Mechanisms of Secondary Dispersions Separation in Particulate Beds

by

MESHAL ABDULLA FAHAD AL-MESHAN

A Thesis submitted to
The University of Aston in Birmingham
for the Degree of Doctor of Philosophy

May 1985

ACKNOWLEDGEMENTS

The author wishes to thank the following

Professor G V Jeffreys

for his supervision and encouragement
throughout the project

Dr C J Mumford

for his constructive criticism and supervision

Members of the Technical and Photographic Staff
of the Department of Chemical Engineering

Miss A E Ferry - for typing this thesis

To my parents and my wife

THE UNIVERSITY OF ASTON IN BIRMINGHAM

"Mechanisms of Secondary Dispersion Separation in Particulate Beds"

Meshal Abdulla Fahad Al-Meshan

Ph.D. May 1985

SUMMARY

The mechanisms by which drops of secondary liquid dispersion ie. <100μm, are collected, coalesced and transferred have been studied in particulate beds of different sizes and heights of glass ballotini. The apparatus facilitated different coalescer cell arrangements. The liquid-liquid system was toluene/de-ionised water. The inlet drop size distribution was measured by microscopy and using the Malvern Particle Size analyser; the outlet dispersion was sized by photography.

The effect of packed height and packing size upon critical velocity, pressure drop and coalescence efficiency have been investigated. Single and two phase flow pressure drops across the packing were correlated by modified Blake-Kozeny equations. Two phase pressure drop was correlated by two equations, one for large ballotini sizes (267μm - 367μm), the other for small ballotini sizes (93μm - 147.5μm). The packings were efficient coalescers up to critical velocities of 3×10^{-2} m/s to 5×10^{-2} m/s.

The saturation was measured across the bed using relative permeability and a mathematical model developed which related this profile to measured pressure drops. Filter coefficients for the range of packing studied were found to be accurately predicted from a modified queueing drop model.

Key words: Secondary Dispersions
Saturation Profile
Particulate Bed
Pressure Drop
Coalescence

CONTENTS

LIST OF FIGURES

LIST OF TABLES

CHAPTER ONE

INTRODUCTION

CHAPTER ONE

INTRODUCTION

The separation of liquid-liquid dispersions is of considerable importance in present day technology. The separation is easier when the dispersed phase consists of drops $>100\mu m$, as in the case of primary dispersions. Provided no stabilisers are present, these dispersions can be separated under gravity due to buoyancy forces. Secondary dispersions contain drops of diameter less than $100\mu m$. The settling velocity for such droplets is very slow and thus prohibitively long settling times are required for adequate separation of the two phases by gravity.

For example, on the basis of Stokes Law,

$$U = \frac{gd^2 (\rho_1 - \rho_2)}{18 \mu} \qquad 1.1.$$

Hence the settling velocity U is proportional to the square of the drop diameter so that a $10\mu m$ drop settles 400 times slower than a $200\mu m$ drop. There are many industrial situations in which secondary dispersions are inadvertantly created, and it is important that they are separated, eg. in the increasing problem of oil pollution of the sea, the contamination of aviation fuel by water, and contamination of produced oil by water.

Generation of a secondary dispersion may arise due to materials transfer (eg. pumping), mixing, or a

change in parameters (eg. temperature) in a liquid-liquid process,or due to vapour condensation.

Various procedures have been used in order to promote rapid coalescence and separation of the dispersed phase from secondary dispersions, These procedures include the use of electrical fields, centrifugation, air flotation, addition of bulk dispersed phase and the addition of chemical coagulants. These processes are often expensive and inefficient, and in the case of the latter may result in residual additives in the separated phases.

One of the most effective separation methods involves coalescence by flow through a fibrous bed, in which droplets are held and grow by coalescence until the surface forces are overcome by other forces acting in the direction of flow; coalesced drops are then released and - given correct operation - are of sufficient size to permit gravity settling. The collection mechanism is critical and if a certain limiting velocity is exceeded both this and retention of the drops on the fibres are adversely affected, ie. 'break through' of fine droplets occurs.

Different types of packing may be used eg. particulate materials such as sand or ballotini, random or woven fibrous materials, or stacked micromeshes. However, the mechanisms of coalescence in porous media are not fully understood and the design of coalescers is based on experimental data, eg. from laboratory tests or on-plant trials.

The objective of the present study was to increase understanding of the mechanisms of droplet collection, accumulation, and travel within beds to reduce the reliance upon specific experimental data and empirical rules for design purposes. A mathematical model was sought to express the efficiency of separation by the filter coefficient, and the energy requirements measured by the pressure drop across the bed.

CHAPTER TWO

FORMATION OF SECONDARY DISPERSIONS

CHAPTER TWO

FORMATION OF SECONDARY DISPERSIONS

2.1. Introduction

The dispersion of one liquid in a second liquid produces a liquid system that has widely differing physical and chemical properties depending upon the drop size of the dispersed phase. Dispersions can be divided into primary dispersions and secondary dispersions. Most previous workers have arbitrarily referred to dispersions of mean droplet diameter which is larger than 100μm as primary dispersions, and less than 100μm as secondary dispersions, while colloids may be defined as systems in which a significant proportion of the dispersed phase molecules lie in, or are associated with the interfacial regions. The two common types of emulsion are oil-in-water (O/W) and water-in-oil (W/O). The continuous and the dispersed phases can be identified easily; the continuous phase can be determined by adding a small amount of one phase, if the emulsion is readily diluted it is the continuous phase that has been added. Alternatively a dye may be added which is soluble in only one of the phases: the dye will diffuse readily to give a general colour if it is the continuous phase in which it is soluble.

2.2. Theory of dispersion formation

The excess energy associated with the formation of new surfaces, for example, subdivision of a liquid within

another liquid always increases the energy of the system and the dispersed phase is thermodynamically unstable with respect to the bulk phase. The energy is also modified by interactions between the surfaces and the bulk phase. Therefore the state of the dispersion is characterised by the excess free energy. Depending on the magnitude of this energy, the colloid may become thermodynamically stable with respect to the bulk phase and form a one-phase colloidal system, or remain unstable with respect to the bulk phase and form a two-phase colloidal system. The processes occurring in the formation and destruction of colloids are illustrated in Figure 2.1.

The particles, however, still behave as individuals separated by thin films of the dispersing medium or by adsorbed layers of surface-active substances. The instability of bulk phase colloids arises from the existence of an energy barrier which has to be surmounted before the two particles can adhere. This energy is a function of the distance of separation between the particles; decreasing as the distance increases.

Figure 2.2(i) is a qualitative sketch of potential energy curves which are the resultant of a repulsive and an attractive component. Such curves may show a maxiumum and two minima, although some of these features may be masked if one contribution greatly exceeds the other. The height of the maximum energy above Energy = 0 is called the height of the energy barrier (P). The deeper minimum is called the primary minimum (M_1), and the more shallow

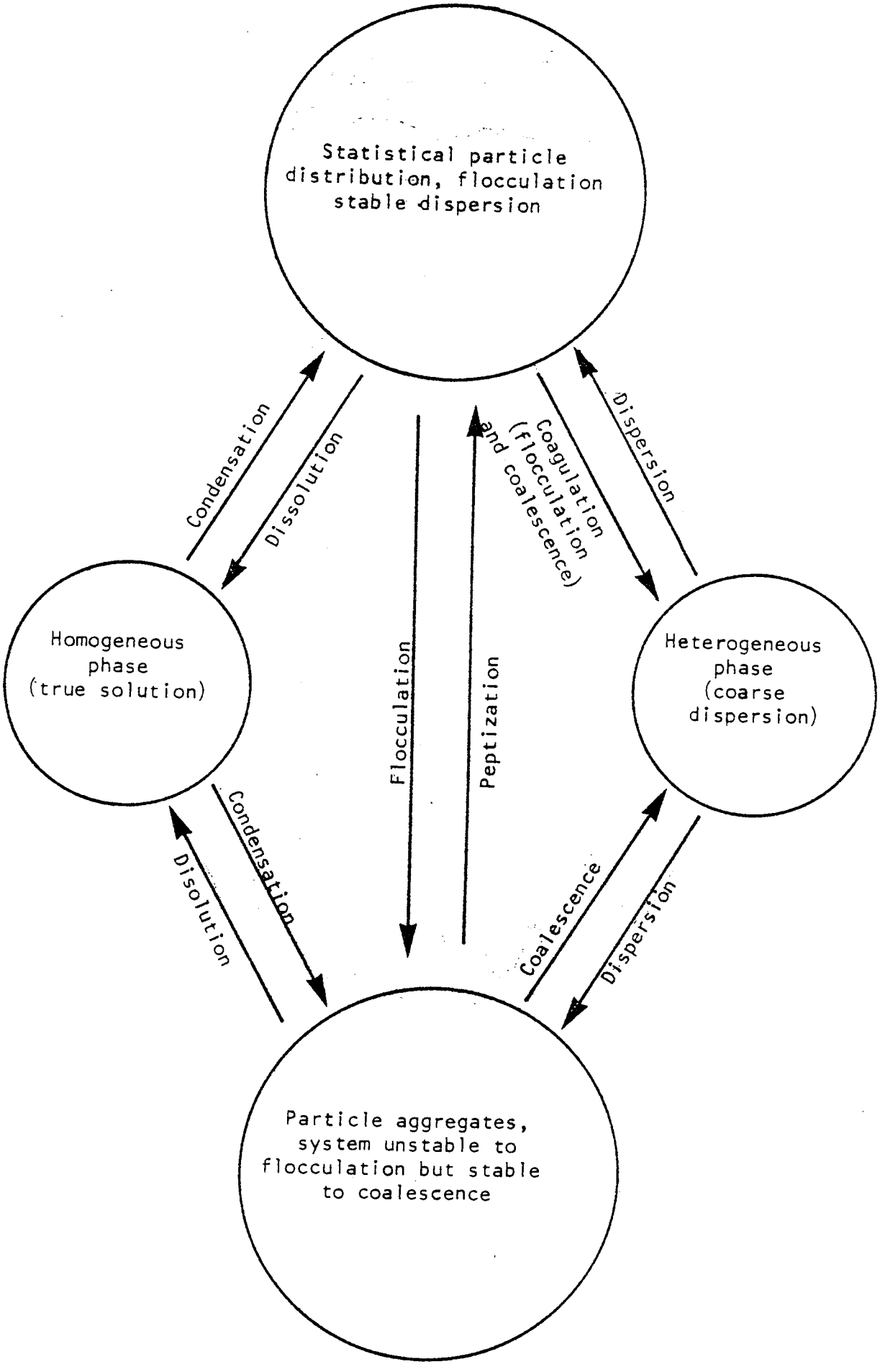

FIG. 2.1 Schematic Diagram of the Processes Involved in the Production or Destruction of Disperse Systems

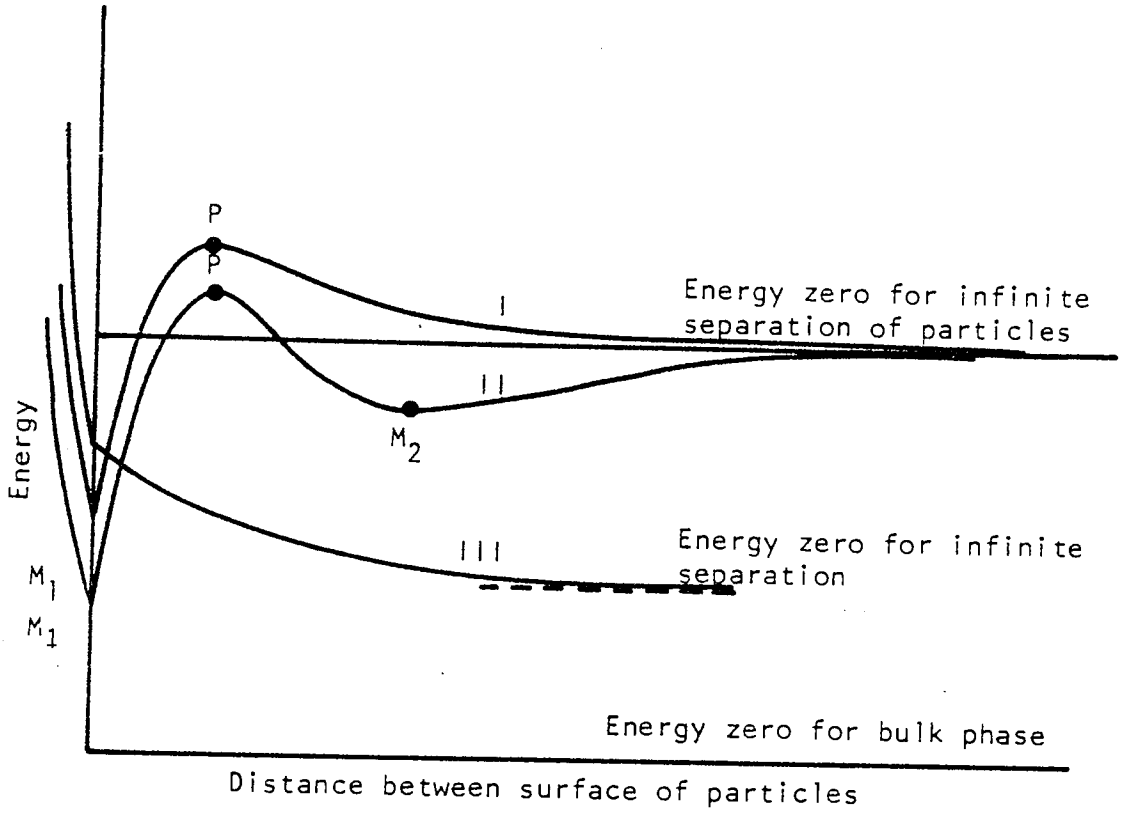

FIG. 2.2 Mutual potential energy of two colloidal particles as a function of the distance of separation between their surfaces:

(i) Curve with primary maximum P and primary minimum M_1

(ii) Curve with primary maximum P, primary minimum M_1 and secondary minimum M_2

(iii) Curve for spontaneous, (unactivated) dispersion

one, the secondary minimum (M_2). Although attraction predominates at large distances - that is, the secondary minimum is generally present - it may be quite shallow, especially in view of the effects of retardation and the medium on attraction. The implication of the potential energy curves shown in Figure 2.2. can be qualitatively considered as follows:

In case I, if no barrier is present or the height of the barrier is negligible compared to the thermal kinetic energy associated with the collision, then the net force of attraction will pull the droplets together as a single kinetic unit. Flocculation has occurred. If the height of the potential energy barrier is appreciable compared to the thermal kinetic energy the particles are prevented from flocculating at the primary minimum. If the depth of the secondary minimum (M_2) is small compared to thermal energy, then the particles will simply diffuse apart. This system is flocculation stable.

There may be situations in which the two droplets may become associated as in case II; here flocculation occurs at the secondary minimum, but the flocs in this case will clearly be much more easily disrupted than those which form by flocculation at the primary minimum and they may later either dissociate or pass over into the primary minimum. Two droplets associated at the primary minimum may remain in this later state or may coalesce to form a larger droplet of a lower surface energy as when an emulsion breaks.

If the interaction curve between two droplets has the form shown in case III, the dispersed state is stable, at constant particle size, so that dispersion of the particles occurs spontaneously.

Curves of the form shown in Figure 2.2. consider the separation between the drops or particles of the size being involved. Therefore to represent different monodispense systems a three dimensional surface shown in Figure 2.3. is used, although the shapes and characteristics of such surfaces depend on many other parameters besides size. Among the more important factors are the continuous phase properties, concentration of the dispersed phase, electrical state of the interface, structure and chemical state of the interface, structure and chemical state of the dispersed phase and the presence of adsorbed films at the interface. Therefore the surface illustrated in Figure 2.3. is only one three dimensional section of a multi-dimensional surface, but useful for a basic description of the phenomena of dispersion and coalescence.

2.3. Preparation of secondary dispersion

It is often required to produce smaller droplets in a short time which necessitates the application of large velocity gradients. To achieve this there are various types of emulsification equipment which can be considered such as simple mixers, colloid mills,ultrasonic devices and homogenizers, Figure 2.4. and Figure 2.5.

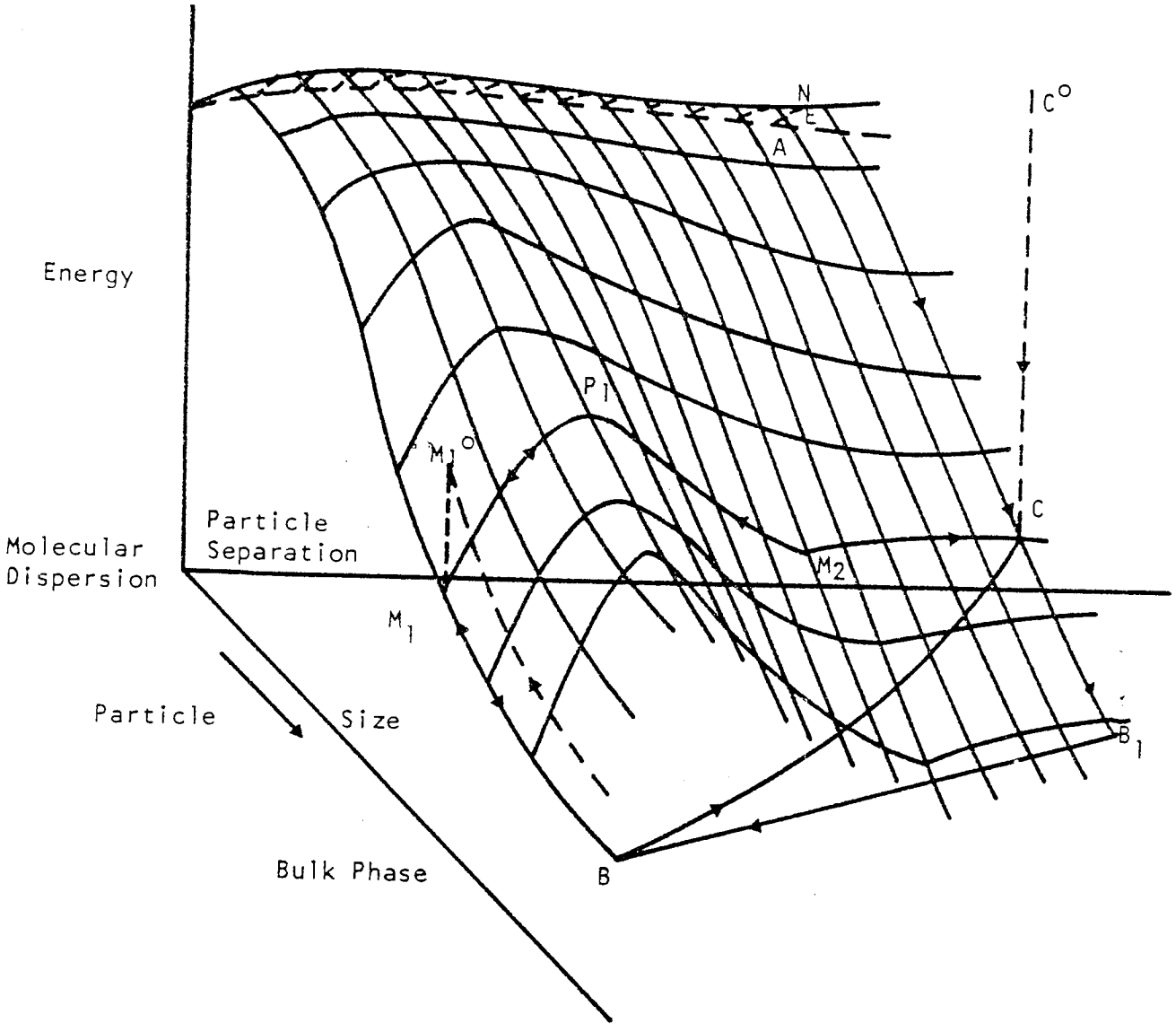

FIG. 2.3 Mutual potential energy surface of two colloid particles of a lyophobic colloid in a liquid medium as function of distance of separation and size of particles, showing routes by which colloid state C can be reached by (i) comminution, routes BC or $BM_1P_1M_2C$ or (ii) by nucleation and growth, ANC; and routes by which coagulation can occur (i) CB_1B and (ii) $CM_2P_1M_1B$. Note that the reverse route CNA in which a colloid would disperse to the molecular state does not in general occur spontaneously. (The short range repulsion "cliff" adjacent to the left hand face of the diagram is omitted for clarity). M_1^o and C^o are points representing energies in a vacuum environment.

IN DESIGNED PROCESSES		By Accident or Malfunction
Deliberate formation of dispersions to increase the rate of a transfer process.	Formation as a result of a physical or chemical change to material being processed.	
1) Liquid-liquid extraction.	1) Condensation of vapour of immiscible liquids.	1) Oil spillage on water.
2) Liquid phase chemical reactions.	2) Azeotropic distillation.	2) Water contamination of oils
3) Direct contact heat transfer.	3) Steam stripping	3) Malfunction of designed apparatus.
	4) Cooling of oils	
	5) Gas compression	

Table 2.1. Methods of Formation of Dispersions and Emulsions.

2.3.1. A Homogenizer

A Homogenizer is a device in which dispersion is effected by forcing the mixture to be emulsified through a small orifice under very high pressure between 70 and 350 bars. Richardson (1) has considered the preparation of an emulsion by injection of one phase into another. Under these circumstances the velocity of flow is extremely important, and break up of the liquid jet is controlled by inertial and viscous forces. The critical velocity Vo from a nozzle of diameter d_n is defined by

$$\frac{\mu_1}{(p_1 \gamma d_n)^{\frac{1}{2}}} = 2000 \left(\frac{\mu_1}{Vo\rho d_n}\right)^{3/4} \qquad 2.1.$$

A production homogenizer will consist of a pump which provides the required pressure, and a special spring-loaded valve which constitutes the orifice and which may be about $10^{-8} m^2$ in area, and which can produce droplets of 1μm.

2.3.2. Colloid mill or blender

Emulsification is carried out by means of a shearing action imparted to the liquid by a rotor, revolving at a speed of from 1,000 to 20,000 rpm, and a stator surface. The emulsion passes between these two opposing faces through a clearance which may be as small as 0.025mm. Taylor (2) deduced a relationship between the radii of droplets formed under conditions of high shear and such parameters as rate of shear, interfacial tension and the viscosities of the two phases. At low speeds, the drop size is given by the approximate expression.

$$\frac{L - B}{L + B} = D \qquad 2.2.$$

where L is the radius of the largest droplet which can exist, B the radius of the corresponding smallest droplet, D is a diameter quantity proportional to the speed of flow. Figure 2.4. shows the mechanisms of break up under shear, based on the work of Rumscheidt and Mason (3).

2.3.3. Sonic and Ultrasonic techniques

In sonic and ultrasonic techniques, electrical energy is converted into mechanical vibrations in the audio or radio frequency range by the use of electro-mechanical transducers. There are three general methods where by acoustic waves of the required energy can be generated. Magnetostriction effects by which certain ferromagnetic metals, particularly nickel, are found to change in length when put in a magnetic field. If an alternating field of the natural frequency of the metal rod is imposed, large amplitude oscillations can be obtained.

Pieszo electric effects, which depend on the fact that certain crystals contract in an electric field. If an alternating current of the same frequency as the natural mode of vibration of the crystal is applied across the crystal's faces, extremely powerful oscillations can be produced.

A diagrammatic representation of the emulsification vessel of a pieszoelectric and of a magnetostrictive emulsifier are given in Figure 2.5.a.

The chief disadvantage of the sonic and ultrasonic techniques is that the methods are most efficient at the

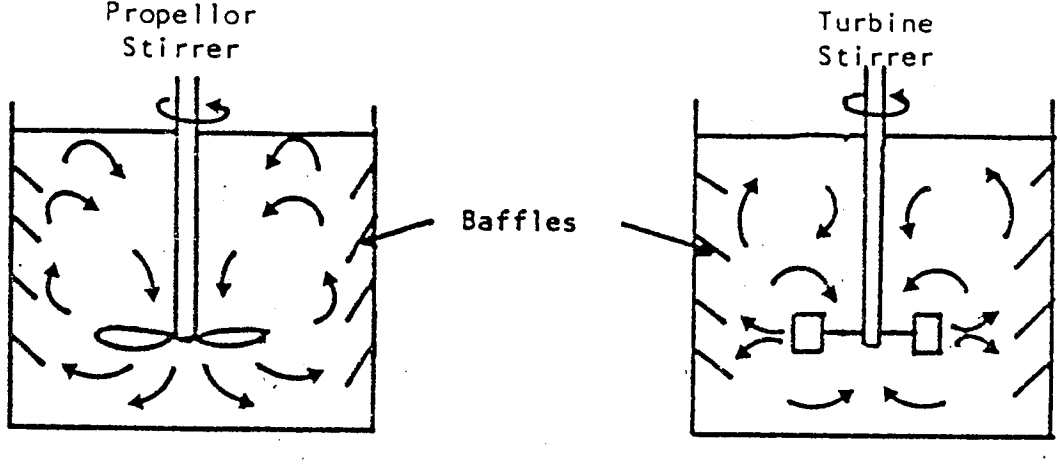

(a) Mixer

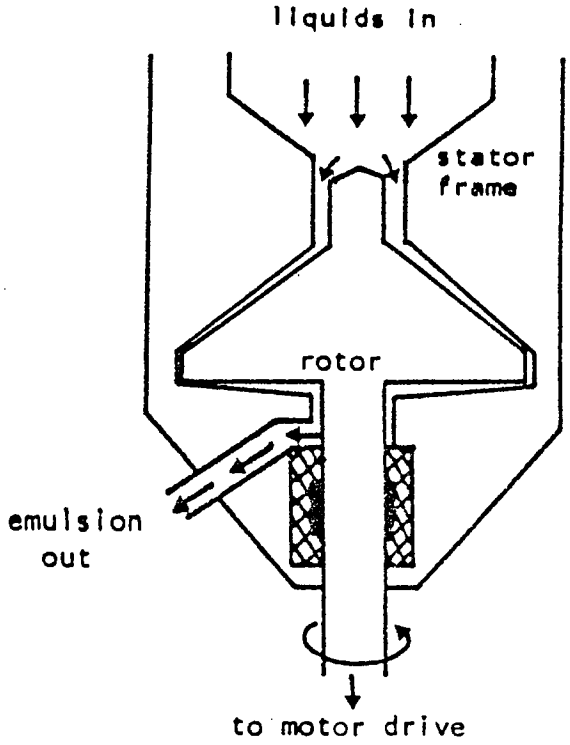

(b) Colloid Mill

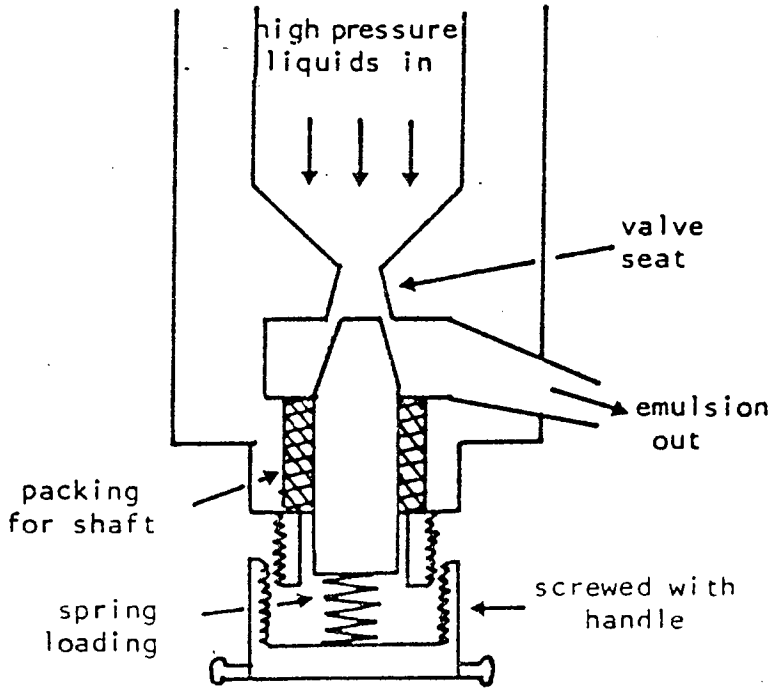

(c) Homogeniser

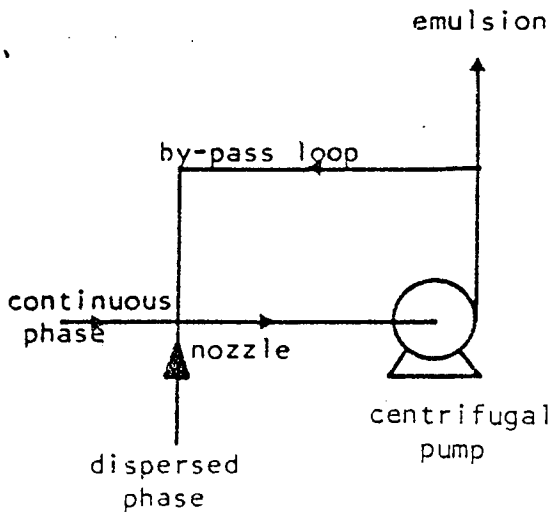

(d) Centrifugal Phase Pump

FIG. 2.4 Mechanical Methods of Emulsification

lower frequencies in the audio range and the use of high intensity sound waves is objectionable on physiological and sociological grounds.

Another method of emulsification is the use of strong electrical stresses, which produce high concentration, monodisperse emulsions on the laboratory scale. The basic equipment is illustrated in Figure 2.5.c. in which application of an appropriate high voltage of about 8kv, between the bulk dispersed and continuous phases produces an aerosol of the dispersed phase which passes into the bulk continuous phase. The disadvantages of this method are that the emulsified droplets are charged and this may seriously interfere with many measurements and interpretation of the results. Also emulsification becomes difficult if the viscosity of either phase is high.

2.3.4. Emulsification by condensation

The essential principle of this method is that the material from which the dispersion is prepared is originally present in true solution, as ions or molecules, and they tend to deposit on any nuclei that may be present in the system. The nuclei may be spontaneously formed by the aggregation of molecules into droplets of submicron size, may be natural impurities of dust or smoke, or may be ions and other seeds that are artificially introduced.

The freeze-heat technique is a condensation method which involves varying the temperature of an agitated mixture of the organic and aqueous phases in a sealed

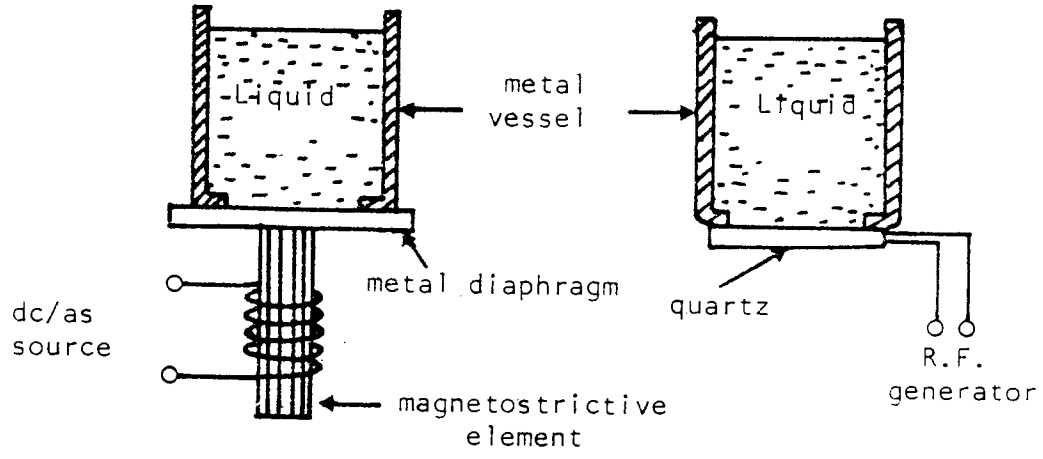

(a) Magnetostrictive and Piezoelectric Emulsifier.

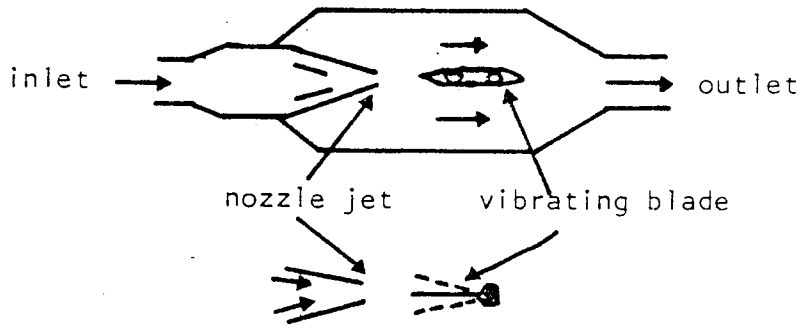

(b) Sonic Emulsification

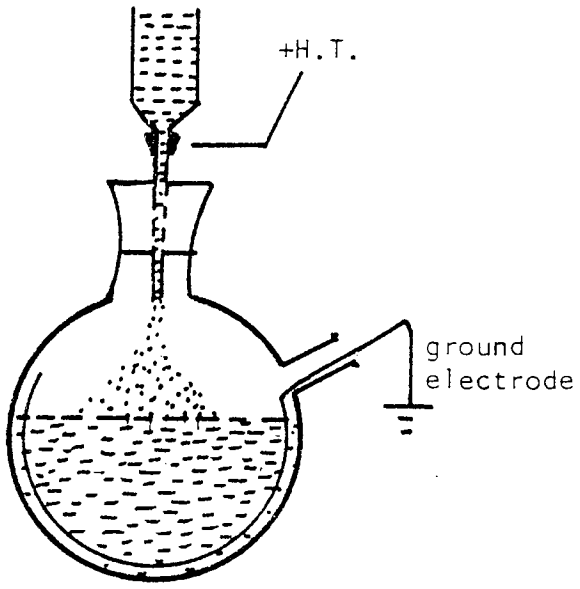

(c) Electric Dispersion of Liquids

FIG. 2.5 Emulsification Using Electromagnetic Transducers

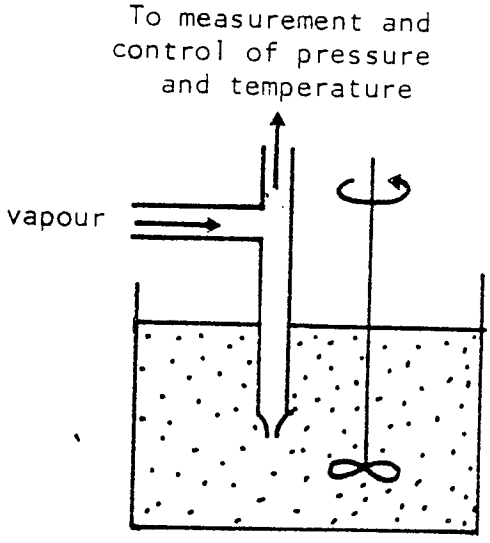

(a) Vapour Injection

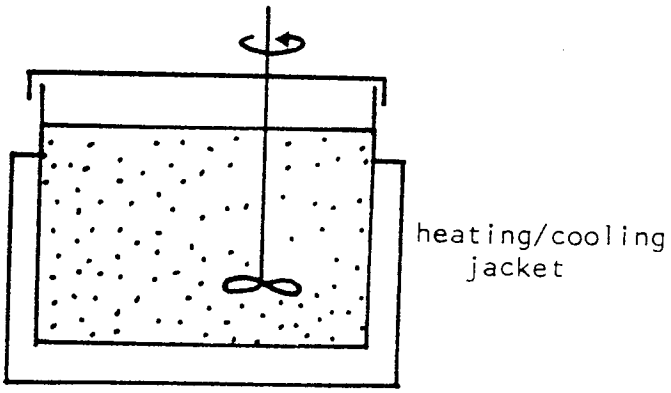

(b) Freeze-Heat Technique

FIG. 2.6 Emulsification by Condensation

system containing an emulsifier until condensation occurs. As it relies upon the temperature dependance of the mutual solubility of the two liquid phases, it is extremely sensitive to temperature changes and may become heterodispersed once formed Figure 2.6.b. This method exists only in the laboratory because of the complexity of the equipment required to control the conditions of formation adequately.

Vapour injection is another condensation method of emulsification which involves the injection of a super-saturated vapour of the dispersed phase using a jet orifice which is submerged in the continuous phase containing a suitable emulsifying agent. The super-saturated vapour condenses as micron-sized drops whose size is dependent on the pressure of the injected vapour, the diameter of the jet orifice, and the emulsifier added to the continuous phase (4). This procedure is illustrated in Figure 2.6.a.

CHAPTER THREE

SEPARATION OF SECONDARY DISPERSIONS

CHAPTER THREE

SEPARATION OF SECONDARY DISPERSIONS

3.1. Introduction

Secondary dispersions can be separated by various techniques, the choice of each technique depends upon many factors; the cost, type of emulsion and the simplicity of the technique.

3.2. Treatment of secondary dispersion

3.2.1. Addition of chemicals

The principle of the chemical treatment is to dissolve the surrounding film of each drop in the emulsion or neutralise surface charges on the drops. For each given emulsion there is a specific demulsifier which will produce optimum results; the nitrosophenols can be used in oil field emulsions (5), alkali metal hexametaphosphates are used for emulsions which contain appreciable calcium ions (6). The disadvantages of this method is the high cost. If the chemicals are surface active they reduce the interfacial tension between the phases of the dispersion leading to formation of very small drops and may be adsorbed onto the surfaces of coalescer elements, thus inhibiting efficient operation.

3.2.2. Centrifugation

This method is most efficient in separating two liquids of low density difference, high continuous phase viscosity

or small drop size. The centrifuging method is not normally applicable to large scale operations as capital and operating costs are too high. This technique is useful in areas where products are expensive and residence time is short as in pharmaceutical or in military applications, such as purification of aviation fuel.

3.2.3. Electrostatic separation

The basic requirements to use this method are that the disperse phase is an electrolyte and the continuous phase in non-conducting.

Sadek and Hendricks (7) state that coalescence can be considered as a four step mechanism in electrical coalescence of water droplets in low conductivity oils:

1. When droplets are passed through an electrostatic field they assume a charge.
2. The charged droplets are propelled by the electrical force towards the oppositely-charged electrode of the field.
3. The droplets collide as they are being propelled with the pole or each other.
4. Coalescence occurs.

This method is suitable just for the separation of water in oil dispersions where the continuous phase is relatively non-conductive and has been applied extensively to the separation of emulsions generated during the desalting of crude oil.

This technique is not suitable for applications where high separation efficiencies are required, and has a

high capital cost.

3.2.4. Air flotation

Air flotation systems cause the suspended drops to be captured by rising air bubbles of 10 to 100 μm diameter and the agglomerates formed float to the surface of the liquid where they can be separated. This method finds extensive application in the treatment of oily wastes from refineries, petrochemical plants and steel mills (8) where quantities of up to 80,000m^3 per day are purified to a dispersed phase concentration of about 20 ppm (9). Flotation processes operate more efficiently when the effluent is pretreated with flocculating agents providing that it is not necessary to recover the dispersed phase from the float which may be contaminated by addition of chemical coagulants.

Generation of the air bubbles may be achieved by chemical reactions, electrolytic methods or by injection of air through a distributor of very small pore size, but dissolved air flotation is the principal method of application due to its simplicity, capacity and versatility.

3.2.5. Coalescence in porous media

The use of porous beds is the most important method of separating secondary dispersions. The mechanism of this method is that small droplets adhere to the packing, droplets in the stream flowing past the fibre strike these stationary droplets and inter-droplet coalescence occurs. This process continues until enough dispersed phase is

gathered at the entrance to form a rivulet which is then pushed through the bed by the drag forces of the continuous phase flowing past it. At the outlet face, enlarged droplets emerge and are separated by gravity as primary sized droplets. The formation of rivulets is however disputed (20).

Because of the current emphasis on pollution control, there has been new interest in porous bed coalescers. A wide variety of porous media has been investigated including pebble beds, ungraded gravel beds and stainless steel gauzes (10). Tuerk (11) and Robertson (12) both indicate that fibrous bed coalescers were initially developed for use on aircraft fuels. Following a series of fatal jet plane crashes in the early 1950's, investigation found the cause to be water in the aircraft fuel.

CHAPTER FOUR

MECHANISMS OF COALESCENCE OF DISPERSIONS IN PACKINGS

CHAPTER FOUR

MECHANISMS OF COALESCENCE OF DISPERSIONS IN PACKINGS

4.1. Introduction

Coalescence phenomena in fibrous beds have been analysed on the basis of three major steps. These are

(i) Approach of dispersed phase drops to the bed.

(ii) Attachment of the drops and flow of the bulk phase through the packing.

(iii) Release of the coalesced drops at the bed exit.

4.2. Requirements for coalescence of secondary drops

The following characteristics are generally accepted as necessary for the coalescence of secondary drops in packed beds.

1. The fibrous bed must be closely packed and possess a high ratio of surface area to volume.
2. The size of the capillary openings must be relatively large.
3. The fibres must be preferentially wetted by the dispersed phase.
4. The surface of the fibres must be rough.
5. The flowrate must be above a certain mimimum but below a certain maximum. A superficial velocity between 0.0012 - 0.005 m/sec has been recommended for separation of water dispersed in petroleum fractions.

6. A bed of several inches is required to coalesce secondary emulsions of submicron drops < 1μm.
7. A high interfacial tension system is more easily coalesced than one of low interfacial tension.
8. Surfactants, dirt, high viscosity tend to inhibit coalescence.

4.3. Approach of dispersion to the packing

The capture of a secondary drop suspended in a continuous phase is theoretically possible by one or more of the following occurences:

(i) Collision with another drop suspended in the dispersion; this is reported to be small by Sareen et al (70)

(ii) Collision with an obstruction in the packing structure. This is an important mechanism especially during the initial, transient operation of a coalescer.

(iii) Collision with another drop which has been captured and is attached to the packing structure. In a study of the coalescence rates of water drops on a single fibre, Bitten (13) observed the growth of a drop attached to the fibre by coalescence with drops captured from a flowing dispersion.

4.3.1.1. Indirect interception

In aerosol filtration and coalescence processes, the diameter of the collector may be comparable to the drop diameter. Under these conditions, the finite size of the drops cannot be neglected and interception between the drop

and collector becomes significant. This mechanism is characterised by the value of the interception number

$$N_R = \frac{d_p}{d_c}$$

The capture efficiency, η is defined as the ratio of the number of drops captured to the number of drops approaching within the projected area of the collector per unit time. Hazlett (14) proposed the use of an equation developed by Langmuir to evaluate the interception mechanism.
This equation determines the capture efficiency of a single cylindrical collector under viscous flow conditions.

$$\eta_I = \frac{1}{2A}\left[2\,(1 + N_R)\,\ell n\,(1 + N_R) - (1 + N_R) + \frac{1}{(1 + N_R)}\right] \quad 4.1.$$

However this equation predicts that as the velocity increases the capture efficiency will increase which is contradicted by experimental evidence (10, 15, 16) Rosenfeld and Wasan proposed an equation for irrotational flow conditions (17)

$$\eta_1 = (1 + N_R) - \frac{1}{(1 + N_R)} \quad ; \quad N_{Re} > 1000 \qquad 4.2.$$

This equation predicts a reduced capture efficiency with increasing N_{Re} which is not a good description of experimental evidence;Davies and Jeffreys (18) concluded that an optimum velocity exists for a given packing; when the local viscous shear forces exceed the force of adhesion between the drops and collector, detachment of the drop, or part of the drop, occurs which is manifested as redispersion. Therefore, assuming the validity of the single collector model, the predicted relationship between capture efficiency and velocity may apply to coalescence processes.

4.3.1.2. Hydrodynamic retardation

Rajagopalan and Tien investigated theoretically the effect of retardation on deep bed filtration (19). Their trajectory analyses, using a single spherical collector model, predicted a monotonic reduction in capture efficiency as N_{Re} was increased. It was also shown that retardation is significant when the drop/collector separation is less than ten drop diameters. Consequently, for large values of N_{Re} hydrodynamic retardation is an important factor, especially when coalescence is induced in low porosity beds. Rajagopalan suggested that, in packed beds, the decrease in capture efficiency is offset by capture of drops by pores whose diameters are less than those of the drops. Although these effects are likely to occur simultaneously, their relative contributions to the drop capture efficiency have not been quantified.

4.3.2. Diffusion onto bed fibres

A particle moving with a fluid will tend to depart from the flow streamline. The most important mechanism affecting this departure is the random transverse motion due to diffusion. Capture of particles by the diffusion mechanism is important at low flow velocities in aerosol filtration. The higher viscosity of liquids would lower the efficiency, whilst the generally lower flow velocities used in liquid filtration would increase the efficiency by this mechanism for water coalescence in a fuel. The viscosity of the fluid is incorporated in the formula for the diffusion coefficient along with the temperature and

particle size. The Peclet number $N_{Re} = \frac{d_c U}{D}$, is often introduced to characterise diffusion and is a measure of the ratio of transport by convective forces to transport by molecular diffusion.

4.3.3. Direct interception

In laminar flow fluid passing a submerged cylinder, such as a glass fibre, will follow stream lines such as those depicted in Figure 4.1 where F is the cross section of a fibre. A water droplet W_1, will follow these flowlines. The droplet shown on streamline S_4 will be intercepted by the fibre when it reaches position W_2. A droplet of somewhat smaller size W_3, following streamline S_2 which is equidistant to S_4 from the centre line, will pass the fibre without any opportunity for interaction, even at the closest approach, W_4. Even such a small droplet will however be intercepted if it follows a streamline closer to the centre line of the fibre. In evaluating the interception mechanism the equation developed by Langmuir is useful (21)

$$\eta_I = \frac{1}{2A} \times (2(1 + R) \ln (1 + R) - (1 + R) + \frac{1}{1 + R}) \qquad 4.3.1$$

η_I = Efficiency of collection by single isolated fibre from a fluid stream of a width equal to the diameter of the fibre.

R = Interception parameter = dp/d_c

dp = Particle diameter (cm)

N_{Re} = Reynolds Number

A = 2 - $\ln N_{Re}$

This mechanism predominates in the coalescence of a primary

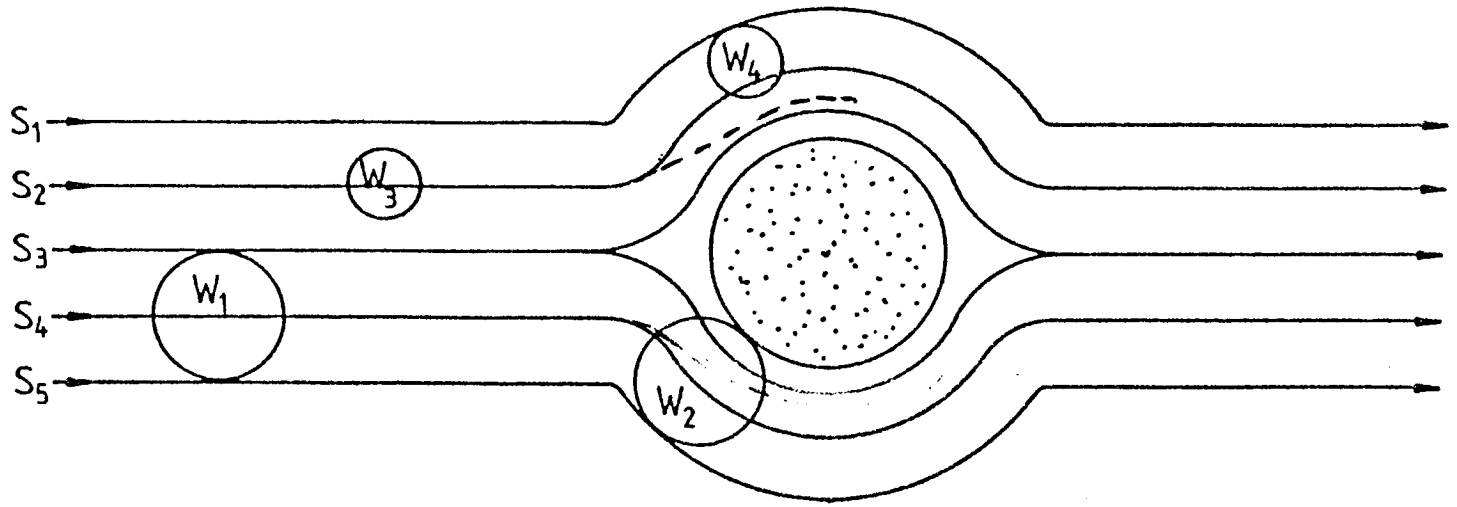

Figure 4·1 Flow patterns for direct interception.

dispersion since it is well known that when the drop diameter is less than the equivalent diameter of the packing interstice, the coalescence rate is very low, even when the dispersed phase wets the packing.

4.3.4. Inertial impaction

A particle with a density different from that of a fluid with which it is flowing will deviate from the flow streamline should the latter be diverted. A more dense particle tends to move in a line less curved than that of the streamline. A possible path for a more dense particle is illustrated in Figure 4.1. where the broken line indicates the departure from streamline S_2; particle W_3, in deviating from the streamline, approaches close enough to the fibre to be captured when it reaches position W_4. Thus the greater the density a particle has, with respect to the continuous phase, the higher the probability that it will be captured. This approach mechanism is termed the inertial impaction process. Hazlett and Sherony suggested this mechanism was relevant to coalescence in fibrous beds and characterised its contribution by the magnitude of the Stokes number (14, 23).

$$N_{stk} = \frac{d_p^2 \rho_c U}{9 \mu_c dc} \qquad 4.4.$$

Impaction becomes significant when N_{stk} exceeds a critical value which depends on the Reynolds number. Langmuir determined N_{stk} to be 0.063. Landahl proposed an empirical expression relating capture efficiency by inertial impaction to the Stokes number, (21).

$$\eta_{II} = \frac{N^3_{stk}}{N^3_{stk} + 0.77\, N^2_{stk} + 0.22} \qquad 4.5.$$

for $N_{Re} < 10$; $N_{stk} > N_{stk\ crit}$

4.3.5. Sedimentation

The density difference between dispersed and continuous phases causes drop trajectories to deviate from the fluid streamlines due to buoyancy forces. Their magnitude is characterised by the Gravity number. $N_G = \frac{d_p^2 (\rho_d - \rho_c) g}{18 \mu_c U}$ which is the ratio of the drop terminal velocity, assuming viscous flow conditions, to the superficial velocity of the dispersion flowing through the bed. Rajagopolan and Tien showed that the capture efficiency is equal to the value of the Gravity number (19)

$$\eta_G = N_G \quad ; \quad N_G > 10^{-3} \qquad 4.6.$$

The condition associated with this equation is not restrictive since the contribution due to sedimentation is negligible for $N_G < 10^{-3}$

4.3.6. Electrical double layer forces

The ionic double layer forms by retention of mobile ions adjacent to the phase boundary by electrostatic attraction to the boundary charge. The interaction between the double layers surrounding the drop and collector may be either repulsive or attractive, depending on whether their respective charges are like or opposite. For low electrolyte concentrations in the continuous phase, double layer forces only become significant when the distance

between drop and collector is less than of the order of 20μm. Spielman and Fitzpatrick proposed the following expression for the double layer force between a drop and collector (24).

$$F_{DL} = \varepsilon \zeta_p \zeta_c N_{DL} \left[\frac{e^{-N_{DL}H}}{1 + e^{-N_{DL}H}}\right] \qquad 4.7.$$

Where ε is the dielectric constant of the continuous phase ζ_p, ζ_c are the zeta potentials of the drop and collector respectively. The Double Layer group, $N_{DL} = \frac{Kd_p}{2}$ where k is the reciprocal Debye length indicates the relative thickness of the double layer. When the Electrokinetic group, $N_{EZ} = \frac{2\zeta_c\zeta_p}{(\zeta_c^2 + \zeta_p^2)}$ is positive, the force given by equation 4.7. is repulsive and when the converse is true, the force is attractive.

Spielman (22) developed a criterion to neglect double layer forces in trajectory analysis which is based on the requirement that, $F_{DL} << F_{Ad}$ at $H = H^*$, where H^* is the dimensionless separation at the rear stagnation point of the critical trajectory. Rajagopalan and Tien (19) proposed that the resultant force, calculated as the sum of the double layer interaction and the retarded London attraction, indicated no barrier against drop collector contact for parameters relevant to coalescence processes. They concluded that these surface interactions, when considered as transport mechanisms, are unimportant providing that their effect is attractive in the vicinity of the collector.

4.3.7. London - van der Waal's forces

Dispersion or London forces arise due to the polarisation of one molecule caused by fluctuations in the charge distribution within an adjacent molecule and vice-versa. These forces are, however, retarded because a finite time is required for propagation of electromagnetic radiation between the particles.

Spielman and Goren (16) recognised that the long range attractive forces between a drop and collector may contribute to drop capture. These London forces increase rapidly as the drop approaches the collector to overcome the hydrodynamic retardation effects or to offset any double layer interaction. Hamakeer derived an expression from which the London attractive force between a sphere and a plane surface may be evaluated (25).

$$F_{ad} = \frac{2Q}{3a_p (H + 2)^2 H^2} \qquad 4.8.$$

where a_p is the sphere radius,

H is dimensionless separation between the sphere and plane surface $H = \frac{h}{a_p}$

Q is the Hamaker constant.

Since the London force depends on separation, knowledge of the motion of a drop in the vicinity of a collector is required to determine the capture efficiency. Rosenfield modified equation 4.8. to describe the attraction between a sphere and cylinder (24).

4.4. Attachment

4.4.1. Coalescence sites

After capture, by either held drops or by a packing fibre,drops will continue to coalesce until hydrodynamic forces cause detachment from the coalescence sites. Coalescence may occur between two freely moving drops with primary dispersions,but experimental observations refute this possibility for secondary dispersion coalescence. Drops captured by direct interception and retained by the collectors, may then trap other approaching drops and subsequently coalesce with them. Wilkinson (27) investigated the behaviour of primary drops, that did not wet the packing, trapped in the interstices of a bed of random packed glass spheres. He showed that drops increase their volume by coalescence until the buoyancy forces exceed the restraining interfacial tension forces. Deformation of the drop then occurs as it is squeezed through the aperture.

When the drops are small compared with the collector and aperture diameter, coalescence may take place between adjacent drops located on the collector surface. Bitten (29) observed that this was a slow process for the coalescence of drops on single fibres compared to growth by acquisition of the dispersed phase from the flowing dispersion.

4.4.2. Drop passage through interstices

Various mechanisms for the passage of drops through the packing voids have been proposed by Wilkinson (27) as illustrated in Figure 4.2. It is clear that the probability

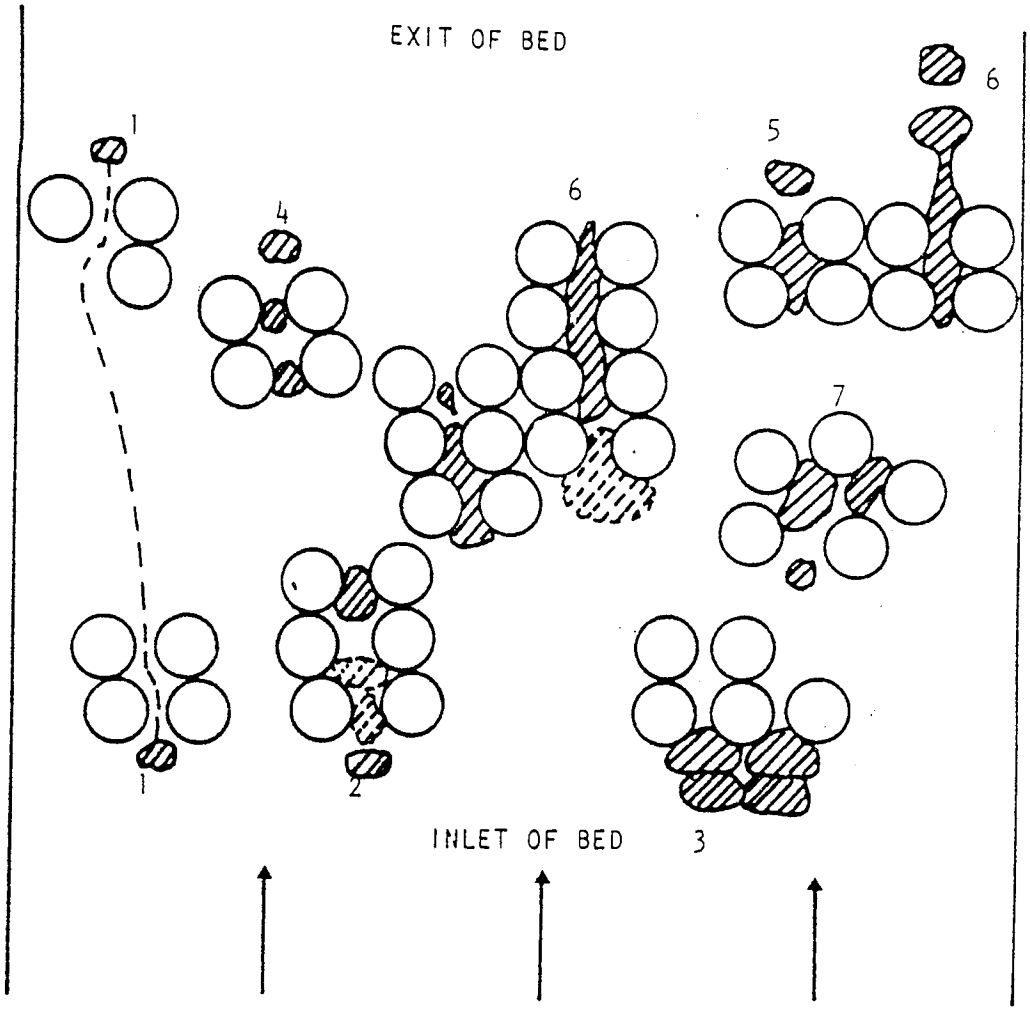

1. Unrestricted drop passage
2. Restricted drop passage (penetration due to kinetic forces)
3. Inlet drop restriction
4. Retention - impact - release
5. Unrestricted drop release
6. Restricted drop release
7. Preferential flow-path

FIG. 4.2 Proposed Droplet Hydrodynamics in a Non-Wetted Packing of Equal-Sized Spheres

associated with each mechanism depends on the value of the direct interception number N_R.

Secondary drops possess more surface energy per unit mass than primary drops due to their size and also buoyancy forces are usually negligible. Therefore drop deformation and drainage of the intervening continuous phase film prior to coalescence is less easily accomplished. For this reason the retention - impact - release mechanism, whereby small individual drops deform to pass through micron size pores, is unlikely to be important for secondary dispersions. Unrestricted drop passage, may also be insignificant since drops attaining a critical diameter for release from a collector are likely to be immediately recaptured by direct interception. This provides evidence that pores may become blocked by large drops, or by simultaneous approach of smaller ones. If this happens frequently, fewer channels are available for flow of the dispersion and the pressure gradient per unit length of the bed will increase. Captured drops will then be induced to retreat to sites where the interstitial velocity is low so offering least resistance to the flow of the continuous phase.

As a result, the drops will tend to concentrate in relatively few channels where they queue in a localised 'dispersion band' type formation until coalescence occurs with adjacent drops and the drop which blocks the pore. As more flow paths become blocked, eventually the increasing pressure gradient will be sufficient to force coalesced drops through the pores. The above discussion has been confined to cases where the dispersed phase is non-wetting.

4.5. Dispersed phase flow regime

Drops which have been collected by the packing fibres and reside in the packing interstices until they are coalesced, act as potential collectors for other drops entering the bed. Therefore, both the number and distribution of drops within the packing are important factors governing capture rate and pressure drop under steady state conditions.

4.5.1. Drop redispersion

Movement of the coalesced dispersed phase may occur by release of the drop from the fibre when the drag forces exceed adhesive and London attractive forces. Vinson states that cohesive failure results when only part of the drop is detached (13). The cohesion mechanism involves formation of threads which subsequently break up into smaller drops which are then redispersed into the flowing continuous phase. The size of these drops depends on attenuation of the liquid threads which is suggested to be a function of the viscosity ratio. Internal drop release by cohesive failure is thought to be responsible for low filter coefficients when the dispersed phase exhibits a high wetting affinity for the packing material. Also the existence of a critical velocity above which redispersion considerably reduces efficiency, has been reported by many workers but the value of this velocity varies over two orders of magnitude. Therefore, these values are of little use in practical coalescer design because they are specific to the liquid systems and properties of the packings studied.

4.5.2. The travelling drop hypothesis

Sherony and Kintner (23), and Rosenfeld and Wasan (17) among others have proposed that drop release is by adhesive failure, after which the large drops travel through the pores of the medium, eventually being released at the downstream face. Their models describe coalescence of a secondary dispersion in high porosity beds and are based on this travelling drop hypothesis.

They assume that a saturation regime prevails within the bed, which precludes the existence of a dispersed phase continuum. Rosenfeld (17) claims that the assumption is justified when the dispersed phase is dilute and because channels should not be present in beds with porosities greater than 0.9. However Brown (32) showed that the dispersed phase passed through the intermediate portion of a bed using the same channels repeatedly. The threads were observed to pulse and they varied in diameter and flowrate with time. In many cases, the threads were discontinuous but, when flow restarted, the same channels were utilised. Similar behaviour was reported by Hazlett when threads of water were observed in a fibrous bed during the coalescence of a water in fuel dispersion (24). This experimental evidence suggests that a saturation regime would better represent the dispersed phase distribution.

4.5.3. Critical drop diameter

The travelling drop models also assume that when drops are detached from fibres their passage through the bed to the exit face remains unimpeded. Their diameter should

therefore be less than the pore diameter. Bitten (29) described visual observations of coalescence of water drops in jet fuel on individual fibres of glass, Teflon, Dacron and nylon. Individual fibres were reported to retain drops having diameters many times those of the fibres without re-entrainment for velocities up to 2×10^{-2} m/s. Glass fibres of 5-6μm diameter could retain 400-500μm drops before release but the polymeric fibres, having diameters in the 11-17μm range, were less retentive as drops were detached when their diameters exceeded 65-75μm. It may be concluded that characteristic interfibre spacings of 2 or 3 fibre diameters will not permit progressive travel of drops which are 90 fibre diameters.

4.5.4. Dispersed phase continuum model

Spielman and Goren (33) assumed that two readily distinguishable regimes of the dispersed phase exist within the packing. One regime consists of drops that are suspended in the continuous phase; the other is coalesced disperse phase that is held up in the pores and assumed to form a network of channels which are sufficiently well connected to sustain viscous flow of the dispersed phase by capillary conduction. This model implies that captured drops are immediately coalesced into the continuum which is contrary to observations since coalescence time is large for drops of secondary dispersions.

Spielman and Su (34) recently proposed an additional regime corresponding to an intermediary coalescing dispersed phase which is a better physical description of the process.

This phase consists of a distribution of drop sizes varying from newly-captured drops which continuously coalesce, to drops which then participate in channel flow. Spielman and Su (34) assumed that the intermediary phase constituted the majority of the total dispersed phase saturation with only a negligible proportion comprising newly captured drops and the capillary conducted phase.

Although feasible, this assumption cannot be universally applied, because, if the diameter of the captured drops are comparable to the mean pore diameter, then the proportion of the intermediary phase would be considerably less. Attarzadeh (20) reported that coalesced drops travel through the bed, and not rivulets.

In conclusion, the dispersed phase flow regime proposed by Spielman and Su (34) is probably the most accurate description and consistent with experimental observations especially for low porosity packings.

4.6. Release

Three factors which affect the size of droplets released are the flow velocity, the surfactant content and the fibre size.

The water droplet size at release from a packed bed is given by the equation (35),

$$dp = \frac{0.9a^{0.71}\ \gamma^{0.71}}{\Delta v\ F^{0.29}\ n^{0.43}} \qquad 4.9.$$

where a = orifice radius at the downstream face of water channel through the fibrous bed - cm.

γ = interfacial tension, dynes per cm

Δv = difference between fuel and droplet velocity cm/sec

F = dimensionless number.

In release of water from the downstream face of the fibre glass bed in the ideal case with a high quality fuel, a water thread passing through the fibrous bed feeds a water drop attached to the downstream face of the bed. The balloon shaped drop formed in this way continues to grow in size until the hydrodynamic forces exceed the interfacial fuel-water forces. See Figure 4.3. (a). The balloon may be fed continuously by a thread, or stepwise transfer of an intermediate size drop from the thread to the growing balloon can occur. The rupture occurs at the neck of the balloon. The size of the drop released is a function of the flow velocity, interfacial tension, and water neck cross-section. A surfactant can also alter the release step in other ways. High speed cine films show that a different type of release is common when surfactants are present in the fuel(36). A water jet then breaks up into uniform, but small droplets by Rayleigh instability. This phenomenon is shown in Figure 4.3.(b) along with the capillary waves which precede the break up of the jet. Water release by the jet mode is associated with irregular water release. The jet will play for a period of time which may involve droplet chains of several hundred drops although the usual number is 10 to 20 drops. The jet then becomes passive but activity is normally reinstituted at the same bed sites.

Surfactants appear to stimulate jet release by encouraging rupture of a water thread passing through the

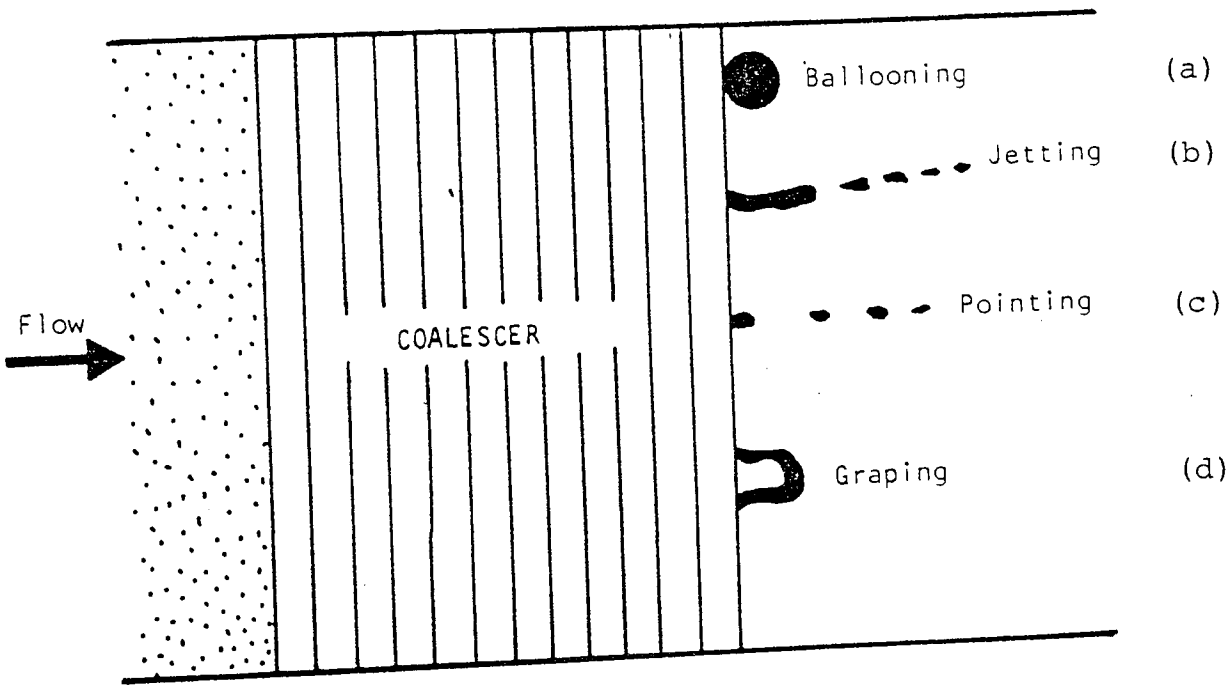

FIG. 4.3 Exit Drop Release Mechanisms

filter bed. The free jet which results passes through the bed pores propelled by the force of the moving fuel. The water jet readily decays to a droplet chain, probably within the bed, rather than growing into a balloon on the downstream face. Lowering the interfacial tension, a likely function of a surfactant, would assist rupture of the water thread.

An unusual type of release is illustrated in Figure 4.3(c) This has been designated 'pointing release'. Fingers of collected water project beyond the filter face. These fingers taper to a point, vibrate and release small drops from the tip. This behaviour is probably a modification of the jet release pattern described above. Subsequent movement of the small drops produced in this manner through the multiple tortuous capillaries of the fibre would yield a random pattern of droplets leaving the bed. An additional type of water release,designated 'graping', has been reported by a number of observers (37, 38). This behaviour is found at high water concentration or with certain additives. Fibres which give low contact angles frequently encourage 'graping'. In this type of release water bridges across a pore; fuel using this pore blows a bubble and in so doing becomes encased in a film of water. Several of these bubbles readily associate with each other to form a cluster.

CHAPTER FIVE

MODELS OF FIBROUS BED COALESCERS

CHAPTER FIVE

MODELS OF FIBROUS BED COALESCERS

5.1. Introduction

Models developed by previous workers (39, 40, 36, 33) were based on assumptions of coalescence mechanisms within the packing and/or observations of drop coalescence on a single fibre.

Mathematical models which have been derived to assist in the design of fibrous bed coalescers are reviewed below.

5.2. Sherony and Kinter's Model

Using a combination of aerosol filtration models and the kinetic theory of gases a model of a fibrous bed coalescer was presented which relates the collision frequency between droplets and fibres to the overall coalescence frequency (120). The basic assumption is that there is a population of drops adhering to the fibres and that this size distribution of drops is some subset of the size distribution in the main stream. Therefore, this model is confined to a sufficiently small concentration of dispersed phase in the entering emulsion, that it does not form a continuum in the bed.

The model took into account coalescence by the following mechanisms:

(a) Impaction: This method of coalescence occurs when a drop in the stream collideswith a drop attached to a

fibre and a coalescence results.

(b) Brownian diffusion: Collision by Brownian motion can occur between two drops in the stream or between a drop in the stream and a drop on the fibre.

(c) Coagulation in a turbulent field: In this mechanism, drops which are associated in pairs as they are squeezed through the capillary passages of the bed eventually coalesce.

As a first order of magnitude they calculated that the collision frequency due to the impaction mechanism was about 150 times higher than turbulent collision and 10,000 times higher than diffusion. Thus only the impaction mechanism was considered. This led to their final equations where filtration coefficient for a coalescer λ_c is given as:

$$\lambda_c = \frac{3}{4} \frac{S}{(1 - S)} \frac{(1 - E)\ (1 + d_{10}/d_c)}{d_c} \eta_c \qquad 5.1.$$

When S is average degree of saturation, η_c is overall coefficient efficiency, E is packing voidage, d_{10} is average inlet drop size.

for S and η_c constant over the bed length

$$Y = \frac{\mu_o(L)}{\mu_o(O)} = \exp\ (-\lambda_c L) \qquad 5.2.$$

Y is the ratio of outlet to inlet drop densities.

This model shows that the performance of a coalescer will increase with (a) decrease in fibre diameter,

(b) larger mean inlet drop size, and (c) increase in packing thickness, in agreement with experimental results (122).

In the model, in order to keep the study of coalescence in a fibrous bed in perspective with aerosol filtration, the overall fibre efficiency was defined as:

$$\eta_c = \alpha\beta \qquad 5.3.$$

where α is ratio of total number of particles striking a fibre to the total number approaching it, and β is fraction of collisions between drops that resulted in coalescence. Calculations indicated that η_c increased with increase in velocity, in agreement with aerosol theory and Hazlett's model but contrary to experimental results with fibrous bed coalescers (11, 14, 42). Clearly therefore the coalescence efficiency predicted from aerosol filtration theory is not applicable to fibrous bed coalescence and a more accurate theory is needed for predicting efficiency.

5.3. Hazlett's model

Hazlett (14) based his model on three major steps:

(a) approach of a dispersed water droplet to a fibre,

(b) attachment of the droplet, and

(c) release.

The approach process was subdivided into direct interception, diffusion and inertial impaction. Direct interception was the most important step. Diffusion may assist direct interception for submicron drops but inertial impaction was insignificant.

5.3.1. Direct interception

Under the laminar flow conditions generally existing in a fibrous bed coalescer fluid will flow past a glass fibre, analogous to a submerged cylinder, in streamlines. The droplets which follow streamlines close to the fibre centre will be intercepted. Using Langmuir's equation to evaluate the interception process:

$$\eta_I = \frac{1}{2(2 - \ln N_{Re})} \left(2(1 + N_{Re}) \ln(1 + N_{Re}) - (1 + N_{Re}) + \frac{1}{1 + N_{Re}}\right) \quad 5.4.$$

This equation predicts an increase in efficiency with increase in velocity, which is contrary to experimental observations (39). In any case it is misleading to relate bed efficiency to single fibre efficiency because packed bed fibres are orientated at different angles to the flow, and there are many intersections, causing different collection efficiencies. At steady state there is also hold up of dispersed phase within the bed which alters the effective voidage. With a single fibre in a fixed position there is no significant hold up and there is no variation in collection efficiencies.

The release mechanism was considered to involve coalesced droplets forming threads through the bed until released as individual drops from the exit face. Drop release occurs when the hydrodynamic force exceeds the adhesive force between the drop and the fibre or fibres. The size of the released drop depends upon flow velocity, surfactant content and fibre diameter. Three possible release mechanisms are presented:

(a) Drop-volume rupture: This equates the drag force exerted on the drop with the restraining forces due to interfacial tension. This yields:

$$\frac{C\ P_c\ U_d^2 \pi (\frac{1}{4}(d)^2 - a^2)}{2} = 2\ a\pi\alpha\gamma \qquad 5.5.$$

(b) Drop elongation rupture: This release is due to the effect of the moving fluid surrounding a drop. For the viscosity ratio of the drop to the continuous phase frequently encountered, 0.5 to 1.0, the elongation at small distortions is proportional to a dimensionless number F:

$$F = \frac{2G\ u_2\ (\frac{1}{2})d}{y} \qquad 5.6.$$

where F is Harkins-Brown factor, G is shear rate, and y is ratio of outlet to inlet drop densities.

(c) Jet rupture: This is the rupture of an extended jet due to Rayleigh instability producing a series of uniform but smaller drops whose size is governed by interfacial tension and nozzle size. Whilst this is a common release mechanism, no equation is presented to describe this process. Thus Hazlett's model is of limited use for designing a fibrous bed coalescer.

5.4. Rosenfeld and Wasan's model

This model (17, 43) is based on the following mechanisms: Droplets impact upon the fibres and adhere; a distribution of retained drops is thus created. Other drops from the main stream impact upon the retained drops and coalesce. Coalescence proceeds until an equilibrium drop size is reached at which the drop is pulled away from the fibre

due to the fluid drag. A design equation was derived based on the following assumptions:

(a) The dispersed phase is dilute and the droplets are small ie. dispersed phase droplets do not affect the flow of the continuous phase. This is in agreement with observations of Spielman and Goren (33).

(b) The saturation in the bed is sufficiently small that a continuum of the dispersed phase does not exist.

(c) Approach to a fibre is mainly by the interception mechanism. London van der Waals forces have been shown to be negligible. This has been accepted by a number of investigators (72, 36, 44, 16).

(d) When a drop strikes a fibre or a retained drop the probability that it will remain on the fibre, or coalesce with the drop, is a constant for one particular system.

(e) Drops grow by coalescence of a retained drop with drops from the free stream. There is essentially no coalescence between two drops in the field stream, which is in agreement with the experimental results of Sareen et al (72) and Bitten (13).

(f) The drop detaches from the fibre after reaching a critical size. This has been observed in single fibre studies (72, 45).

(g) Each drop can be considered independently of the overall distribution. Spielman and Goren found that for dilute emulsions, eg. 0.1% concentration, provided the dispersed phase viscosity is not too large compared

with the continuous phase viscosity, the coalescence efficiency for any given drop size is independent of the size distribution.

A set of equations were formulated and solved to give a final theoretical design equation as follows:

$$\lambda = \frac{8\ \beta\ (1 - E)d}{\pi^2 E\ (1 - S)d_c^2} \times \frac{2d_{ce} + d}{d_{ce} + d} \qquad 5.7.$$

Comparison of equation 5.7. with Spielman's experimental data (40, 24), showed that it is only valid at low velocities of less than $1.5 \times 10^{-3} ms^{-1}$ for $\beta = 0.24$, when the turbulence in the bed is insignificant. At larger velocities, the effect of turbulence grows until the equation is no longer valid. A purely empirical extension of the above equation is made to fit this data. This leads to:

$$\lambda = \frac{8\ \beta\ (1 - E)d}{\pi^2 E\ (1 - S)\ d_c^2} \times \left(\frac{V'_{cr}}{V'}\right) 0.5 \times \left(\frac{2d_{ce} + d}{d_{ce} + d}\right) \qquad 5.8.$$

Although this theoretical model is an improved version of the Sherony et al (36) model various workers (41, 42) have obtained results showing that it is inadequate for velocities $< 0.5 \times 10^{-2} ms^{-1}$.

5.5. Vinson and Churchill model

This model assumes that drops collide with fibres and have a probability of being retained. They then move along the fibre onto other fibres, and coalesce with other retained drops. The model further assumes that the drops are captured

by interception and the thinning of the continuous phase film and the van der Waals attraction. The drop filament adhesion, together with the wettability, determines whether a drop remains on the fibre long enough to coalesce with other drops. Their equation represents the best fit of the data taken for a system where photoetched screens were used to simulate a fibrous bed (15).

$$\lambda = \frac{-\log_e \{0.128\ (U\ d_c\ \mu_c)^{-0.4} - 0.089\}}{L} \qquad 5.9.$$

where the units of the independent variables are (gm)(micron)/s^2.

The obvious shortcoming of this model is that no equations are presented which can be used to correlate the data, ie. it is qualitative model. Also it has some shortcomings, in that photographic studies (43) indicate that while drops strike the fibres they also strike drops which are attached to the fibres. Also whilst van der Waals attraction was considered in the film thinning process, they failed to consider this force as a factor in holding a drop on a fibre.

5.6. Spielman and Goren model

This model (31, 33) assumes that when a dispersion flows through a fibrous bed, the suspended drops are transported to the fibres and entrapped liquid interfaces where they are captured and coalesced into the bulk of previously captured liquid. This coalesced liquid drains through the bed and leaves the bed at the same rate as the rate at which suspended drops are coalesced within the bed. Each immiscible fluid is considered to flow within a fixed

channel, with the non-wetting fluid flowing on the inside. Each channel is described by Darcy's Law.

They suggested that London van der Waal's forces are of sufficient magnitude to overcome any hydrodynamic retardation effects and were included in the evaluation of capture efficiency. Their equation for continuous phase wetted beds was obtained by correlation of experimental data with a modified adhesion number.

$$\gamma = 0.29 \frac{d_p 2}{dc^3} \left\{ \frac{Q\, d_c^{\,2}}{\mu_c\, U\, d_p^{\,4}} \right\}^{0.25} \qquad 5.10.$$

The main shortcoming of this model, is that it is unique only for geometrically similar solids, having the same dispersed phase saturation.

CHAPTER SIX

EXPERIMENTAL INVESTIGATION

CHAPTER SIX

EXPERIMENTAL INVESTIGATION

6.1. Introduction

The equipment was designed to supply a secondary dispersion of known drop size and dispersed phase concentration at a specified flow rate to the coalescence section. In this section, collection and coalescence of the drops in the secondary dispersion produced primary droplets at the top of the bed, where they separated under gravity.

6.2. General arrangement

The flow diagram of the apparatus is shown in Figure 6.1. and the general arrangement is presented in Figures 6.2. and 6.3. The continuous phase was produced by distillation of tap water using an electrically heated boiler. The water which left the boiler at 330°K was allowed to cool to ambient temperature in a $350m^3$ capacity tank of stainless steel construction. The maximum liquid level inside the tank was automatically controlled by using a pressure sensor connected to the boiler power supply. It was very important to cover the storage tank because the partially de-aerated water would absorb air during cooling and be evolved at many points throughout the equipment. A gravity-fed, stainless steel centrifugal pump with Viton seals was used to transfer the distilled water through the flow equipment, coalescence device and to a gravity settling vessel, and then to drain.

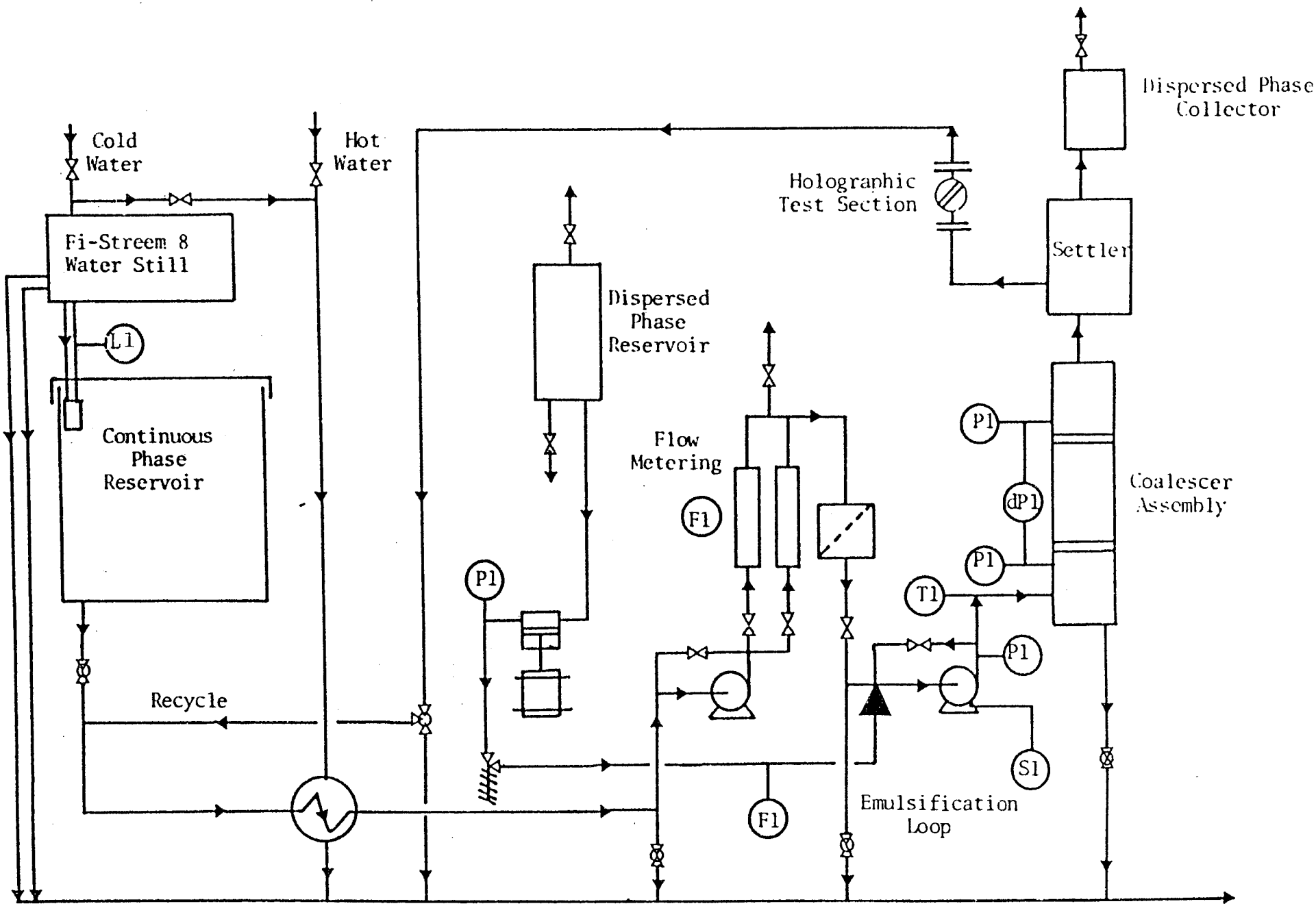

FIG. 6.1 Flow Diagram of Equipment

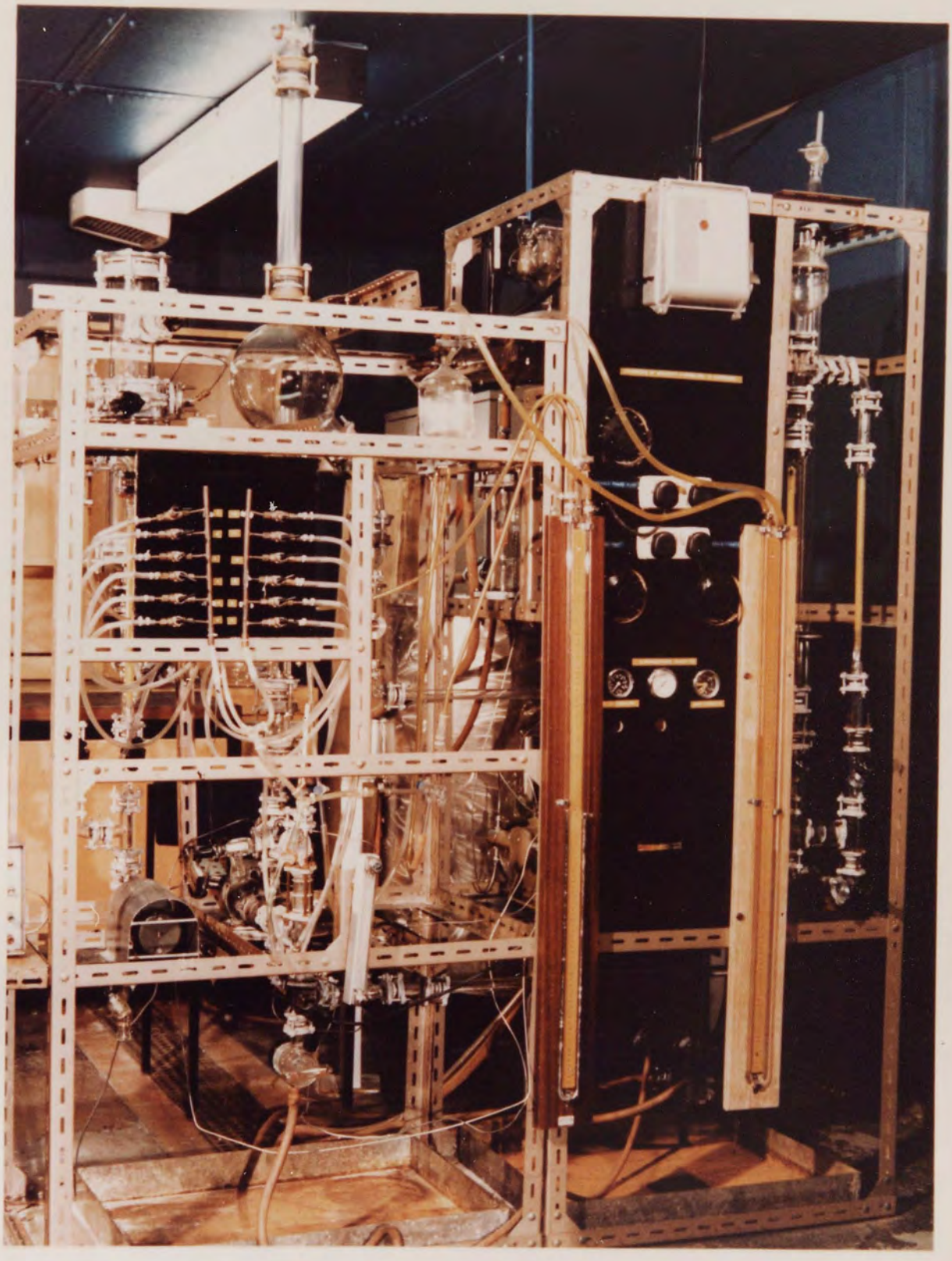

Figure 6.2

GENERAL ARRANGEMENT OF EQUIPMENT
Dispersion generating loop and Coalescer
are mounted in the middle.

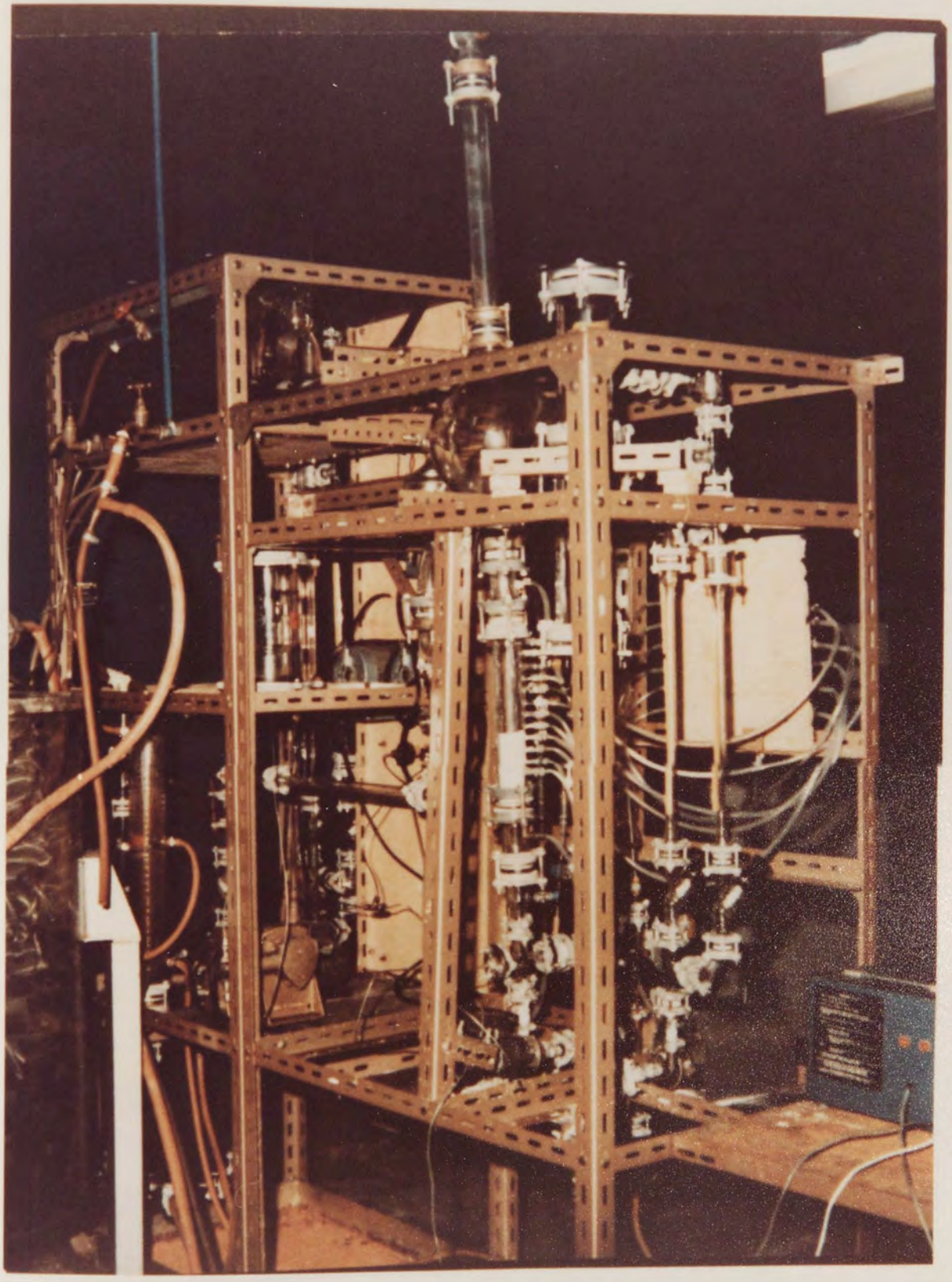

Figure 6.3

REAR VIEW OF EQUIPMENT
Distilled water tank on the left side
Rotameters and Manometers on the right side.

The selected flow rate was maintained using a control valve on the delivery line and a control valve on the loop line between the delivery and suction sides of the pump. Flowrates were monitored using two glass rotameters with stainless steel floats which provided a range of superficial velocity from 0 to 7 x 10^{-2} m/s based on the cross sectional area of the coalescer. From a storage vessel, the dispersed phase was gravity fed to a centrifugal pump through 3mm bore stainless steel tubing. Using a pressure relief valve, the delivery pressure was maintained at 3 bar which ensured efficient operation of the non return valves in the pump head during the suction stroke and prevented excess flow due to the head of the liquid in the storage vessel during delivery. A flow meter with a stainless steel float was installed after the pressure relief valve to ensure that the pump delivered the desired flowrate. A centrifugal pump was used to generate secondary dispersion; the pump speed determined the mean drop size, and this speed was monitored using an electronic tachometer. The liquid temperature was measured up stream of the coalescer using a thermometer inserted in the recycle loop. After passing through the coalescer, the primary dispersion produced was recovered in a 685mm diameter settler placed above the bed.

6.3. Coalescer design

As shown in Figure 6.4. the coalescer vessel was constructed from Q.V.F. glass pipe, 5cm inside diameter, and 30cm high. It was provided with pressure tappings one

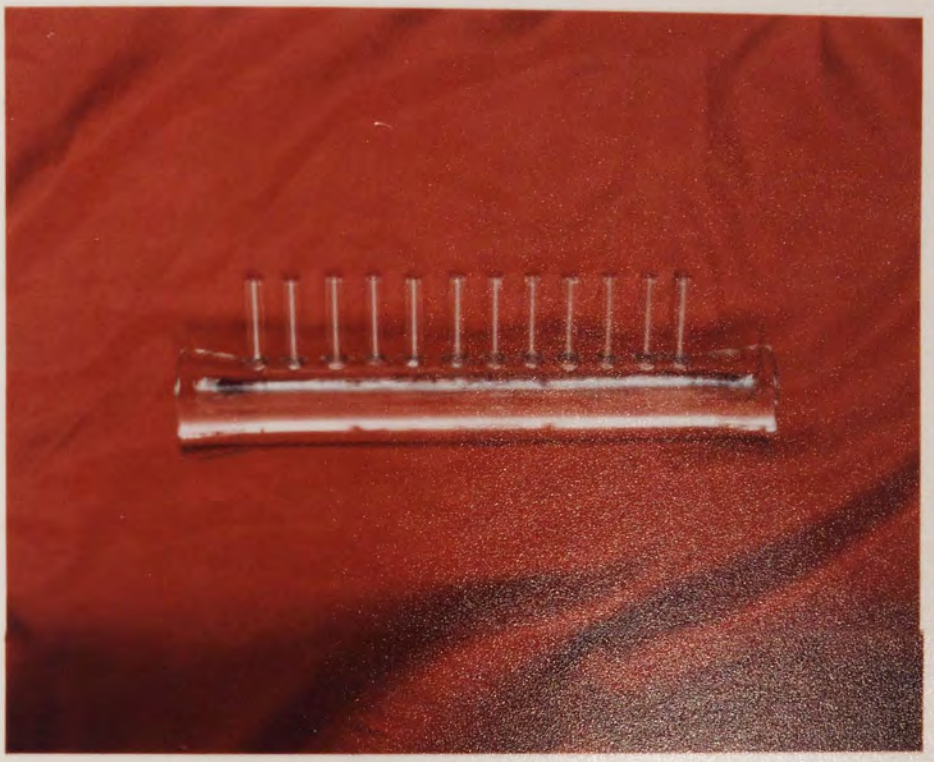

Figure 6.4

COALESCER
30 c.m. length with 12 side arms

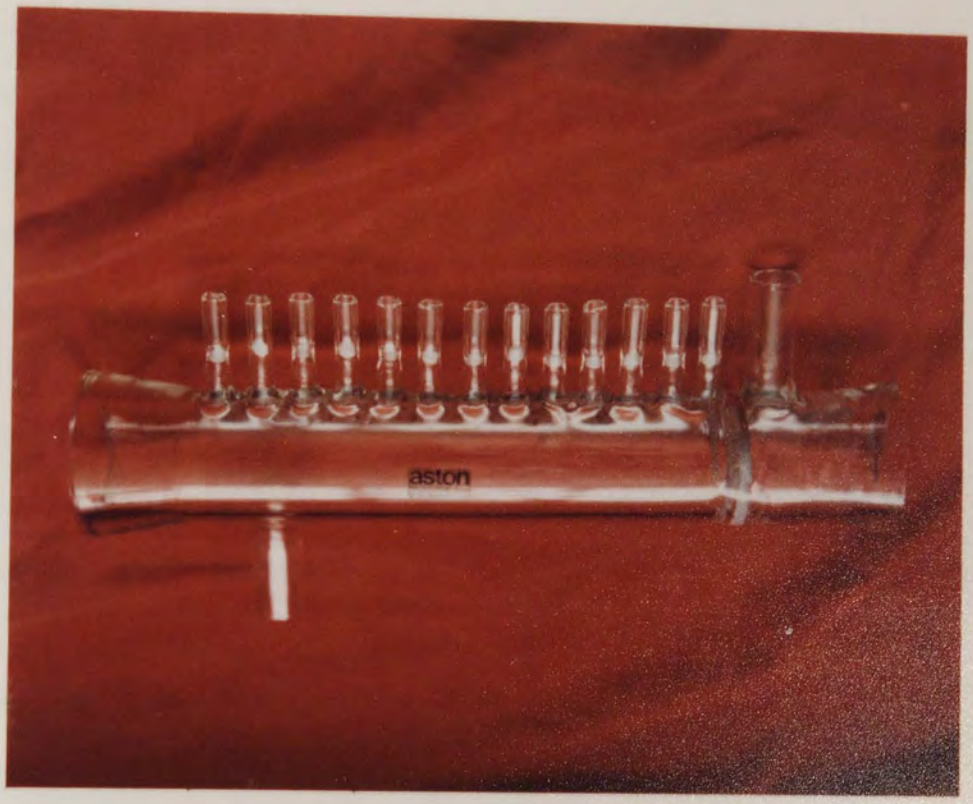

Figure 6.5

COALESCER
With glass mesh holder

above the other, one centimeter apart. These tubes were connected to two manometers containing, carbon tetrachloride or mercury, to measure the pressure drop across each section of the coalescer. A glass mesh was fitted at the end of the coalescer to restrain the packing; the material of the mesh was chosen especially to avoid any differences in the surface energy between the packing and the holder. This glass mesh was found in practice to have an effect on coalescence performance and pressure drop due to its thickness. The glass ballotini packing was then confined to the column by using Becosyn, stainless steel meshes Figure 6.6. supplied by Begg Cousland Ltd, with P.T.F.E. rings to be used as the gaskets when assembling the column to the rest of the equipment. The mesh size used was the largest which would retain the granular material for each particular experiment. This minimised any coalescence effects at the inlet of the dispersion and also made the least pressure drop across the support.

6.4. Packing selection and preparation

Many recent investigations into the coalescence of secondary dispersions in packed beds have employed randomly arranged matrices usually consisting of glass fibres (48, 49, 17, 33). Glass as a raw material is favoured because it is relatively inexpensive, is resistant to the extreme thermal and chemical environment commonly used in cleaning procedures and its wetting properties may be modified by the attachment of silicone groups to the surface of the fibres (50).

Figure 6.6

STEEL MESH HOLDER

Simple compression of a quantity of fibrous material to the required voidage fraction produces an acceptable structure, but frequently the glass fibres used have a distribution of diameters and the above packing technique produces a bed with a pore size distribution and where the fibre orientations are unknown. The lack of an accurate geometrical description of the bed has favoured investigations where the coalescer packing consists of layers of fine woven meshes. Where the fibre orientation is known the different packing characteristics can be expressed mathematically in terms of these known factors.

Fibrous media, which can be made to have both higher porosities and higher specific surface than granular media, are observed to give more complete phase separation than granular solids for the same bed depth and operating conditions. This makes fibrous media appear more attractive from the standpoint of space requirements. However, even small amounts of suspended solids, which are sometimes unavoidably present, can rapidly accumulate to block fibrous media to such a degree that their use over extended periods is prevented. Also, their permanent structure hinders periodic cleaning so frequent replacement would very likely be necessary, although Shah (51) has made progress in regenerating fibrous media. Unconsolidated, coarse granular media have a much longer operating period and in the less frequent event of excessive solids build-up, they can be periodically cleaned by fluidisation.

In many unit operations, packings of various geometries have been related to that of a sphere by a shape factor, where a sphere has a shape factor equal to 1.0. In this respect it is envisaged that the use of spheres as a packing may facilitate the use of a shape factor to equate the effect of surface area to volume ratios on the coalescence efficiency of different packings.

The theory and practice of packing arrangements of spheres has been widely reported in the literature (52, 53, 54, 32). Co-ordination numbers and voidage relationships have been evaluated from both regular and random packing of spheres. Pore sizes and channel diameter variations have been evaluated from a theoretical (52) and experimental (55) standpoint. Therefore, from these properties, it is possible to quantify the packing geometry and its effects on coalescence. Most of the previous work has not included an analysis of packing geometry and has restricted the geometrical description to that of a voidage value. Whereas voidage values are important with respect to limiting flow conditions, they do not provide any information with regard to coalescence mechanisms within the bed. Furthermore, examination of local voidage variations of either Rashig Rings or knitted mesh packing in small diameter columns show that very large wall effects exist. This is also true for spheres and indicates the importance not only of packing selection, but also of using a column of adequate diameter. Ridgeway and Jarburk (54) who investigated local voidage variation of spheres in cylindrical columns, concluded that the wall effects were virtually eliminated

within two particle diameters from the wall. In this study the ratio of column diameter to grain diameter was always greater than 35:1, thus eliminating wall effects.

The non-porous glass ballotini was obtained from Englas, English Glass Company Limited. Their properties are listed on Table 6.1. Glass ballotini diameters measured by volume displacement and by microscopy were within 5 to 10 per cent of the arithmetic mean of the manufacturer's reported sieve range.

6.4.1. Surface properties of glass ballotini

Coalescence mechanisms and droplet hydrodynamics within packed columns are, to a large extent, dependent on the surface energy of the packing. Considerable information is available on the surface properties of glass and its relationship to the contact angle, and wetting effects with many liquid-liquid systems.

This study was restricted to the coalescence process in a non-wetted packing. Glass, having a high surface energy value, was thus well suited when organic liquids were used as the dispersed phase.

To obtain a reproducible packing surface, the packing was subjected to the preferential wetting technique described by Thomas (56). The ballotini were first cleaned in chromic acid, then thoroughly washed with distilled water. After washing, the packing was placed in an oven at 150°C for 8 hours. The dried beads were stored in sealed polyethylene containers for subsequent use. The

TABLE 6.1 PROPERTIES OF GRANULAR COALESCER MEDIA

Composition: Lead Glass

Physical Properties:

Specific gravity (approx.)	2.95
Refractive index	1.6
Thermal conducitivity (at 20°C Kcal.m/m^{2}h deg C)	0.0018
Specific heat (between 20 and 100°C Cal/g. deg C)	0.156
Hardness (Moh's scale)	5.7
Linear coefficient of expansion (between 0° to 300°C x 10^{-6}/°C)	9×10^{-6}
Maximum working temperature °C	350
Softening point °C	470

Diam.Range mm.	Test Sieves B.S. 410 : 1969 Pass	Retain	Approximate Weight per m^3 in kg.
0.045 - 0.070	63	53	1740
0.060 - 0.095	50	63	1720
0.210 - 0.325	300	250	1780
0.440 - 0.530	500	425	1840

Approximately 80% in "Diameter Range" specified. Less than 5% irregular shapes.

effect of surface renewal by acid etching and the thorough drying proved to be a suitable method of producing a highly active surface.

Thomas (57) stated that this surface, if then immersed in either organic or aqueous phase, would be preferentially wet by the liquid which first came into contact with the surface; this effect was possible irrespective of the solid surface energy. Therefore, glass, which has a high surface energy and is preferentially wetted by water, could be made to be wet by the organic phase. However in this study, surfaces wet by the continuous aqueous phase were produced by immersion in distilled water. A technique for rendering the glass surface hydrophobic has been described by Wilkinson (27).

6.5. Liquid system description

The equipment was designed for coalescence of an organic liquid dispersed in distilled water. Toluene was selected as a relatively non-toxic, non-corrosive and inexpensive solvent. G.P.R. grade toluene was distilled to within 17°K of its boiling point and stored in clean, dark glass bottles to prevent exposure to sunlight which has been reported to cause degradation(60).

Any effects due to the mutual solubility of toluene and water were minimised by allowing the two phases to attain mutual saturation by contact for over 24 hours before use. Mass transfer effects could not be completely eliminated due to the temperature coefficients of solubility.

Since accurate temperature control was impractical due to heat generation by pumping and emulsification, the physical properties of the system were determined as a function of temperature and are presented in Appendix (A). The high sensitivity of both continuous and dispersed phase viscosities, and hence pressure drop to temperature changes emphasises the need for monitoring during single and two phase flow experiments. The continuous phase rotameters were calibrated experimentally at 20°C and the effect of temperature fluctuation was evaluated theoretically from the Calibration Handbook (62). An 8°C change in temperature was found to cause a 5% maximum error in flowrate. Instruments of this type possess inherent errors, due to random flow disturbances, and accuracies of better than 3 or 4% would not be realised in practice. Temperature correction of the calibration curves was therefore unwarranted.

6.6. Pressure drop measurement

Initially, pressure drop was measured across the coalescer. This was done by using two differential 'U-tube' manometers. A mercury manometer was used to measure pressure drops greater than 100mm Hg and one containing carbon tetrachloride used for the lower range of values. The manometers were connected in parallel to pressure tappings upstream and downstream of the coalescer by tubes containing distilled water. Location of the interface between the carbon tetrachloride and water was improved by colouring the organic phase using a dye, 'Oil Soluble Yellow' (71). Since the ambient temperature varied,

the density of the carbon tetrachloride was determined gravimetrically and was found to be 1604 kg/m^3; it varied less than 0.4% over the temperature range 10-30°C.

During the experiments for single phase flow through the coalescer, it was discovered that a different value of pressure drop was obtained for the same superficial velocity depending on whether the flowrate was progressively increased or decreased. Modification of the manometer system as described in Figure 6.7. eliminated this hysteresis effect which was only detectable using the carbon tetrachloride manometer. This phenomenon, which has been observed previously in low pressure drop measurement (63) may be attributed to an advancing and receding interfacial contact angle as the pressure drop rises and falls. The liquid levels in the water reservoirs were equalised before the measurements were taken from either manometer.

When the coalescer column was modified to measure pressure difference over its entire length, the manometer system already described was kept with the addition of pressure tappings which were isolated from one another by means of valves. Each pressure tapping on the coalescer column as well as the one upstream of the coalescer, measured differential pressure with respect to the pressure taping downstream of the coalescer. The new system is illustrated in Figure 6.8.

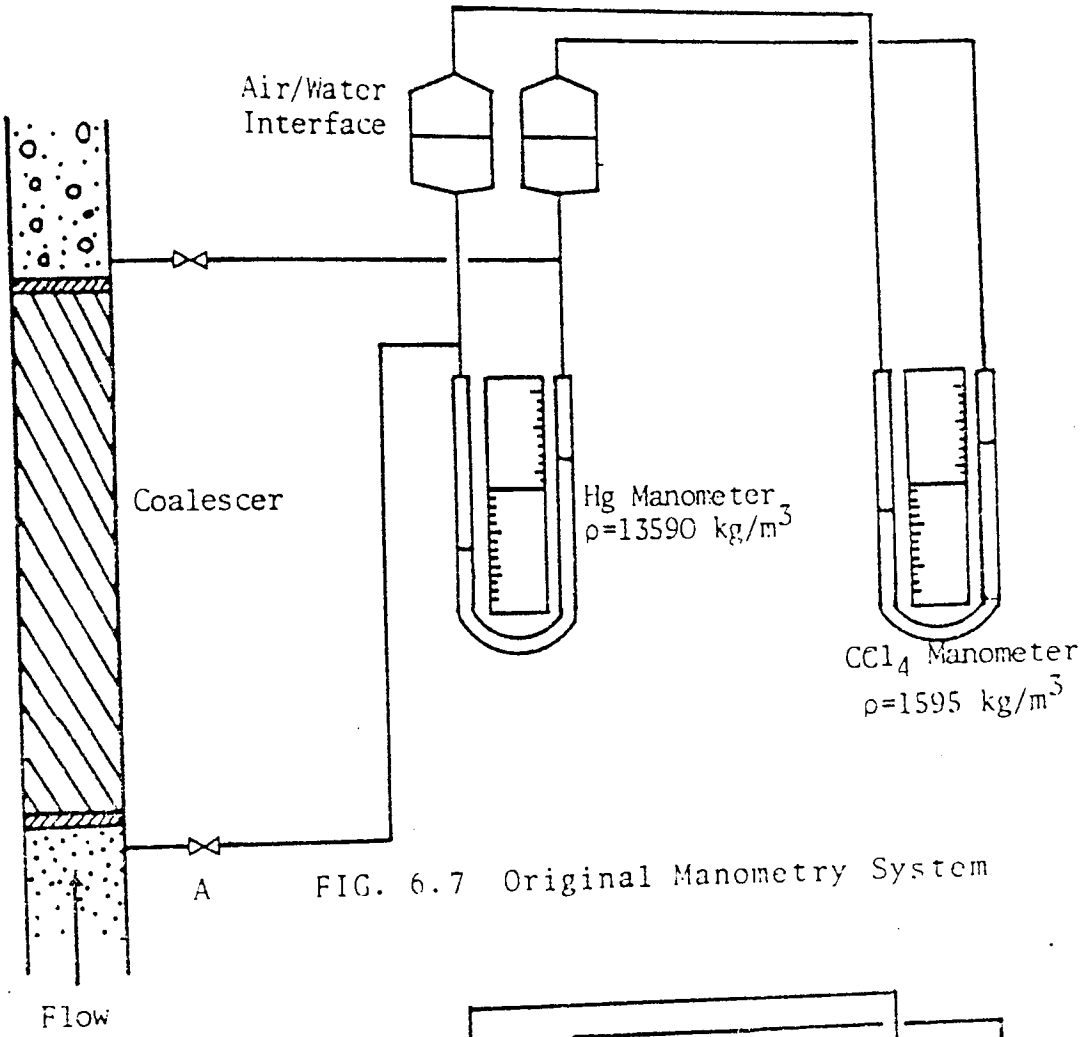

FIG. 6.7 Original Manometry System

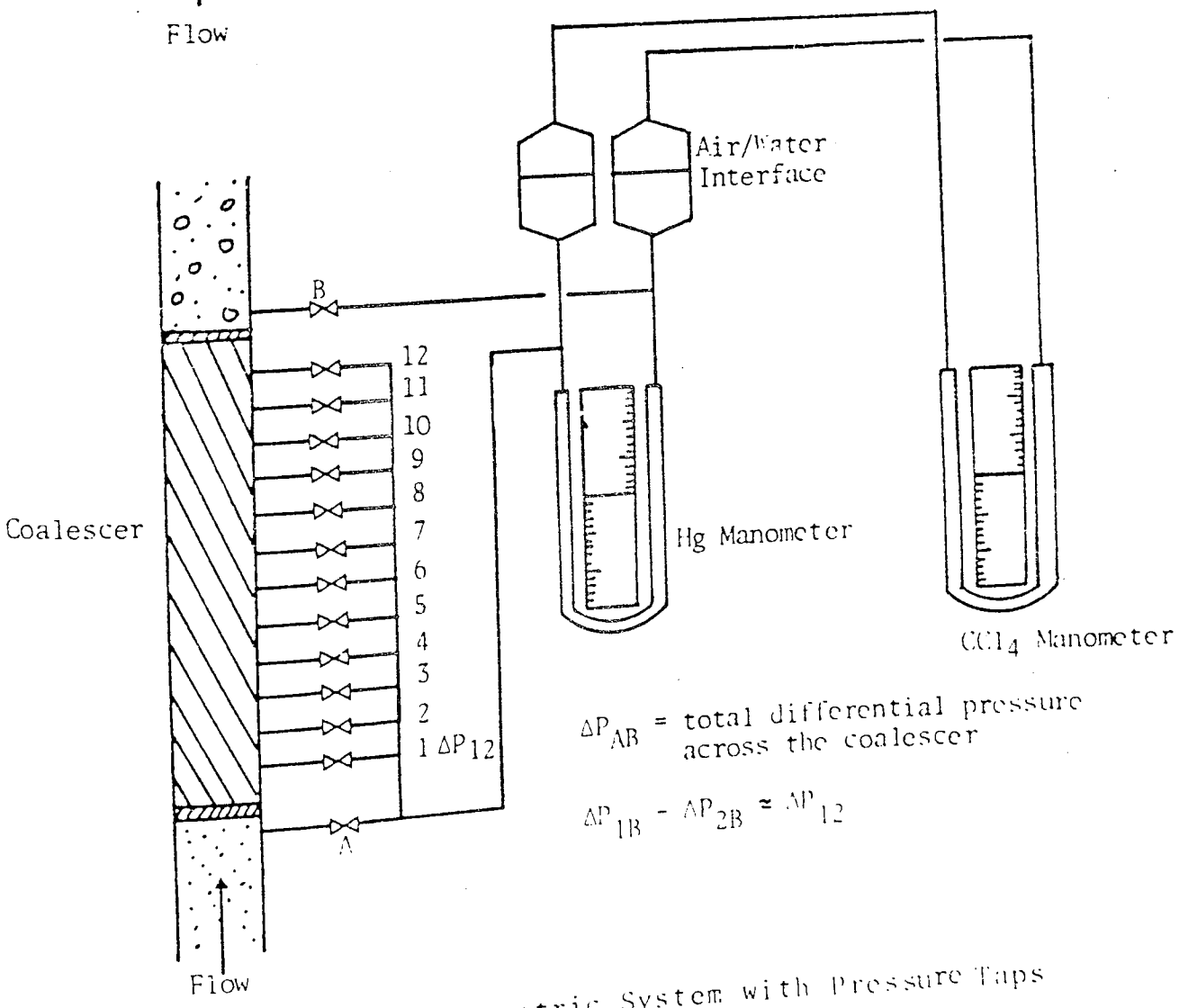

FIG. 6.8 Modified Manometric System with Pressure Taps

6.7. Operating procedure

Following assembly, the equipment was filled with a 2% v/v solution of Decon 90 and allowed to stand for 24 hours with periodic recirculation of the cleaning solution. After soaking, the whole apparatus was rinsed thoroughly with tap water, followed by distilled water. Further contact with surface active agents was avoided to prevent contamination of the liquid system since minute quantities of surfactants which may be absorbed onto glass surfaces are extremely detrimental to the coalescence process.

To pack the coalescer the column was half filled with the continuous phase, then a pre-weighed quantity of uniform glass beads were added through the top of the column by gently taping the column wall to eliminate the possible accumulation of air bubbles and to ensure uniform porosity along the whole column.

After assembly, the equipment was operated in the recycle mode when only flow of the continuous phase was permitted. The temperature and pressure drop were recorded for a range of superficial velocities from $0\text{-}5 \times 10^{-2}$ m/s. This procedure provided sufficient data for single phase flow analysis and ensured correct assembly of the coalescer through pressure drop checks.

The isolation valves were then adjusted to alter the operating mode from recycle to a 'once through' condition and the flow regulated to the desired value. The emulsification pump was started, followed by the dispersed

phase metering pump and after the appearance of a milky haze in the pump recycle loop, characteristic of secondary dispersion, the temperature and pressure drop were recorded at regular intervals on each pressure tap. The performance of the bed was monitored throughout the transient period, typically of several hours duration, until steady state conditions were attained. At this stage, samples of the inlet dispersion and the effluent from the coalescer were taken for determination of mean drop size.

6.8. Bed voidage determination

The initial bed voidage was determined using a displacement method. Distilled water was pumped through the bed at high flowrates, for fifteen minutes to displace all air bubbles. Some of the water was then drained down the bed to a predetermined level fifteen centimetres above the packing. A measured volume (twenty millilitres) of water was removed from the column and the distance the water level dropped was measured. This procedure was repeated until the water level was about one centimeter above the packing. These initial measurements were used to obtain an average value for the water level drop per twenty millilitres since the column diameter could not be assumed uniform with the addition of the pressure taps. Following this, twenty millilitres were collected and the water level receded to beneath the packing. This reduction in the water level was measured, from this value together with the bed depth, packing bulk volume and the initial average value recorded, the bed voidage was calculated as shown in Appendix (B).

6.9. Operating conditions

In this study, preliminary experiments were carried out to determine the optimum operating variables at which a high separation efficiency could be achieved. The aim was to obtain large exit drop diameters and thus, high separation efficiency, with low pressure drop and high superficial velocity. There is a wide range of ballotini sizes available and the selection of sizes was made based on the fibre diameters used in previous coalescence studies (9,15). (Decreasing the ballotini size,increases the pressure drop, decreases the exit drop size and lowers the value of superficial velocity at which drop redispersion occurs. Increasing the ballotini size increases the exit drop size, decreases the pressure drop and permits higher throughout.) A set of experiments was devised whereby the changes in ballotini size, bed depth, superficial velocity and dispersed phase concentration were measured as changes in the pressure drop, exit drop size, effluent drop size and separation efficiency.

CHAPTER SEVEN

DETERMINATION OF DROP SIZE DISTRIBUTION

CHAPTER SEVEN

DETERMINATION OF DROP SIZE DISTRIBUTION

7.1. Introduction

As discussed in Chapter 4 the mean drop size and the distribution of the dispersed phase has a critical effect upon the mechanisms of coalescence. In addition the capture efficiency of drops also depends on drop diameter. The methods used for measurement of the drop size of secondary droplets are

1. Lazer analysis
2. Optical microscopy
3. The Coulter Counter

Whereas the method generally used to measure primary droplets size is still photography.

The methods used in this study will now be reviewed.

7.2. Measurement techniques for droplets in secondary dispersions

7.2.1. Lasers : Malvern 2200 particle sizer

This instrument is applicable to particle size distributions in the range of 1 to 100 microns. It depends on the principle of Fraunhofer. Diffraction from the particles as the means of measurement, as illustrated in Figure 7.1. A low power visible laser transmitter produces a parallel monochromatic beam of light which is arranged to illuminate the particles residing in an appropriate

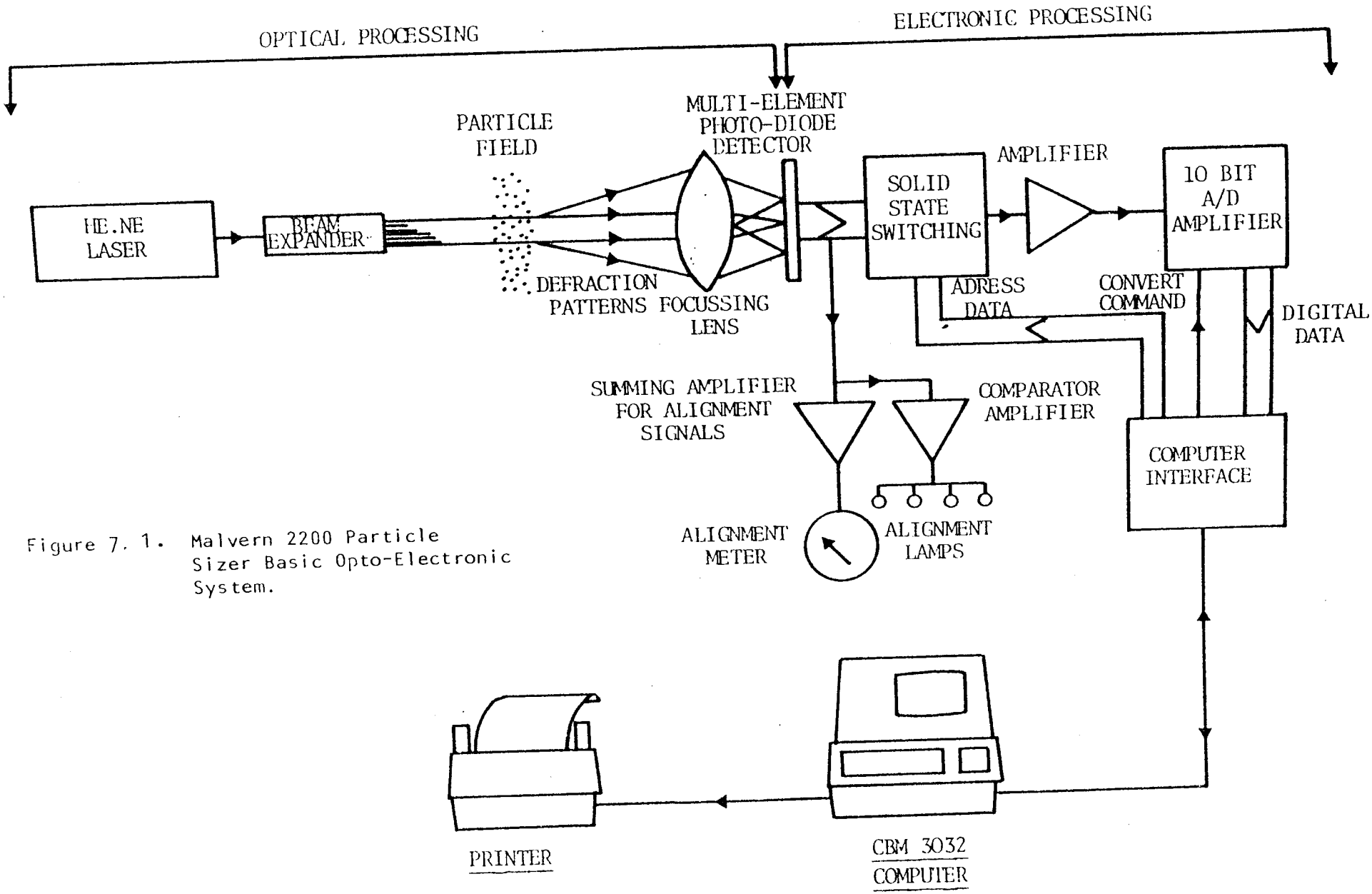

Figure 7. 1. Malvern 2200 Particle Sizer Basic Opto-Electronic System.

sample cell. The incident light is diffracted by the illuminated particles to give a stationary diffraction pattern regardless of particle movement. As particles enter and leave the illuminated area the fraction pattern "evolves", always reflecting the instantaneous size distribution in this area. Thus by integration over a suitable period and a continuous flux of particles through the illuminated area a representative bulk sample of the particles may contribute to the final measured diffraction pattern.

A Fourier transform lens focusses the diffraction pattern onto a multi-element photo-electric detector which produces an analogue signal proportional to the light intensity received. The detector is interfaced directly to a computer allowing it to read the diffraction pattern and perform the necessary integration digitally. Having measured a diffraction pattern the computer uses the method of non-linear least squares analysis to find the size distribution that gives the closest fitting diffraction pattern. The size distribution can be analytically generated from the well known two parameter models Rosin Rammler, Log Normal and Normal.

The results of the analysis, a size distribution of the sample by weight, may be displayed graphically on the VDU screen of the computer or printed as a hand copy result on a line printer. The size distribution can be presented as the weight in size bands, the cumulative weight below a size, and the cumulative weight above a size.

RUN NO.	TIME	OBSCURATION
22	00-55-00	0.30

INDEX	SIGNAL	BACKGROUND	DATA
1	91.75	10.04	45.00
2	92.39	10.42	49.41
3	101.17	10.74	57.03
4	102.38	9.87	62.63
5	107.15	8.61	68.28
6	113.00	8.36	68.44
7	122.74	8.24	78.41
8	110.69	7.02	75.34
9	107.88	6.25	75.31
10	117.38	6.56	85.73
11	113.58	5.96	85.32
12	111.73	5.59	85.63
13	108.38	5.55	84.94
14	103.93	5.47	82.22
15	101.34	5.54	81.41
16	99.81	5.54	80.97
17	99.58	5.07	81.47
18	103.04	5.47	84.38
19	107.39	5.27	89.13
20	113.95	5.22	96.00
21	121.00	5.48	103.03
22	124.00	5.93	106.25
23	109.73	6.18	94.00
24	73.10	6.23	61.31
25	34.96	8.51	26.28
26	13.64	7.10	6.13
27	9.15	8.32	0.75
28	9.22	9.27	- 0.06
29	10.68	11.00	- 0.31
30	12.00	13.22	- 1.22

Figure 7.2. Malvern 2200 Particle Sizer Background Reading Printout.

MALVERN 2200/3300 PARTICLE SIZER V3.1

MALVERN INSTRUMENTS LTD,SPRING LANE,MALVERN,ENGLAND.

PRINTING PARAMETERS

RUN NO.	TIME	MODEL	X BAR	N	LOG ERROR
3	00-14-40	ROS-RAM	50.19	2.60	5.55

PRINTING RESULTS FROM DATA BLOCK 1

SAMPLE CONCENTRATION = 0.0211% BY VOLUME OBSCURATION = 0.21

SIZE BAND UPPER	SIZE BAND LOWER	CUMULATIVE WT BELOW	WEIGHT IN BAND	CUMULATIVE % WT ABOVE
320	310	100.0	0.0	0.0
310	300	100.0	0.0	0.0
300	290	100.0	0.0	0.0
290	280	100.0	0.0	0.0
280	270	100.0	0.0	0.0
270	260	100.0	0.0	0.0
260	250	100.0	0.0	0.0
250	240	100.0	0.0	0.0
240	230	100.0	0.0	0.0
230	220	100.0	0.0	0.0
220	210	100.0	0.0	0.0
210	200	100.0	0.0	0.0
200	190	100.0	0.0	0.0
190	180	100.0	0.0	0.0
180	170	100.0	0.0	0.0
170	160	100.0	0.0	0.0
160	150	100.0	0.0	0.0
150	140	100.0	0.0	0.0
140	130	100.0	0.0	0.0
130	120	100.0	0.1	0.0
120	110	99.9	0.4	0.1
110	100	99.4	1.4	0.6
100	90	98.0	3.6	2.0
90	80	94.4	7.4	5.6
80	70	87.0	12.5	13.0
70	60	74.5	17.2	25.5
60	50	57.3	19.4	42.7
50	40	37.9	17.7	62.1
40	30	20.2	12.6	79.8
30	20	7.6	6.3	92.4
20	10	1.3	1.3	98.7
10	0	0.0		

Figure 7.3 Malvern 2200 Particle Sizer Sample Analysis Printout using Two Parameter Model.

MALVERN 2200/3300 PARTICLE SIZER V3.1

MALVERN INSTRUMENTS LTD,SPRING LANE,MALVERN,ENGLAND.

PRINTING RESULTS FROM DATA BLOCK 1

TIME 00-11-30 RUN NO. 4 LOG ERROR = 5.62

SAMPLE CONCENTRATION = 0.0319 % BY VOLUME
OBSCURATION = 0.40

SIZE BAND UPPER	SIZE BAND LOWER	CUMULATIVE WT BELOW	WEIGHT IN BAND	CUMULATIVE WT ABOVE	LIGHT ENERGY COMPUTED	LIGHT ENERGY MEASURED
118.4	54.9	63.8	36.2	0.0	2047	2047
54.9	33.7	33.7	30.2	36.2	1790	1930
33.7	23.7	20.3	13.4	66.4	1565	1543
23.7	17.7	14.7	5.5	79.7	1357	1373
17.7	13.6	9.3	5.5	85.3	1257	1245
13.6	10.5	6.3	3.0	90.7	1243	1237
10.5	8.2	6.3	0.0	93.7	1259	1169
8.2	6.4	6.3	0.0	93.7	1285	1148
6.4	5.0	3.7	2.6	93.7	1375	1205
5.0	3.9	0.0	3.7	96.3	1617	1426
3.9	3.0	0.0	0.0	100.0	1705	1766
3.0	2.4	0.0	0.0	100.0	1447	1429
2.4	1.9	0.0	0.0	100.0	1028	323
1.9	1.5	0.0	0.0	100.0	946	16
1.5	1.2	0.0	0.0	100.0	1276	0

Figure 7.4 Malvern 2200 ParticleSizer Sample Analysis Printout.

After loading the computer with the analytical model, processing and then checking the optical alignment of the equipment, a background reading of the continuous phase in the sample cell is made. These readings must not exceed 30. An example of background reading is shown in Figure 7.2.

When a size distribution of the dispersion is made, the log error for the two parameter programmes should be less than 5 to establish that the model is adequately fitting the sample data.

A printed output of sample analyses using both the two parameter and the independent models are shown in Figure 7.3. and 7.4. respectively. Further details on the technique and the mode of operation are to be found in the 2200 Particle Sizer Handbook (64).

7.2.2. Optical microscopy

The use of the optical microscope is most effective in the range 0.25 to 20μm; the lower limit is imposed by the resolving power of the microscope; the upper limit is determined by the diameter of the drop in relation to the depth of field of the optical system. The following procedure is applied for the estimation of drop size. A sample of the dispersion is diluted and then placed in the well of a glass slide and under the microscope with a graticule. More than 300 drops per sample are counted in order to obtain statistically valid results for a poly-dispersion (65).

7.2.3. The Coulter Counter

The Coulter Counter is an apparatus for measuring the size distribution of solid particles or immiscible droplets in a dispersion, in a liquid continuous phase of low resistivity, by measurement of the resistance change between two electrodes. A sample of the dispersion is taken, stabilized with surfactant and diluted in an electrolyte. The sample is then withdrawn through an aperture whose diameter is accurately known and which is positioned between two electrodes. Since the conductivity of the dispersed phase droplets is considerably less than that of the continuous phase, the resistance between the electrodes changes instantaneously as a drop passes through the aperture. Voltage pulses, whose magnitude depends on the diameter, are produced and screened electronically by a series of threshold circuits. By selection of different threshold levels and recording the number of pulses, data is obtained for plotting the cumulative frequency against drop size. A typical result is shown in Figure 7.5. from which the mean diameter is obtained corresponding to 50% cumulative weight per cent oversize.

The instrument must be calibrated for each orifice tube and electrolyte combination prior to use. Calibration is ideally performed using 'monosized' particles provided by Coulter Electronics Ltd. The most effective calibration results when the particle size is between 5% - 20% of the aperture diameter of the orifice tube selected. This method is more complicated and takes more time than the laser technique (66).

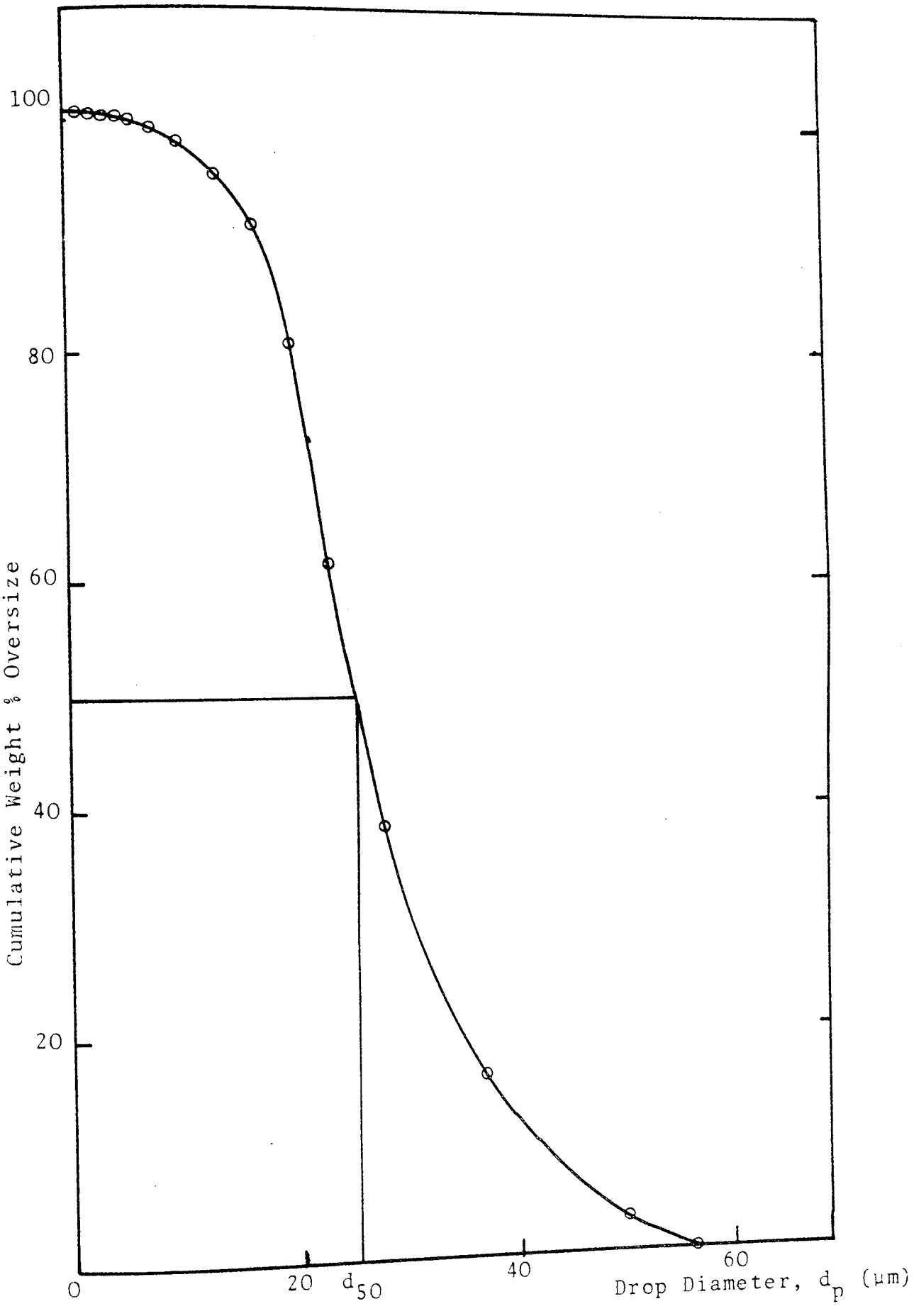

FIG. 7.5. Typical Size Distribution of Inlet Dispersion

7.3. Measurement techniques for primary droplets

7.3.1. Photography

The effluent primary dispersion leaving the coalescer has been successfullly analysed previously by photographic means. Photographs of the dispersion leaving the coalescer were obtained using an Asahi Pentax camera fitted with an Asahi micro-lens on Kodak Trix-Pan 33mm, 400 ASA film. Shutter speeds of less than 4×10^{-3} were employed to eliminate image distortions caused by drop movement. Illumination of the dispersion from the rear was provided by 2500w photo-flood bulb through a diffuser.

The circular pipe section, which retained the flowing dispersion did not cause detectable distortion or magnification of the drops thus eliminating the need for any special optical arrangement. Enlargements of the prints to approximately 5 x magnification was found to be satisfactory with respect to size and contrast for the counting procedure; typical photographs are reproduced as Figures 8.7. to 8.14. A metric scale was placed on the outer tube wall for calibration purposes.

Manual counting of the drops recorded on the photographs was accomplished using a Zeiss T63 particle counter to identify and record the two characteristic dimensions.

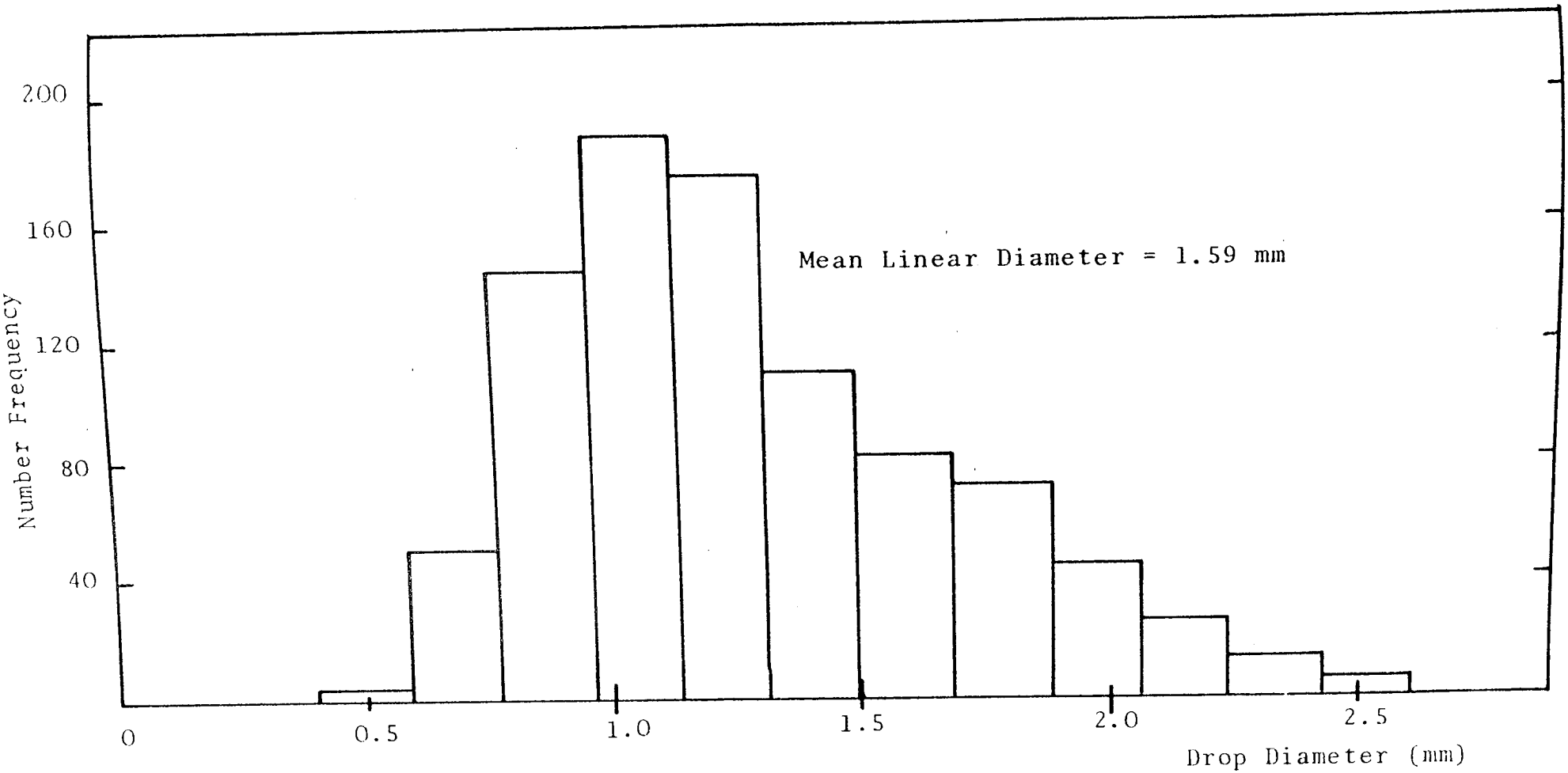

FIG. 7.6 Typical Size Distribution of Coalesced Drops Leaving Exit Face

CHAPTER EIGHT

EXPERIMENTAL RESULTS

CHAPTER EIGHT

EXPERIMENTAL RESULTS

8.1. Inlet drop size

The mean drop size of a secondary dispersion produced by a centrifugal pump in a by-pass loop depends on the pump speed (67,48, 68, 69). A recent study (70) showed that the level of turbulence in the vicinity of the pump impeller far exceeds that inside the loop so that drop break-up by viscous shear is the most likely mechanism. When the pumping velocity increases, the residence time of the dispersion in the loop is reduced, so it is important to analyse the dispersion for each velocity. Figure 8.1., indicates that the mean drop size decreases significantly at low flowrates for a constant phase ratio, but it is independent of superficial velocity above 1.5×10^{-2} m/s. Figure 8.2. shows that below 0.44%v/v phase ratio, for constant velocity, the mean inlet drop size increases with increasing phase ratio for low velocities. Above 0.44%v/v ratio, the mean inlet drop size is independent of phase ratio.

8.2. Coalesced drop size

8.2.1. The effect of velocity on exit drop size

The mean size of exit drops, was found to decrease with an increase in superficial velocity as shown in Figure 8.3. This is in agreement with other workers (67, 71).

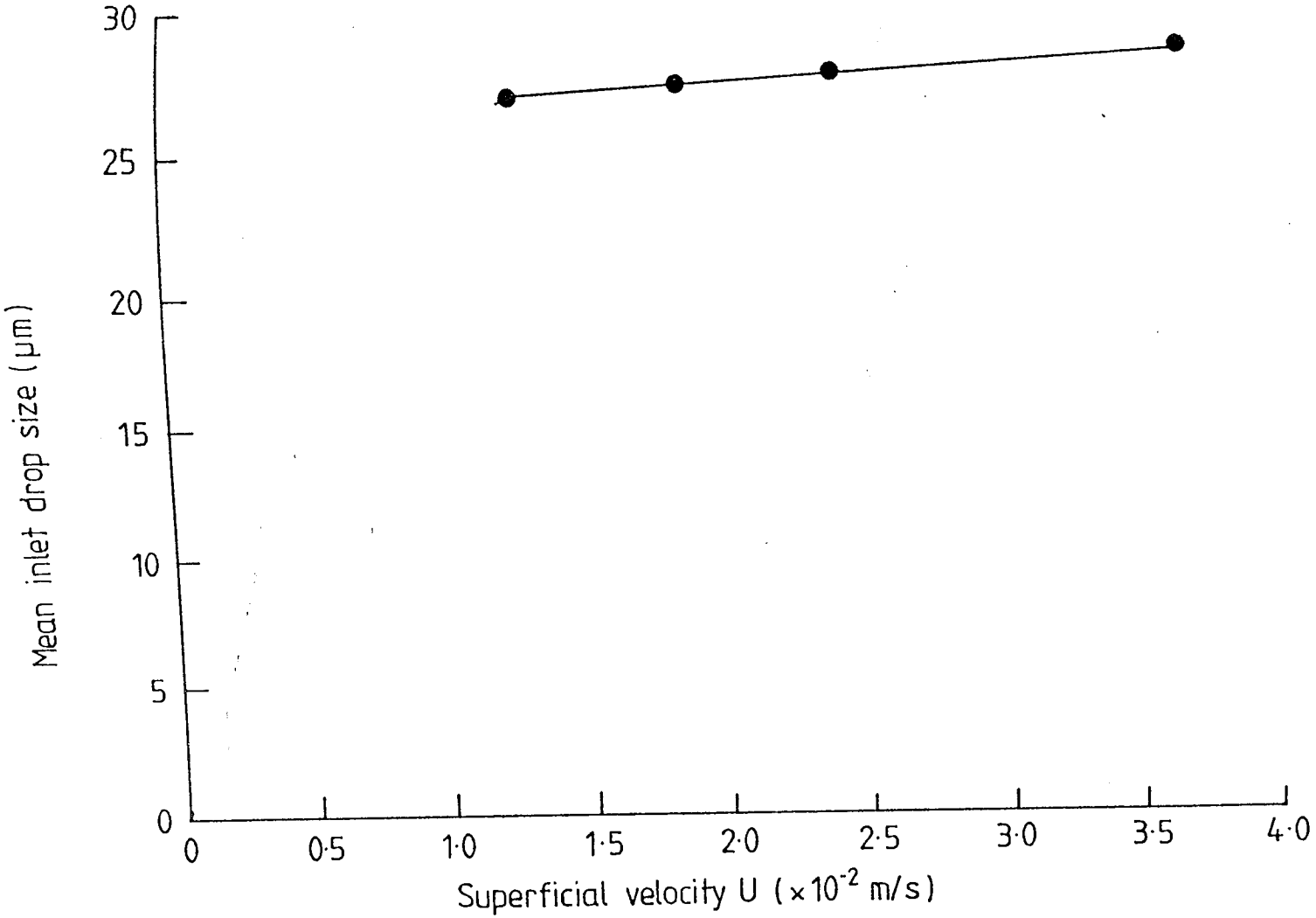

Figure 8·1 Variation of Inlet drop size with velocity for 1% V/V dispersed phase concentration

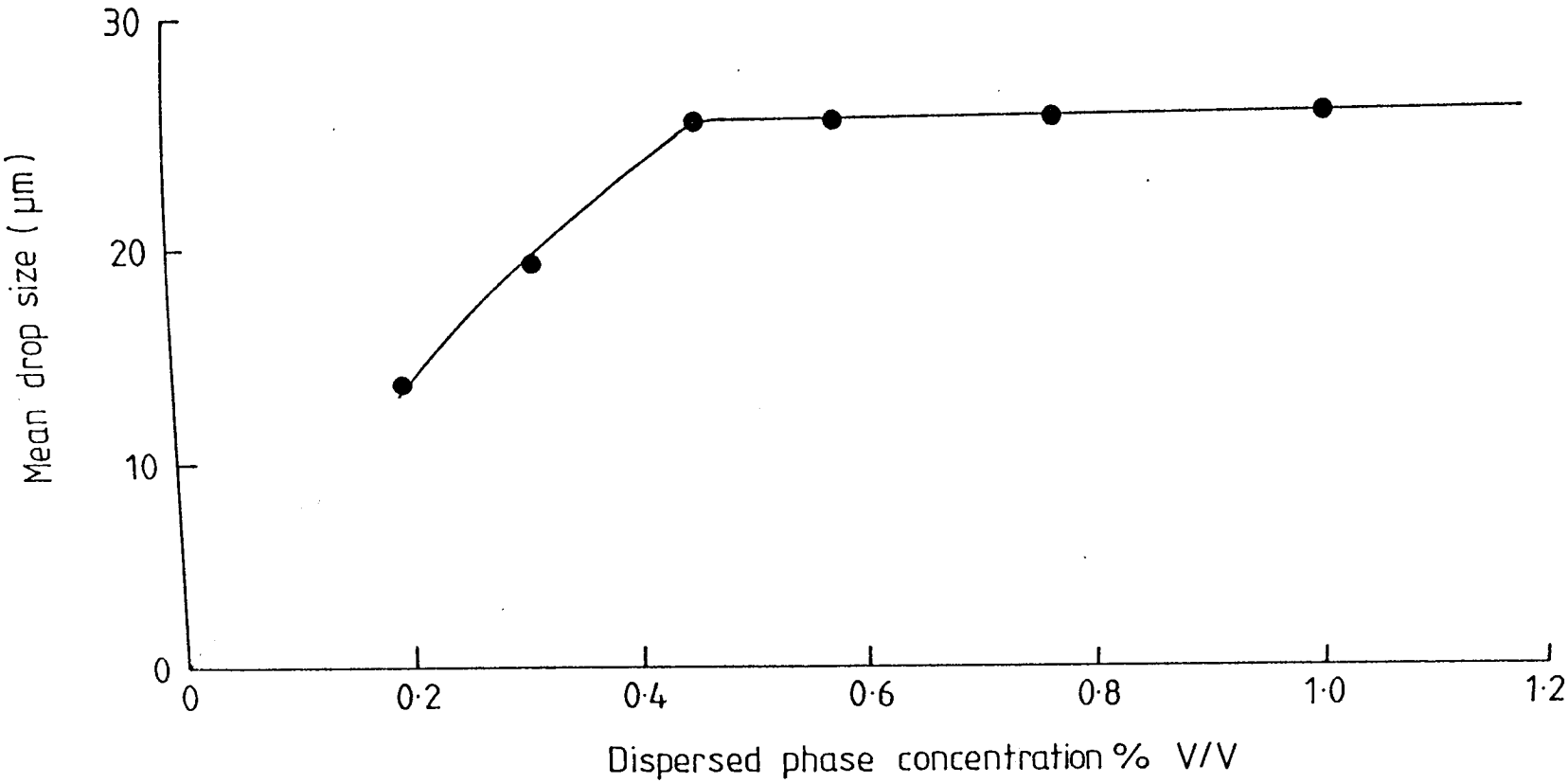

Figure 8·2 Variation of mean drop size with concentration of dispersed phase at $1{\cdot}6 \times 10^{-2}$ m/s.

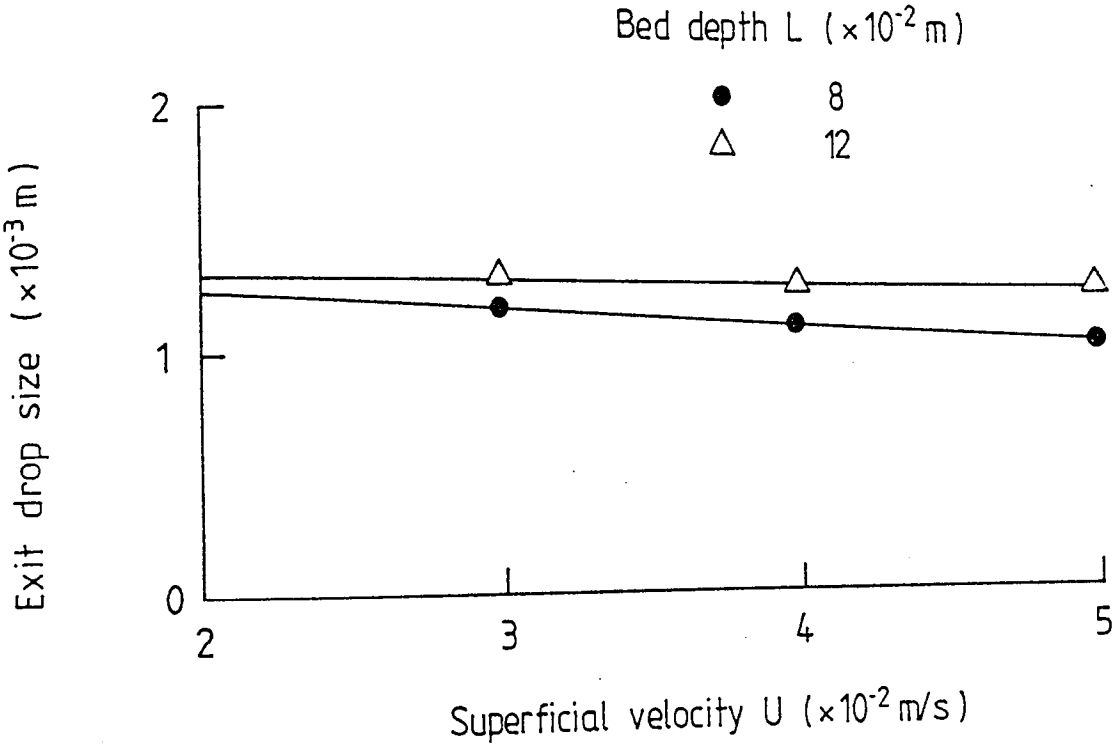

Figure 8·3 Variation of Exit drop size with velocity for Ballotini size 267 μm.

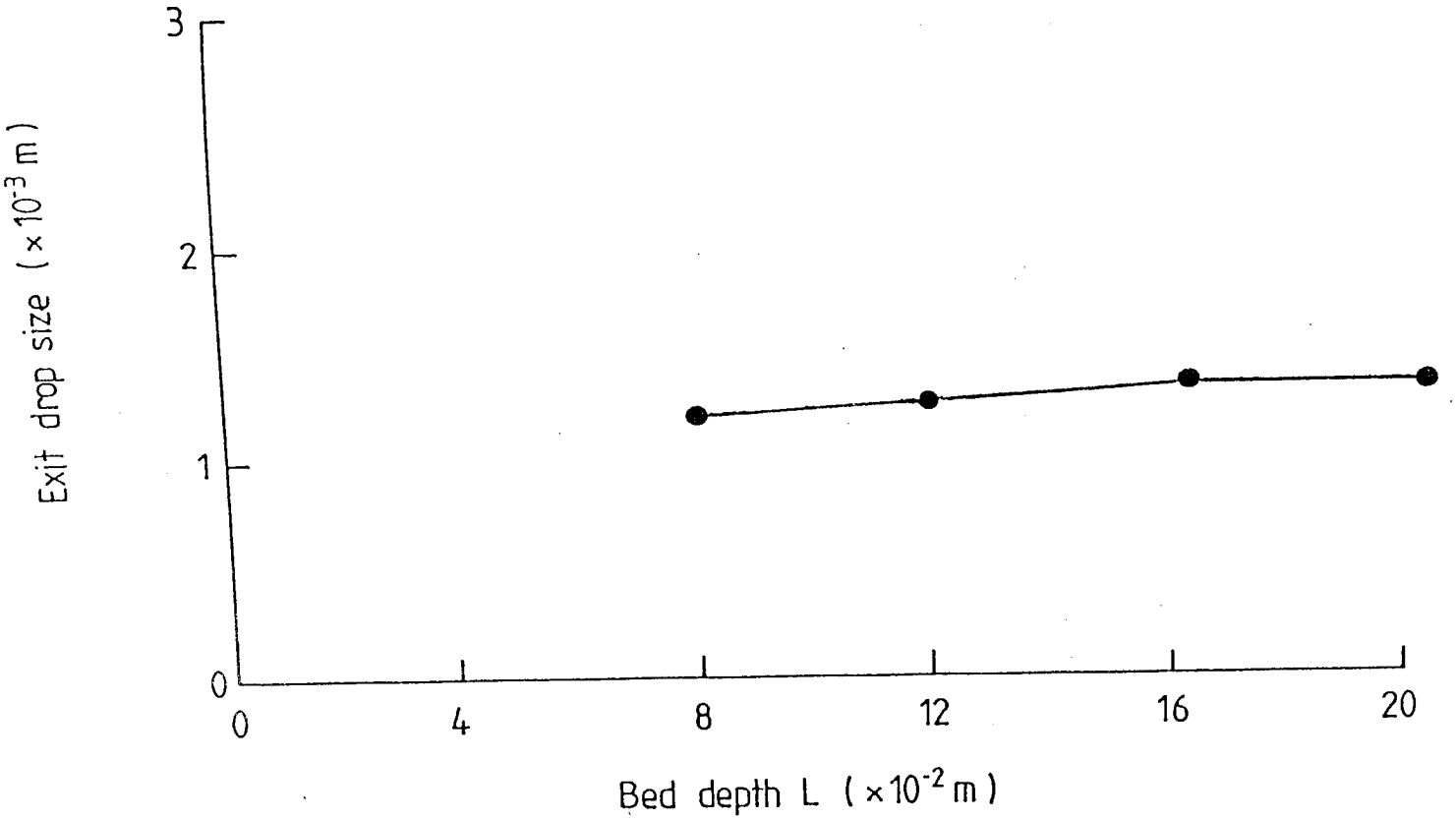

Figure 8·4 Variation of Exit drop size with Bed depth for Ballotini size 267 μm and superficial velocity 5×10^{-2} m/s

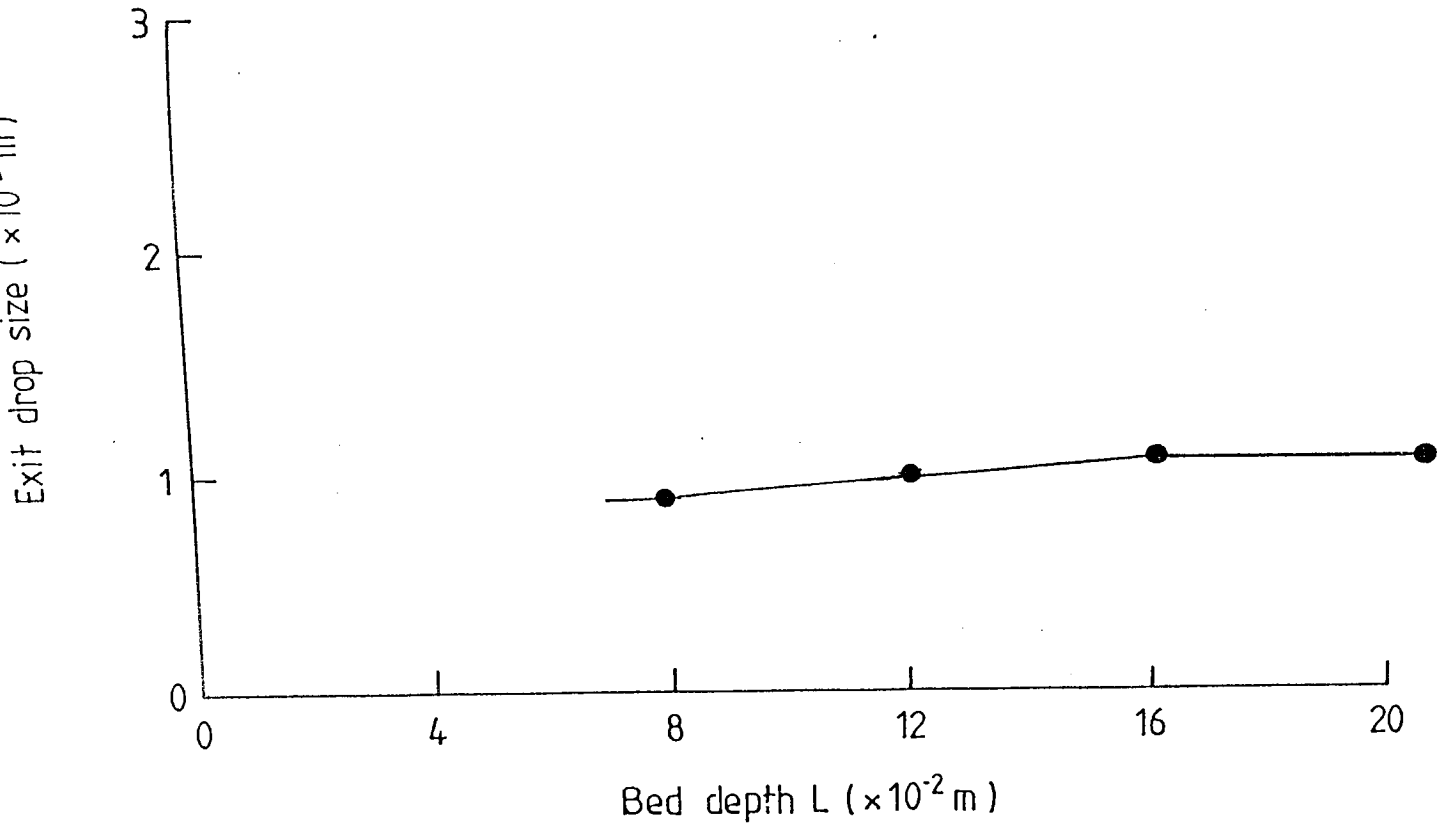

Figure 8·5 Variation of Exit drop size with Bed depth for Ballotini size 93 μm and superficial velocity 3×10^{-2} m/s

This can be attributed to some combination of less growth of primary drops and a variation in the release mechanism with velocity.

8.2.2. Effect of bed depth on exit drop size

The exit drop size was found to increase by increasing the bed depth, as shown in Figure 8.4. and 8.5., but there was an optimum bed depth after which any increase in it did not result in a corresponding increase in exit drop size. This is also in a complete agreement with the previous workers (73, 48). From Figure 8.3., it can be noticed that as the bed depth increased the effect of velocity on exit drop size decreased, until the bed depth reaches an optimum height after which the velocity has no effect on the exit drop size.

8.2.3. Effect of ballotini size on exit drop size

An increase in ballotini size led to an increase in exit drop size as shown in Figure 8.6. This increase in the exit drop size with ballotini size arises because, for any random packing of spheres, the mean void diameter must increase as the packing particle size is increased. Also from Figure 8.6. it can be noticed that the effect of ballotini size decreases as the bed depth increased, until the ballotini size has no effect on the exit drop size. In other words, there is a maximum bed depth after which ballotini size has no effect on exit drop size.

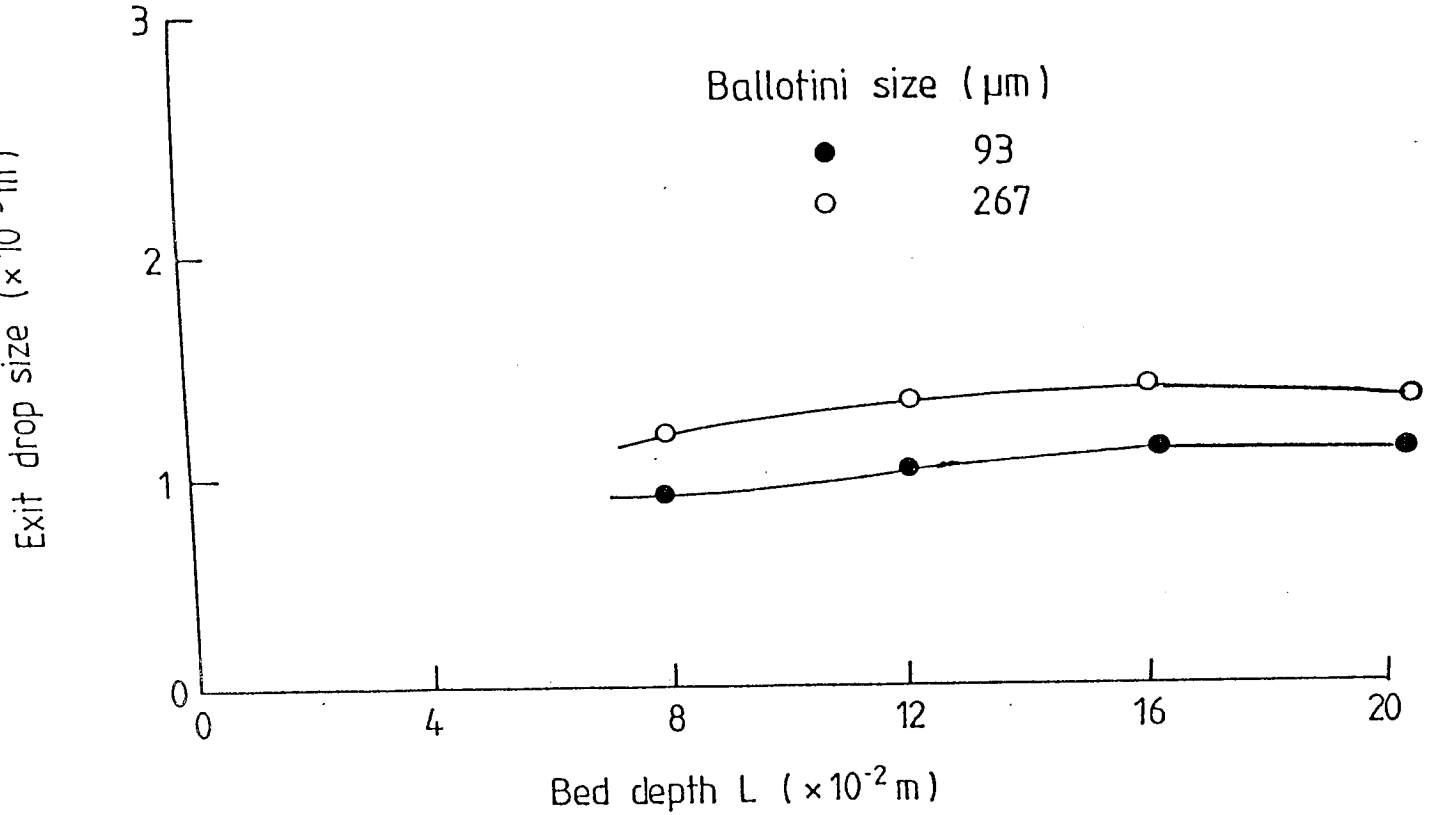

Figure 8·6 Variation of Exit drop size with Bed depth for velocity 3×10^{-2} m/s

8.2.4. Effect of phase ratio on exit drop size

Within the phase ratio in the range 0.4%v/v to 1.0%v.v, the exit drop size was independent of phase ratio, table 8.1. This indicates that the degree of coalescence was independent of the ratio of dispersed phase entering the bed. This is in agreement with other workers' results (71, 68).

8.2.5. Effect of bed depth on separation efficiency

From Figure 8.15. and Figure 8.18., it was noticed that as the bed depth increased the separation efficiency also increased, until the bed depth reached an optimum height after which it had no effect on separation efficiency. This is due to coalescence mechanism which takes place in the third forepart of the bed. Also it can be noticed from Figure 8.16. and 8.18., that as the ballotini size in the bed decreased, the optimum effective height decreased, ballotini size 267μm the optimum height was 0.12m, whereas in 367μm the optimum height was 0.16m, this was because the mean void diameter must increase as the packing particles size is increased.

8.3. Drop release

The drops release was observed to take place in the form of clusters having a wide range of sizes between 0.2mm-5mm, at different time intervals, from fixed points at the exit of the bed. The time interval between each cluster was almost constant but depended on size of ballotini in the bed and flow velocity. As the ballotini size in the

Velocity $x10^{-2}$ m/s	Bed Depth m	Phase Ratio %v/v	Exit Drop Size m x 10^{-3}
5	0.12	0.4	0.91
3	0.12	0.4	1.15
5	0.12	0.6	0.89
3	0.12	0.6	1.18
5	0.12	1.0	0.92
3	0.12	1.0	1.15

Table 8.1. Effect of Phase Ratio on Exit Drop Size for Ballotini Size 93µm.

bed increased, the exit drop size increased also, so the number of exit drops would be more as the ballotini size decreased.

This phenomena suggested that the dispersed phase in channels did not exist as a continuum, but as single coalesced drops travelling together through the coalescer. As the drops became larger by coalescence, they moved upward as a thread in a zigzag motion, at a speed of 3.2cm/sec for ballotini size 267μm and a superficial velocity of 4×10^{-2}m/s.

For a low velocity and ballotini which was used in previous experiments, the exit drops accumulated at the outlet of the bed, and the total height of accumulation of these primary drops sometimes reached 8cm.

Chaining release mechanism, Figure 8.8. was noticed for the first time with the toluene-water system, due to the small size of the ballotini 93μm. This was probably caused by redispersion resulting from high local velocities. (Attarzadeh (20) reported this phenomena for the water-toluene system in fibrous packings). Figure 8.12. illustrates a different effect, three primary drops attached to each other; this did not happen while the drops were travelling through the bed but whilst they were resting at the bed exit, and was not observed in any other experiments. With all the previous release mechanisms, the exit primary drops eg. 0.2cm, always had smaller size drops eg. <0.05cm attached to them. These satellite drops eventually

coalesced normally at the aqueous-organic interface.

8.4. Separation efficiency

The separation efficiency is determined from a material balance over the coalescer. Superficial velocity and ballotini size have different effects on this efficiency. An increase in velocity leads to a decrease in separation efficiency. Decrease in ballotini size leads to an increase in the separation efficiency, as shown in Figures 8.16., 8.17. and 8.18.

An increase in the dispersed phase ratio increases the separation efficiency Table 8.2., and decreases the time required to achieve steady-state operation. This suggests that, as the number of inlet drops increase, they will fill the interstices of the bed faster than at a lower rate of inlet drops. Presoaking improves the separation efficiency for the large ballotini sizes, but it does not have any effect on small ballotini sizes in the range of 93μm and lower. This is due to the different bed voidage, ie. presoaking simply serves to partly fill the interstices, so that steady state is reached more rapidly. Therefore the effect would be expected to be more pronounced with large ballotini size.

Since the efficiency for large ballotini reached a similar value eventually, whether or not it was presoaked 'wetting', in the conventional sense, was not a factor.

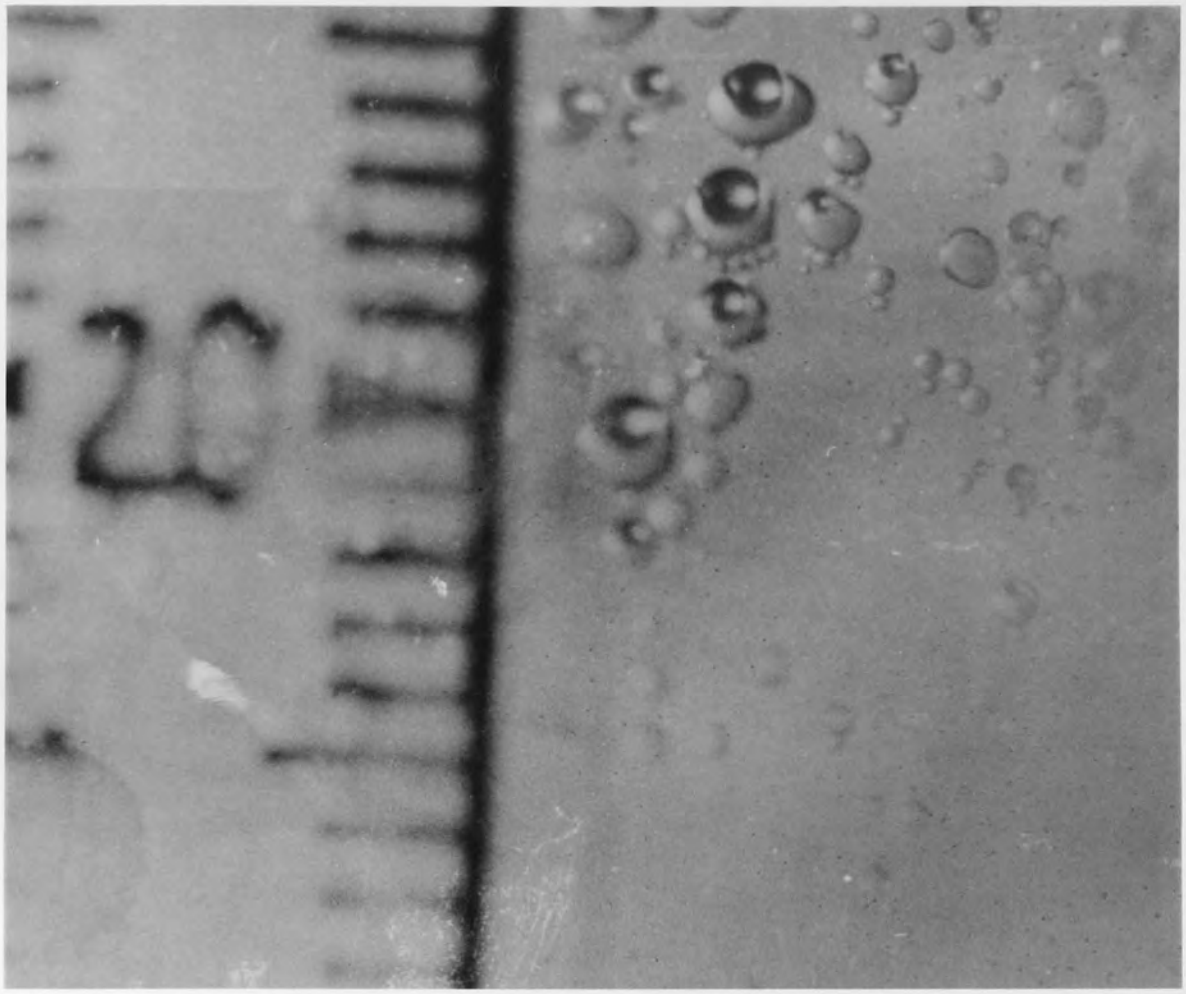

Figure 8.7 Normal Exit Drops

Exit Drops	Toluene/Water
Phase Ratio:	1%V/V
Velocity:	4×10^{-2} M/S
Bed Height:	0.12 m
Ballotini size:	367 µm

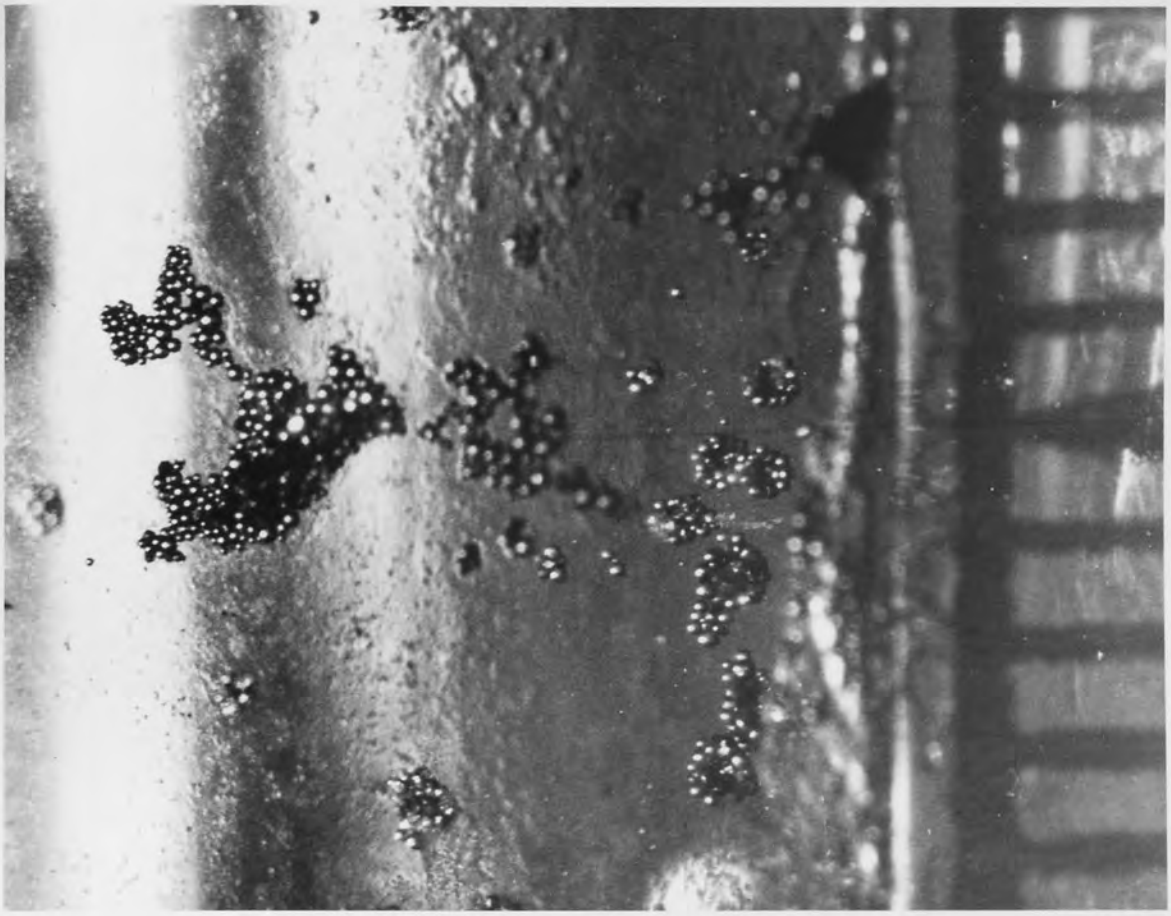

Figure 8.8 Drops Released by Chaining

Exit Drops	Toluene/Water
Phase Ratio:	1%V/V
Velocity:	4×10^{-2} M/S
Bed Height:	0.12 m
Ballotini size:	147.5 μm

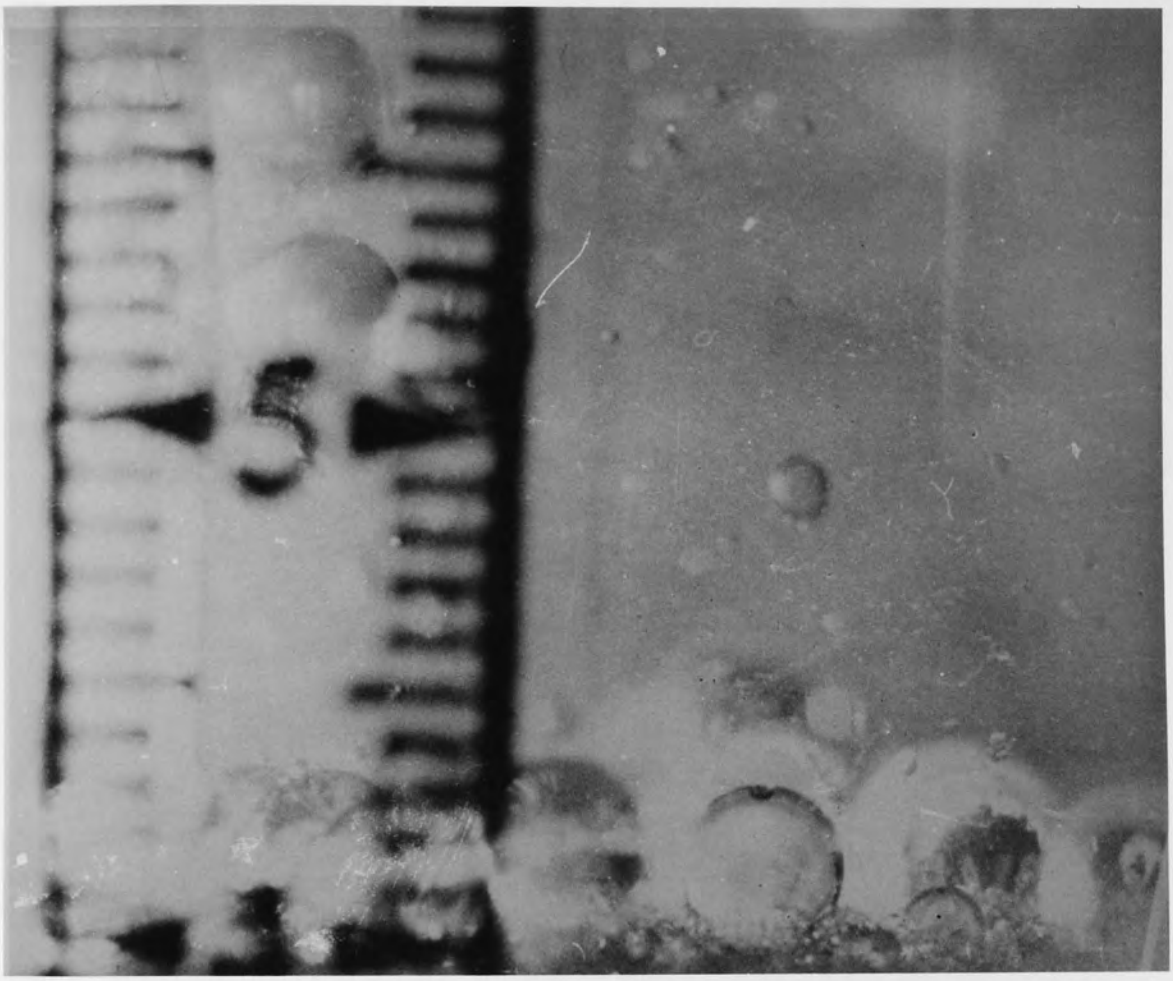

Figure 8.9 Normal Exit Drops

Exit Drops	Toluene/Water
Phase Ratio:	1%V/V
Velocity:	3×10^{-2} M/S
Bed Height:	0.12 m
Ballotini size:	267 μm

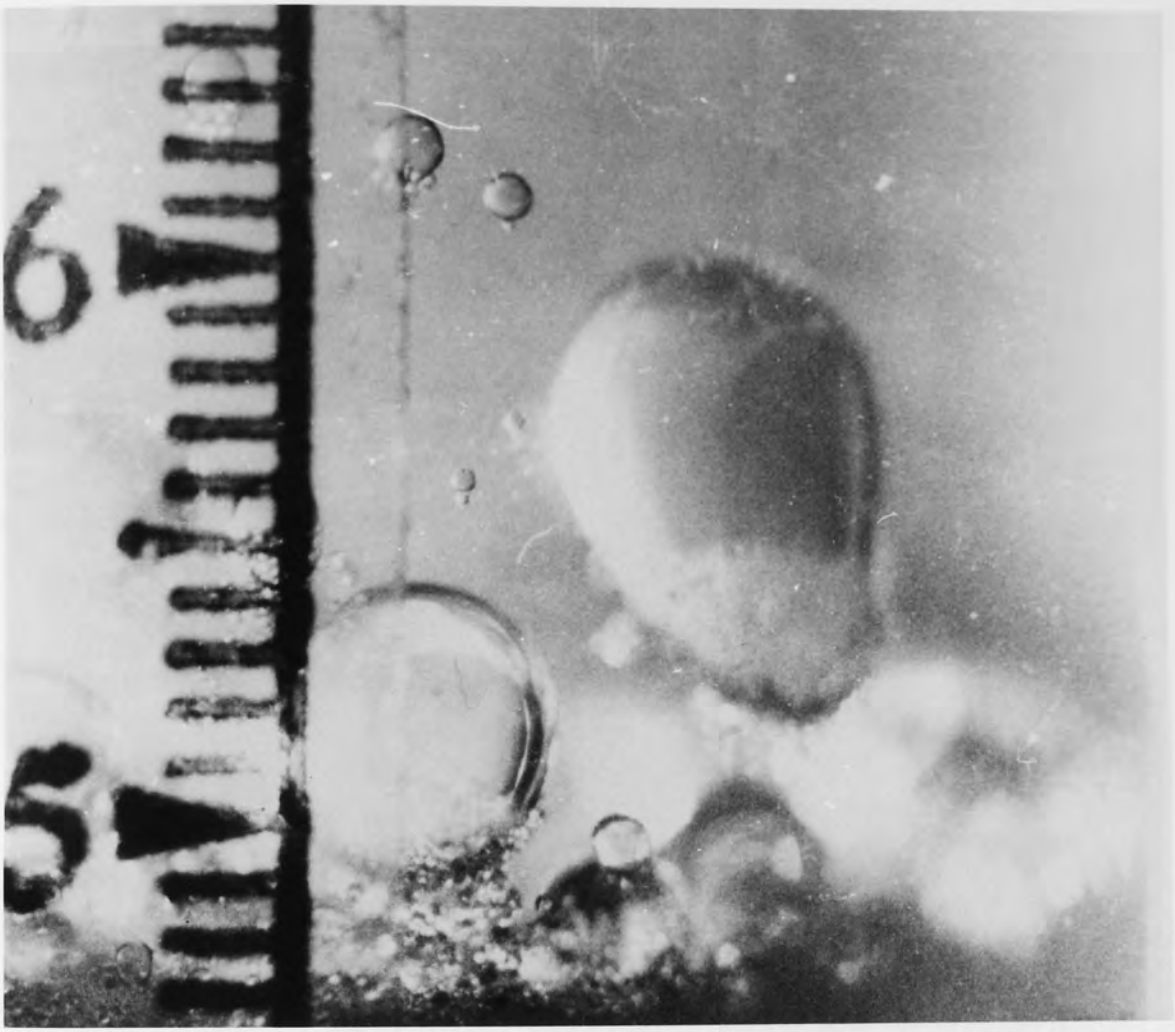

Figure 8.10 Exit Release Mechanism

Exit Drops	Toluene/Water
Phase Ratio:	1%V/V
Velocity:	3×10^{-2} M/S
Bed Height:	0.12 m
Ballotini size:	267 µm

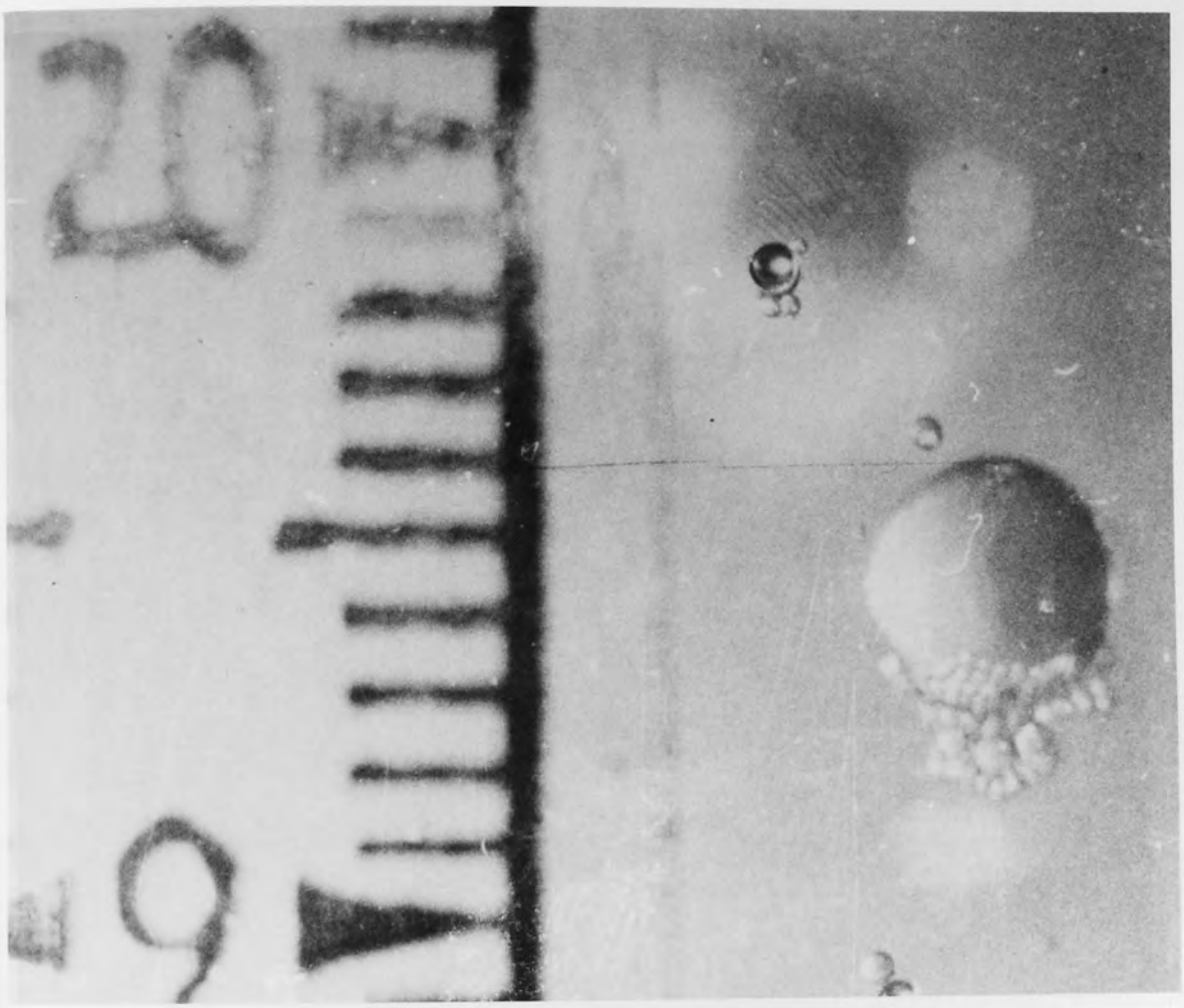

Figure 8.11 Normal Exit Drops

Exit Drops	Toluene/Water
Phase Ratio:	1%V/V
Velocity:	3×10^{-2} M/S
Bed Height:	0.12 m
Ballotini size:	267 µm

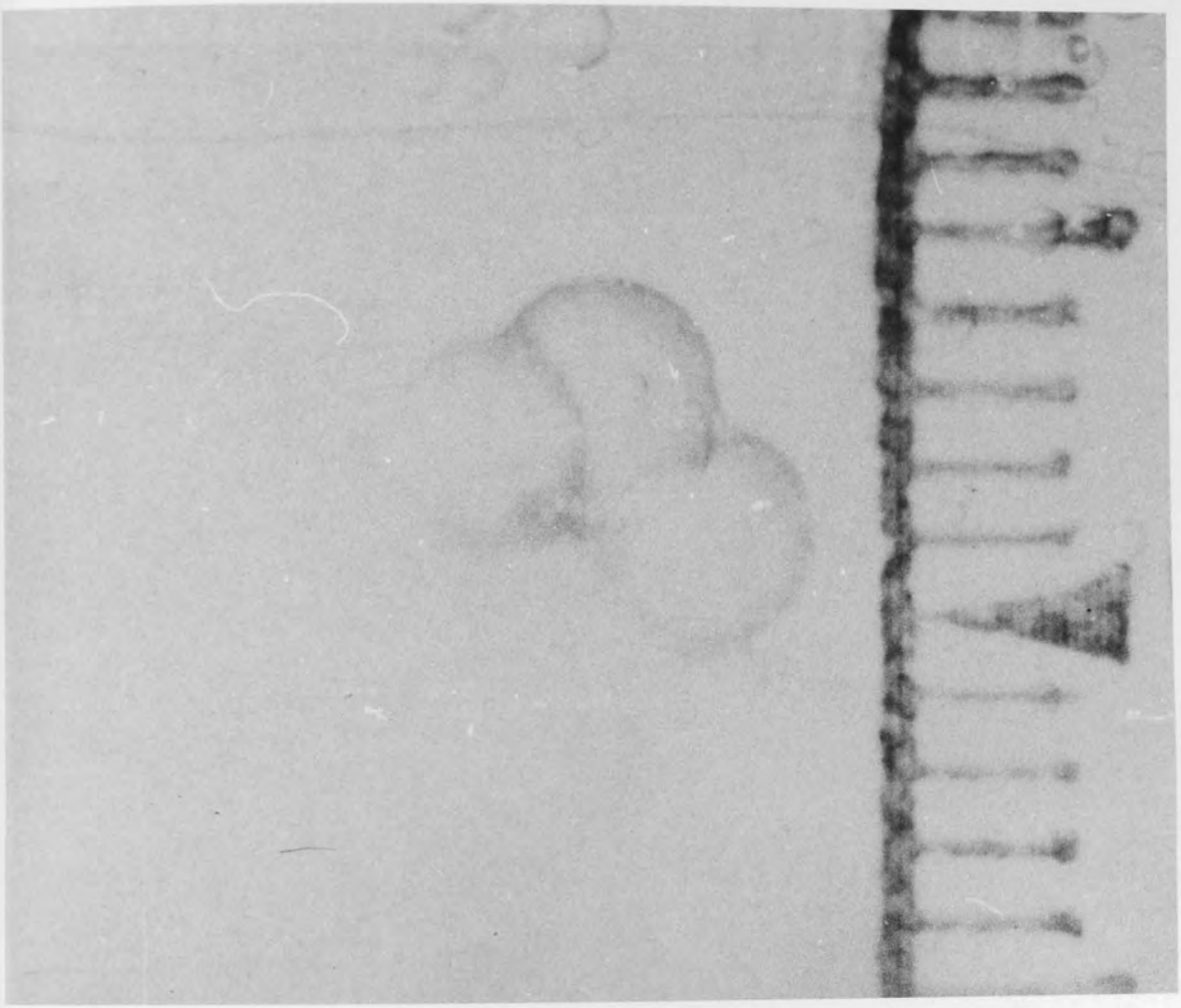

Figure 8.12 Triple Drop EXit

Exit Drops	Toluene/Water
Phase Ratio:	1%V/V
Velocity:	4×10^{-2} M/S
Bed Height:	0.12 m
Ballotini size:	367 µm

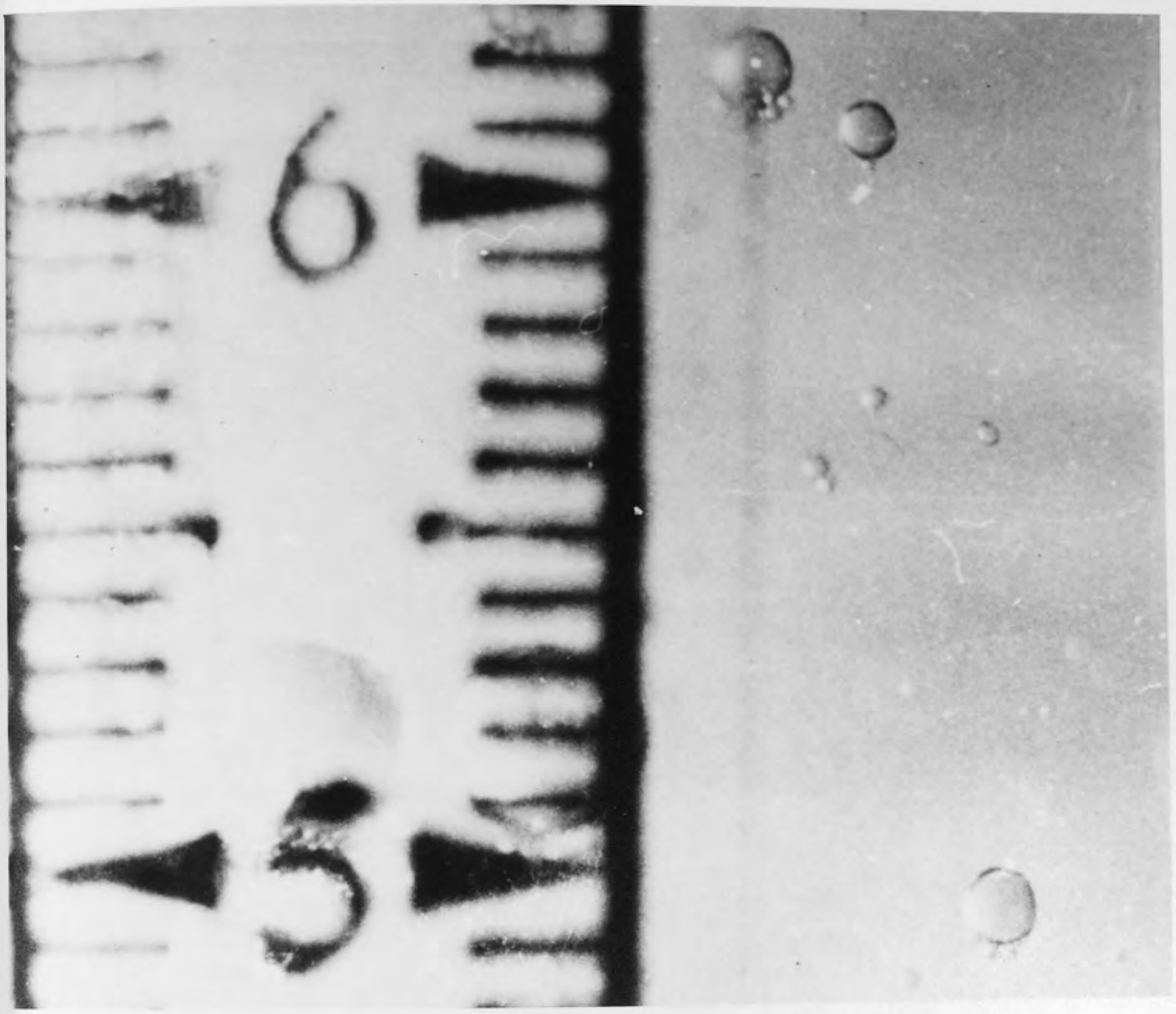

Figure 8.13 Normal Exit Drops

Exit Drops	Toluene/Water
Phase Ratio:	1%V/V
Velocity:	3×10^{-2} M/S
Bed Height:	0.12 m
Ballotini size:	267 μm

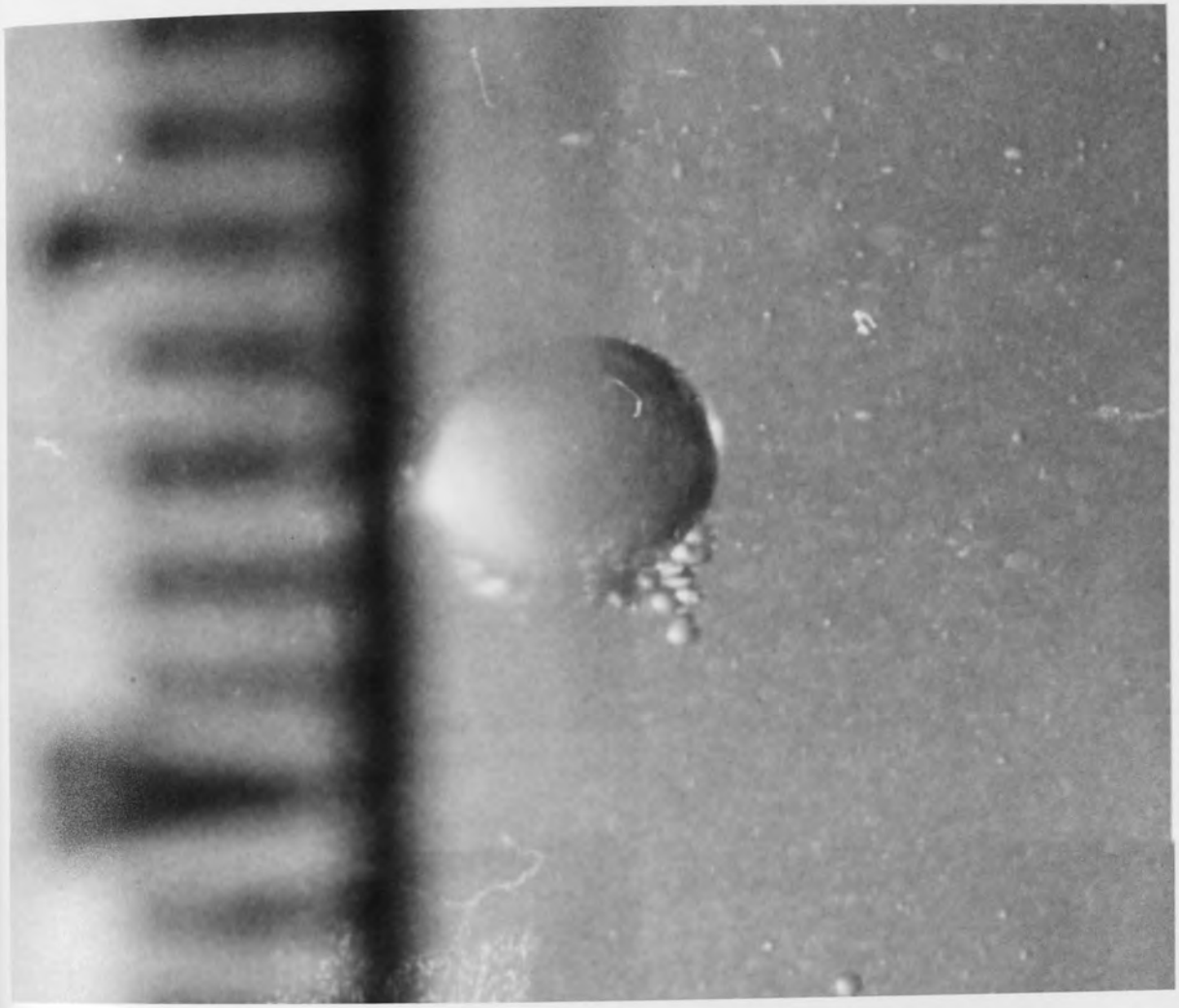

Figure 8.14 Normal Exit Drops

Exit Drops	Toluene/Water
Phase Ratio:	1%V/V
Velocity:	3×10^{-2} M/S
Bed Height:	0.08 m
Ballotini size:	267 μm

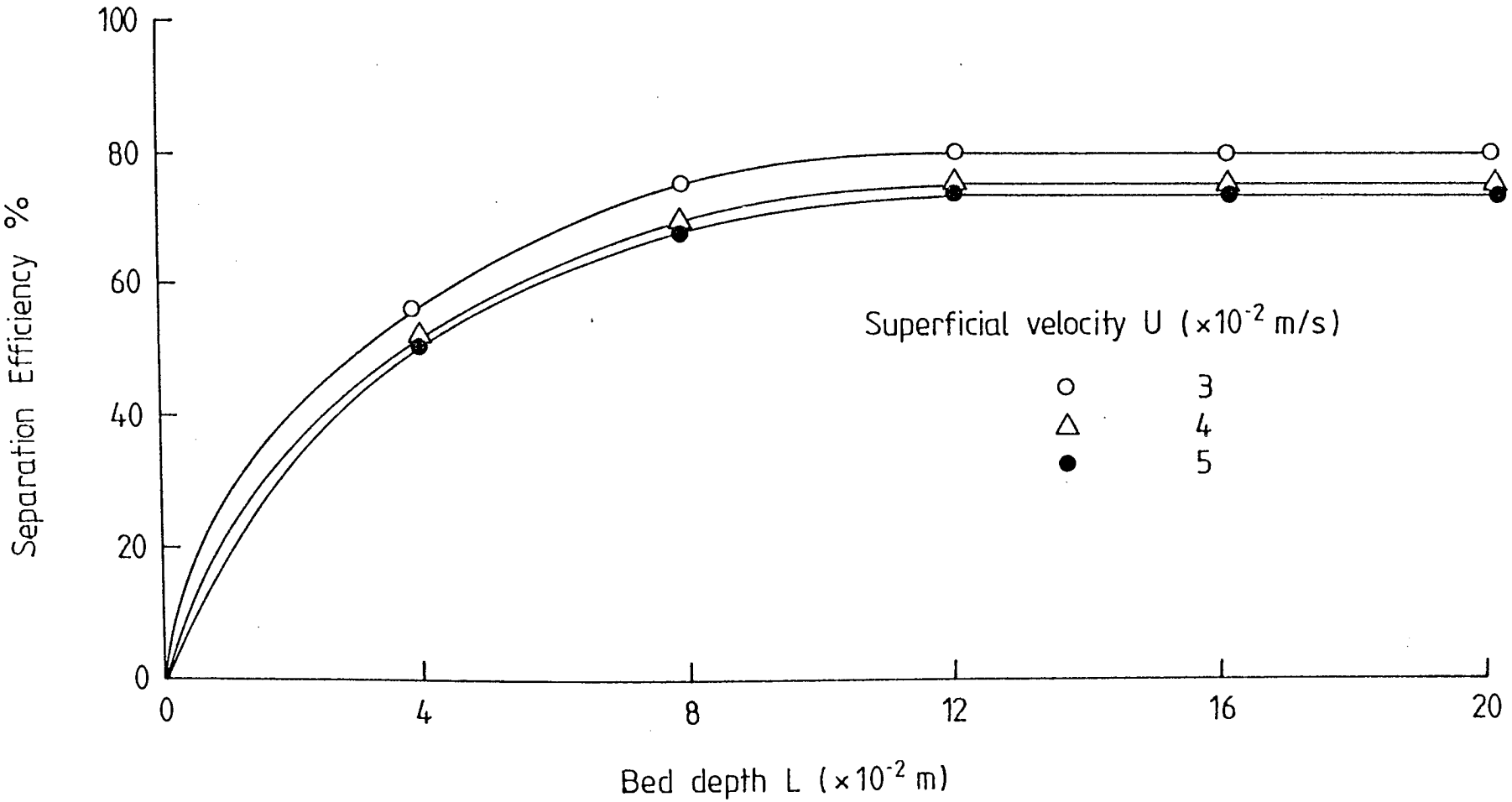

Figure 8·15 Variation of separation efficiency with Bed depth of Ballotini size 267 μm.

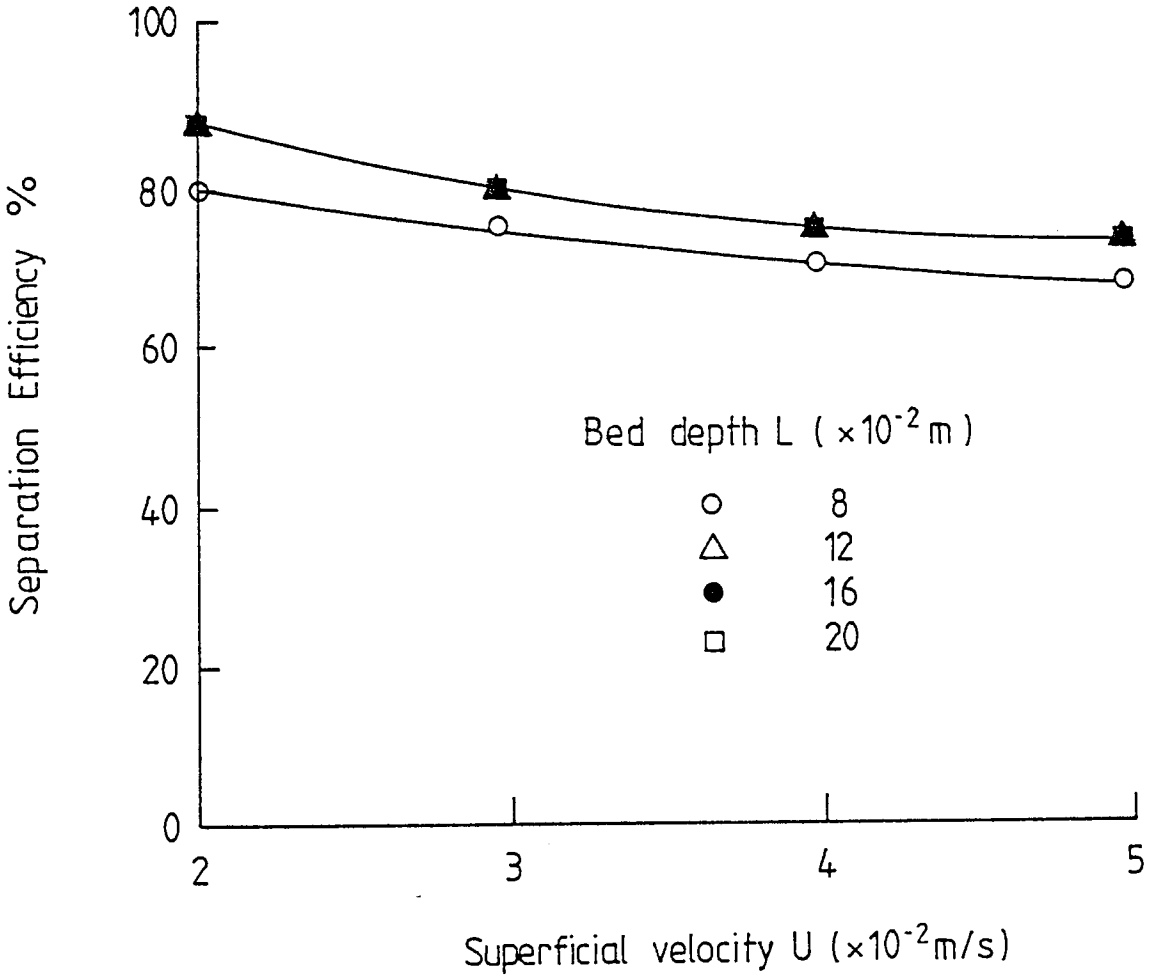

Figure 8·16 Variation of separation efficiency with velocity for Ballotini size 267 μm.

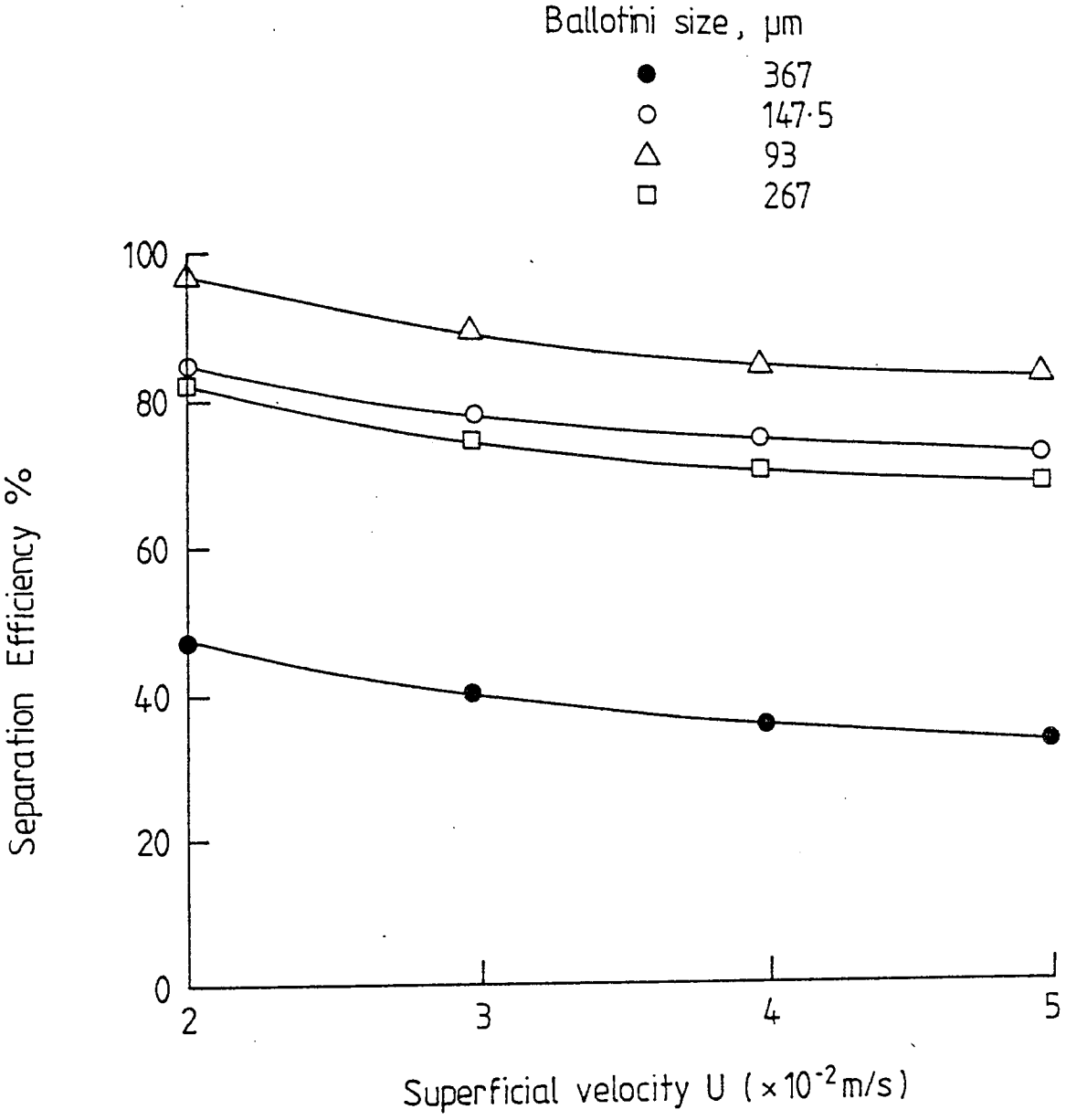

Figure 8·17 Variation of separation efficiency with velocity for different sizes of Ballotini

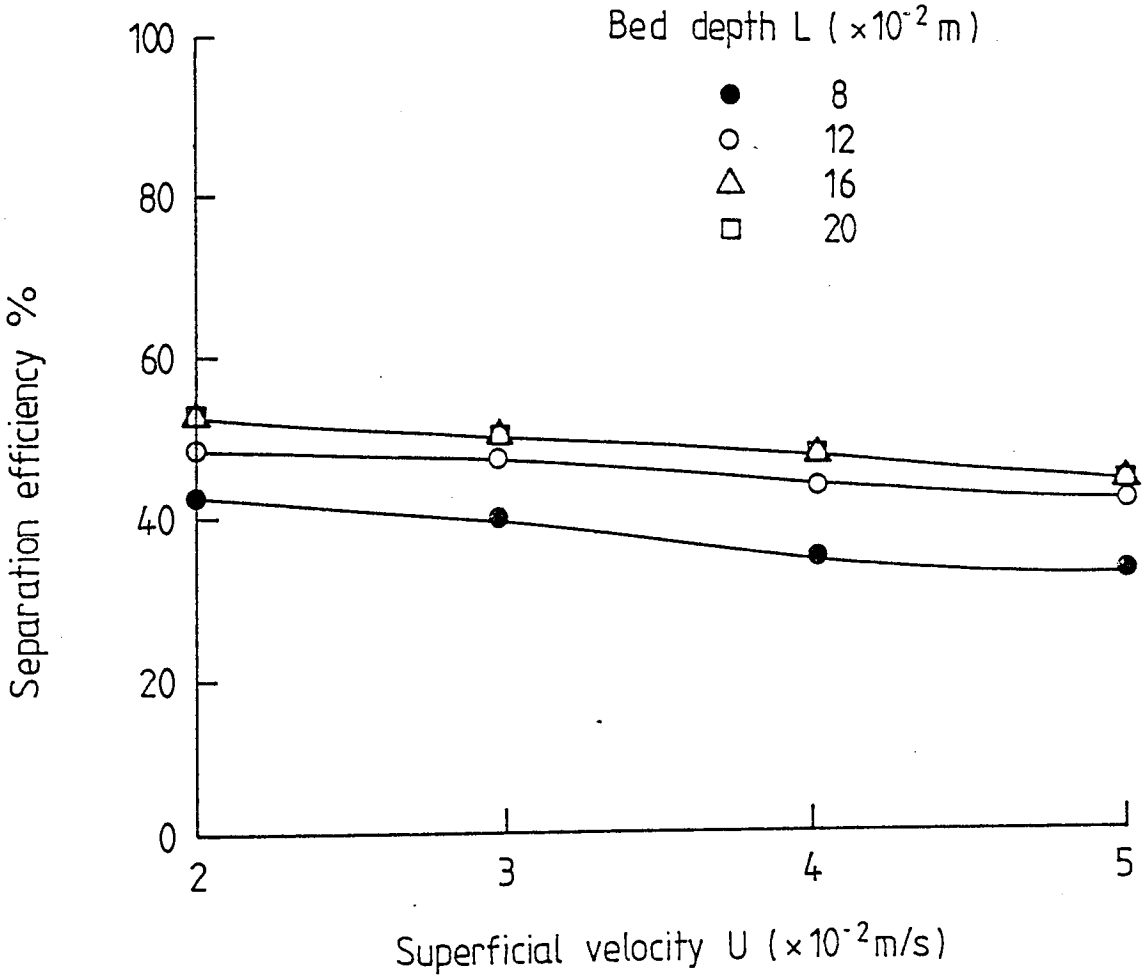

Figure 8·18 Variation of separation efficiency with velocity for Ballotini size 367 μm.

Bed Height (m)	Phase Ratio	Separation Efficiency
0.08	0.4	73
0.08	0.6	75
0.08	1	79
0.12	0.4	78
0.12	0.6	80
0.12	1	82
0.16	0.4	82
0.16	0.6	84
0.16	1	85

Table 8.2. Effect of phase ratio on the separation efficiency.

CHAPTER NINE

ANALYSIS OF PRESSURE DROP DATA

CHAPTER NINE

ANALYSIS OF PRESSURE DROP DATA

9.1. Single phase flow pressure drop

A study was made of single phase pressure drop to compare the phenomena observed with pressure drop for two phase flow during coalescence. It also served to determine the flow characteristics of the packing media used, to check the reproducibility of the coalescer assembly, and to detect ingress of air or particulate matter into the bed.

Many equations have been applied to describe single phase flow in packed beds, the Ergun equation (73) is the most frequently applied

$$f_p \left[e_1^3/(1 - e_1)\right] = (150/N_{Re})\ (1 - e_1) + 1.75 \qquad 9.1.$$

where

$$f_p = \frac{1750}{N_{Re}} + 28$$

substituting for f_p and N_{Re} and rearranging the equation

$$\frac{\Delta p_1}{L} = \frac{150\ \mu_c\ U(1 - e_1)^2}{d_c^2\ e_1^3} + \frac{1.75\ \rho_c\ U^2(1 - e_1)}{d_c\ e_1^3} \qquad 9.2.$$

for low values of Reynolds number, when $N_{Re} < 1$

Macdonald et al (74) recently tested the Ergun equation using more data than was previously available and found the following relation to give the best fit for all the data,

$$\frac{\Delta p_1}{L} = \frac{180\ \mu_c\ U(1 - e_1)^2}{d_c^2\ \ e_1^3} + \frac{1.8\ \rho_c\ U^2(1 - e_1)}{d_c\ \ e_1^3} \qquad 9.3.$$

for low Reynolds numbers, this reduces to the Carman-Kozeny equation.

$$\frac{\Delta p_1}{L} = \frac{180\ \mu_c\ U(1 - e_1)^2}{d_c^2\ \ e_1^3} \qquad 9.4.$$

The high correlation coefficient obtained for linear regression analysis on the pressure drop data confirmed the first order dependence on velocity.

From equation 9.4.

$$\frac{\Delta p_1}{L} = \frac{36\ K\ \mu_c\ U(1 - e_1)^2}{d_c^2\ \ e_1^3} \qquad 9.5.$$

Rearrangement of this equation yields

$$\left(\frac{\Delta p_1}{\mu_c}\right)\left(\frac{e_1^3\ \ d_c^2}{(1 - e_1)^2\ 36L}\right) = KU \qquad 9.6.$$

The first term, $\left(\frac{\Delta p_1}{\mu_c}\right)$ describing the pressure drop, contains the only property pertaining to the continuous phase, and it is almost independent of temperature fluctuations of 17°C to 23°C. The second term $\left\{\frac{e_1^3\ \ d_c^2}{(1 - e_1)^2\ 36L}\right\}$ embodies all the

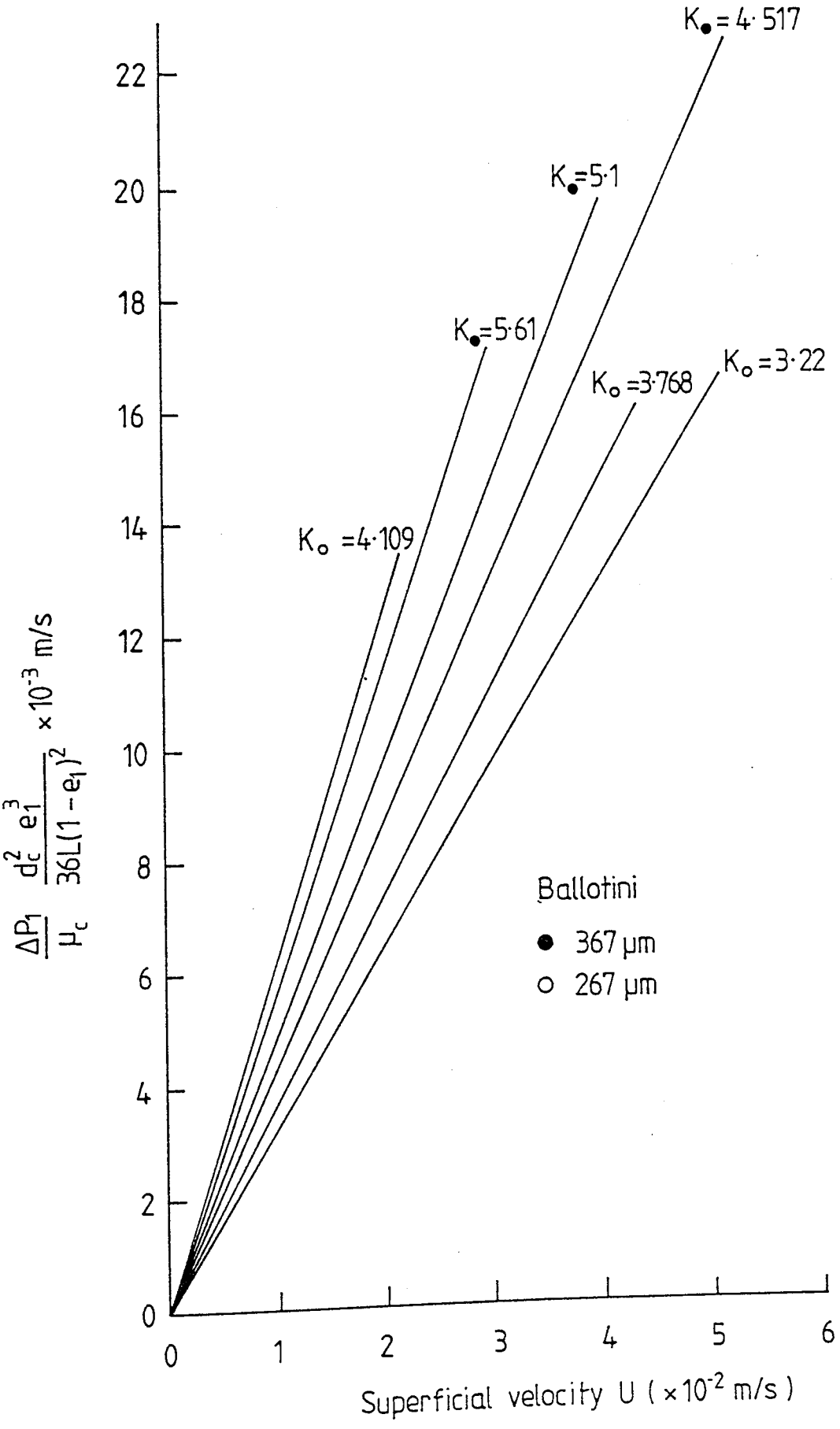

Figure 9·1 Correlation of single phase pressure drop for different Ballotini sizes.

properties of the packing which were evaluated experimentally.

Using equation 9.5., the single phase pressure drop data for different ballotini sizes were correlated against superficial velocity. The results are shown in Figure 9.1. and Figure 9.2., where the slope of the best fit line is equal to Kozeny constant. From the same figures it can be seen that the Kozeny constant exhibits some variation for the same ballotini size due to the influence of the container wall on the arrangement of the particles and bed depth.

The effect of the ratio of the diameter of the container, D, to that of the particle, d_c, has been studied in many different systems. It was concluded by Carman (110) that the wall effect is locally negligible if $D/d_c > 10$; in view of the work summarised by Rose and Rizk (135) concerning the magnitude of the wall effect when the ratio exceeds about 40, no attempt was made to correct the experimentaldata for wall effects in this study, as the ratio of D/d_c for the largest ballotini size used is over 95.

When applying the Ergun and Macdonald equations to the experimental data, it was found that Macdonald equation fitted the data better than the Ergun equation, ie. Equation 9.3. correlated the results within ±10.9%, but equation 9.2. correlated results within ±25.8%.

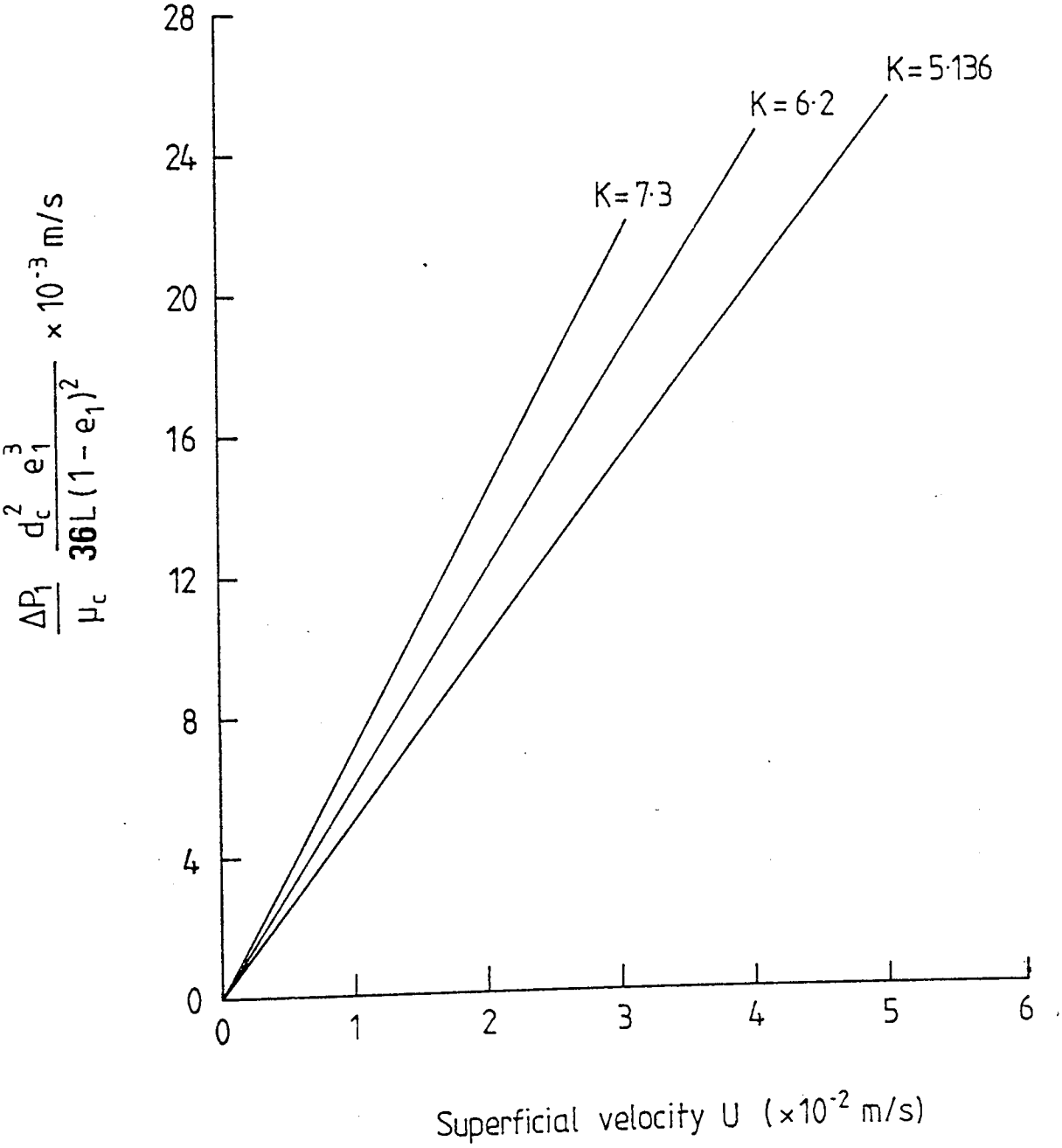

Figure 9·2 Correlation of single phase pressure drop for Ballotini size 147·5 μm.

9.2. Two phase pressure drop

To account for variations in packing technique and operating temperature, the two phase pressure drop is presented as a ratio,

$$\left(\frac{\Delta p_2}{\Delta p_1} \quad \frac{\mu_{c1}}{\mu_{c2}}\right)$$

This ratio was found to be similar (albeit with some variation) for the different ballotini sizes as shown is Tables 9.1/2/3/4. This suggests that the dispersed phase saturation was of the same order of magnitude, and therefore a function of the bed voidage, since all the packings have similar voidages. From the previous tables and from Figures 9.3. and 9.4. the ratio

$$\left(\frac{\Delta p_2}{\Delta p_1} \quad \frac{\mu_{c1}}{\mu_{c2}}\right)$$

was found generally to decrease as both superficial velocity and bed depth increased. This implies that the dispersed phase saturation increases as both velocity and bed depth decrease.

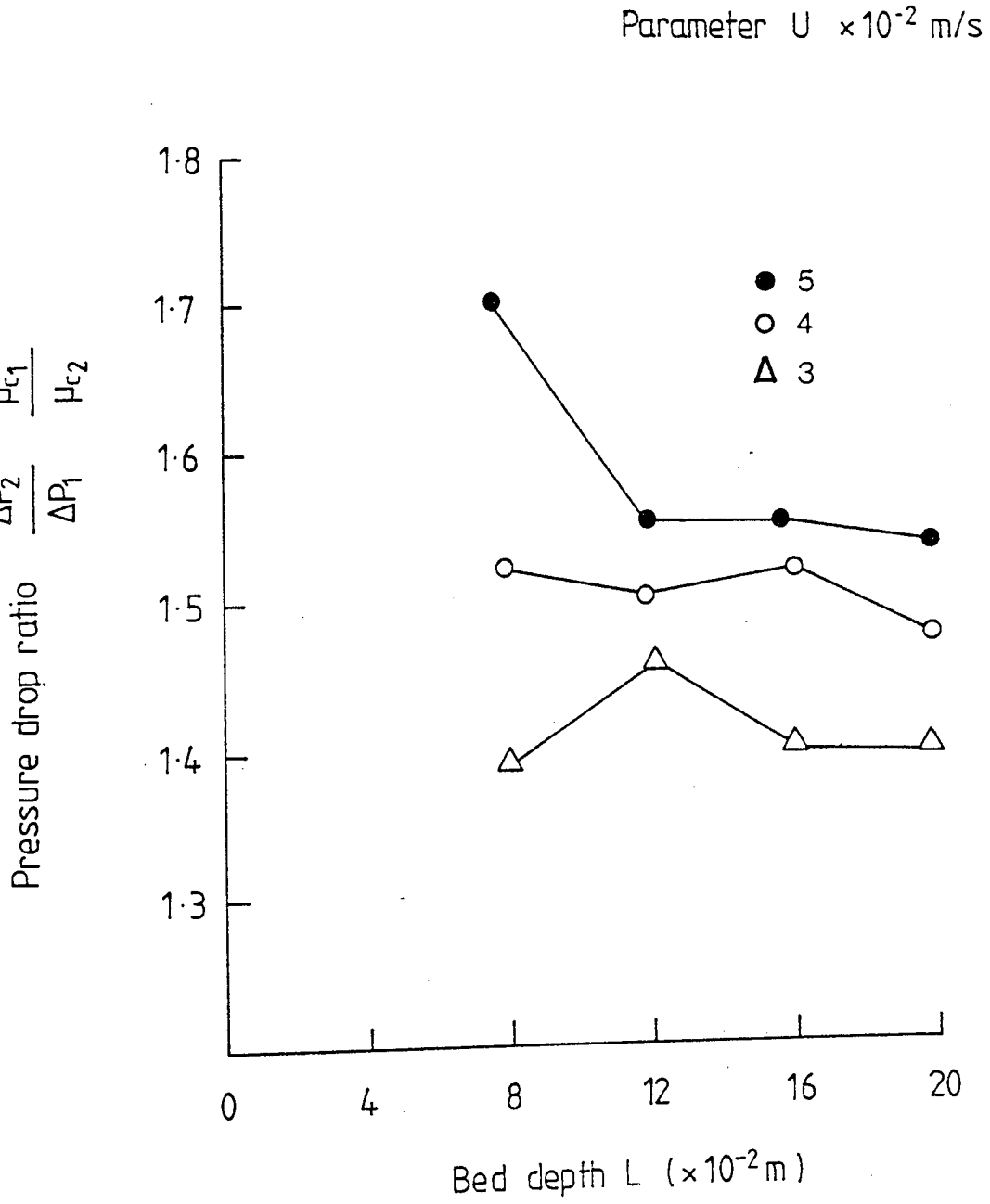

Figure 9·3 Variation of pressure drop ratio with velocity for 147·5 μm Ballotini size and 1% V/V Dispersed phase.

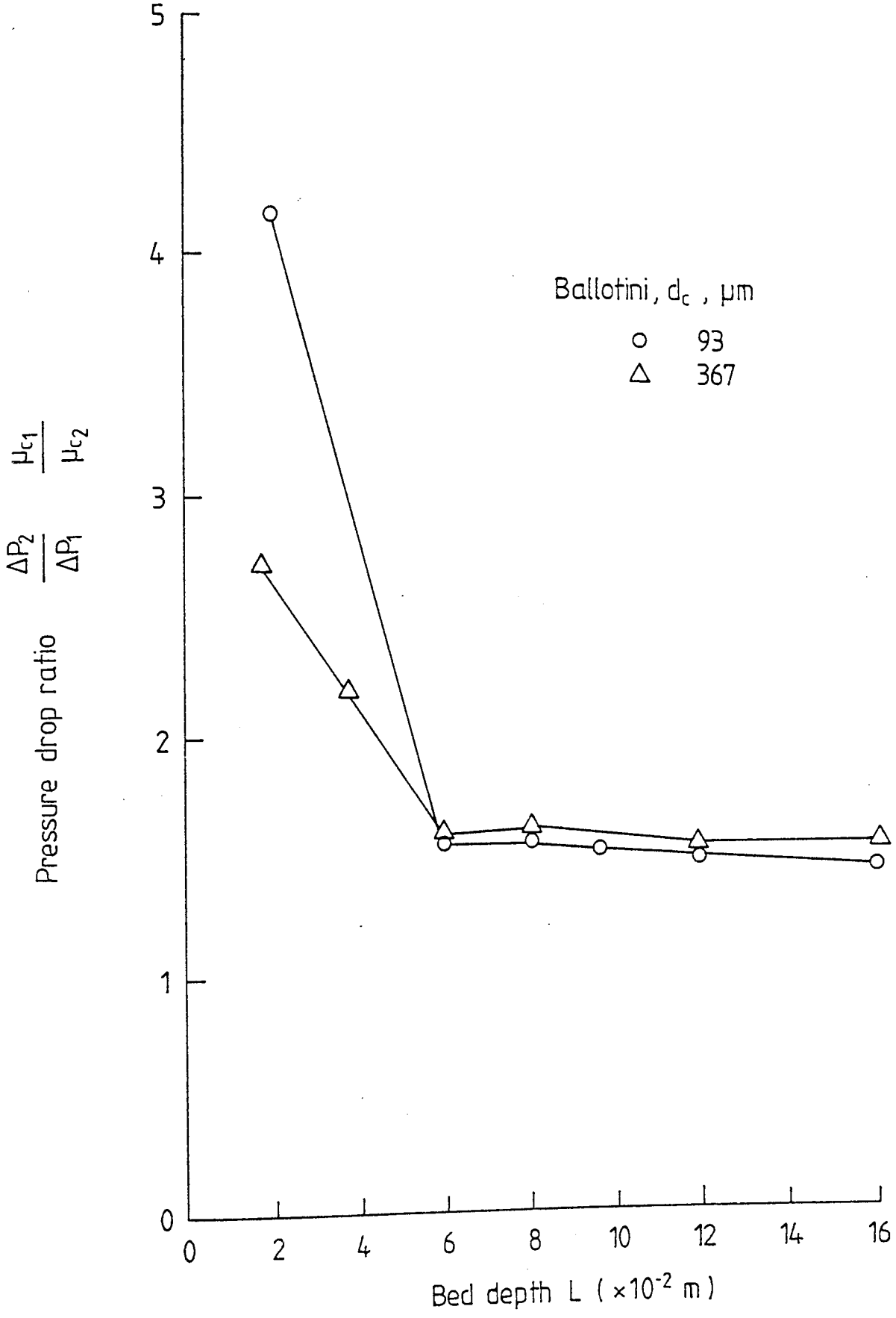

Figure 9·4 Effect of Ballotini size on pressure drop ratio vs. Bed depth

Bed Height (m)	Superficial Velocity m/s ($x10^{-2}$)	$\frac{\Delta p_2}{\Delta p_1} \frac{\mu_{c1}}{\mu_{c2}}$
0.08	3.04	1.345
0.08	3.978	1.487
0.08	5.038	1.589
0.12	3.04	1.289
0.12	3.978	1.423
0.12	5.038	1.504
0.16	3.04	1.338
0.16	3.978	1.433
0.16	5.038	1.435
0.2	3.04	1.29
0.2	3.978	1.233
0.2	5.038	-

Table 9.1. The Effect of Superficial Velocity on the Ratio $\frac{\Delta p_2}{\Delta_{p1}} \frac{\mu_{c1}}{\mu_{c2}}$ for Ballotini size 93μm.

9.3. Saturation profiles

The oil saturation, ie. the volume fraction of voids occupied by oil, is a very important parameter in coalescence operations, since the oil saturation explicitly appears in recent attempts to model the process. It has also been observed that the pressure drop and coalescence efficiency increase significantly as deposited oil accumulates during the approach to steady state from an initial oil-free condition.

It was important to measure the oil saturation across the bed without disturbing the flow, and because of the considerable changes of the oil saturation throughout the bed, pressure taps were therefore used.

Jones (75) correlated relative permeability data to the continuous or dispersed phase saturations using the expressions

$$\frac{K_d}{K_o} = (1 - 1.11\ S_c)^2 \qquad 9.7.$$

$$\frac{K_c}{K_o} = (1 - S_d)^3 \qquad 9.8.$$

For two phases flowing through a short column of porous media with uniform cross section, the effective permeability of the water phase may be defined as

$$K_c = \frac{U_2\ \mu_c\ \Delta L}{\Delta p_2} \qquad 9.9.$$

Bed Height (m)	Superficial Velocity m/s ($x10^{-2}$)	$\frac{\Delta p_2}{\Delta p_1} \frac{\mu_{c1}}{\mu_{c2}}$
0.08	3.04	1.383
0.08	9.978	1.937
0.08	5.038	1.705
0.12	3.04	1.4606
0.12	3.978	1.50
0.12	5.038	1.55
0.16	3.04	1.40
0.16	3.978	1.52
0.16	5.038	1.55
0.2	3.04	1.39
0.2	3.978	1.479
0.2	5.038	1.544

Table 9.2. The Effect of Superficial Velocity on the Ratio $\frac{\Delta p_2}{\Delta p_1} \frac{\mu_{c1}}{\mu_{c2}}$ for Ballotini size 147.5μm.

Bed Height (m)	Superficial Velocity m/s ($x10^{-2}$)	$\frac{\Delta p_2}{\Delta p_1} \frac{\mu_{c1}}{\mu_{c2}}$
0.08	3.04	1.453
0.08	3.978	1.513
0.08	5.038	1.676
0.12	3.04	1.513
0.12	3.978	1.556
0.12	5.038	1.729
0.16	3.04	1.3
0.16	3.978	1.572
0.16	5.038	1.66
0.2	3.04	1.434
0.2	3.978	1.54
0.2	5.038	1.626

Table 9.3. The Effect of Superficial Velocity on the Ratio $\frac{\Delta p_2}{\Delta p_1} \frac{\mu_{c1}}{\mu_{c2}}$ for Ballotini Size 267μm.

Bed Height (m)	Superficial Velocity m/s ($x10^{-2}$)	$\frac{\Delta p_2}{\Delta p_1} \frac{\mu_{c1}}{\mu_{c2}}$
0.08	3.04	1.441
0.08	3.978	1.581
0.08	5.038	1.729
0.12	3.04	1.509
0.12	3.978	1.60
0.12	5.038	1.876
0.16	3.04	1.371
0.16	3.978	1.591
0.16	5.038	1.572
0.2	3.04	1.394
0.2	3.978	1.572
0.2	5.038	1.528

Table 9.4. The Effect of Superficial Velocity on the Ratio $\frac{\Delta p_2}{\Delta p_1} \frac{\mu_{c1}}{\mu_{c2}}$ for Ballotini Size 367μm.

The permeability of the medium to a single phase is defined by Darcy's law as

$$K_o = \frac{U_1 \mu_c \Delta L}{\Delta p_1} \qquad 9.10.$$

If the superficial velocity U_1 for single phase flow is adjusted to equal the value U_2, the superficial velocity of the water phase in two-phase flow at the same temperature conditions then from equation 9.9. and 9.10., the ratio $\frac{\Delta p_1}{\Delta p_2}$ is equal to $\frac{K_c}{K_o}$.

Therefore, the relative permeability can be calculated from the ratio $\frac{\Delta p_1}{\Delta p_2}$ for each pressure tap across the packed bed.

$$\frac{K_c}{K_o} = \left(\frac{\Delta p_1}{\Delta p_2} \frac{\mu_{c2}}{\mu_{c1}}\right) \qquad 9.11.$$

from equation 9.4.

$$K_o = \frac{dc^2 \, e_1^3}{180 \, (1 - e_1)^2} \qquad 9.12.$$

The permeability of the medium to water for different sizes of ballotini was calculated using both equation 9.10. and 9.12. The results are shown in table 9.5. and table 9.6., for ballotini sizes 367μm and 267μm. Both values are very close which supports the assumption that for these large sizes, the Carman-Kozeny equation can be used to predict the single phase flow of the system.

However for the other ballotini sizes 147.5μm and 93μm the equation 9.12. did not fit the experimental data which means that this equation needs modification for smaller

ballotini sizes.

Figures 9.5. to 9.7., which are examples of oil saturation profiles, show that the oil saturation is higher at the inlet of the packed bed and decreases sharply to remain at an almost constant value throughout the bed. Also as the inlet dispersed phase concentration increases the sudden drop in oil saturation is more steep, which suggests intuitively that capture by interception is the predominant mechanism at the inlet of the bed.

From Figure 9.8. to 9.10., the inlet saturation is higher for the smaller size ballotini suggesting that drop capture by interception is aided as the size of the interstice is decreased. For the remainder of the bed, the saturation is almost the same for the different sizes of ballotini which is contrary to the results of Baez (71). To confirm these results another set of experiments was carried out using two different sizes of ballotini in the same bed, where the smaller size, 147.5μm was the bottom 8cm of the bed, and the larger size, 367μm was at the top. The total bed height was 16cm. The exit drop sizes were found to be almost identical to the exit drop sizes when the bed just contained the 147.5μm size. This indicates that the coalescence mechanism in the middle and the top of the bed is the same for all the different sizes of ballotini covered in this work.

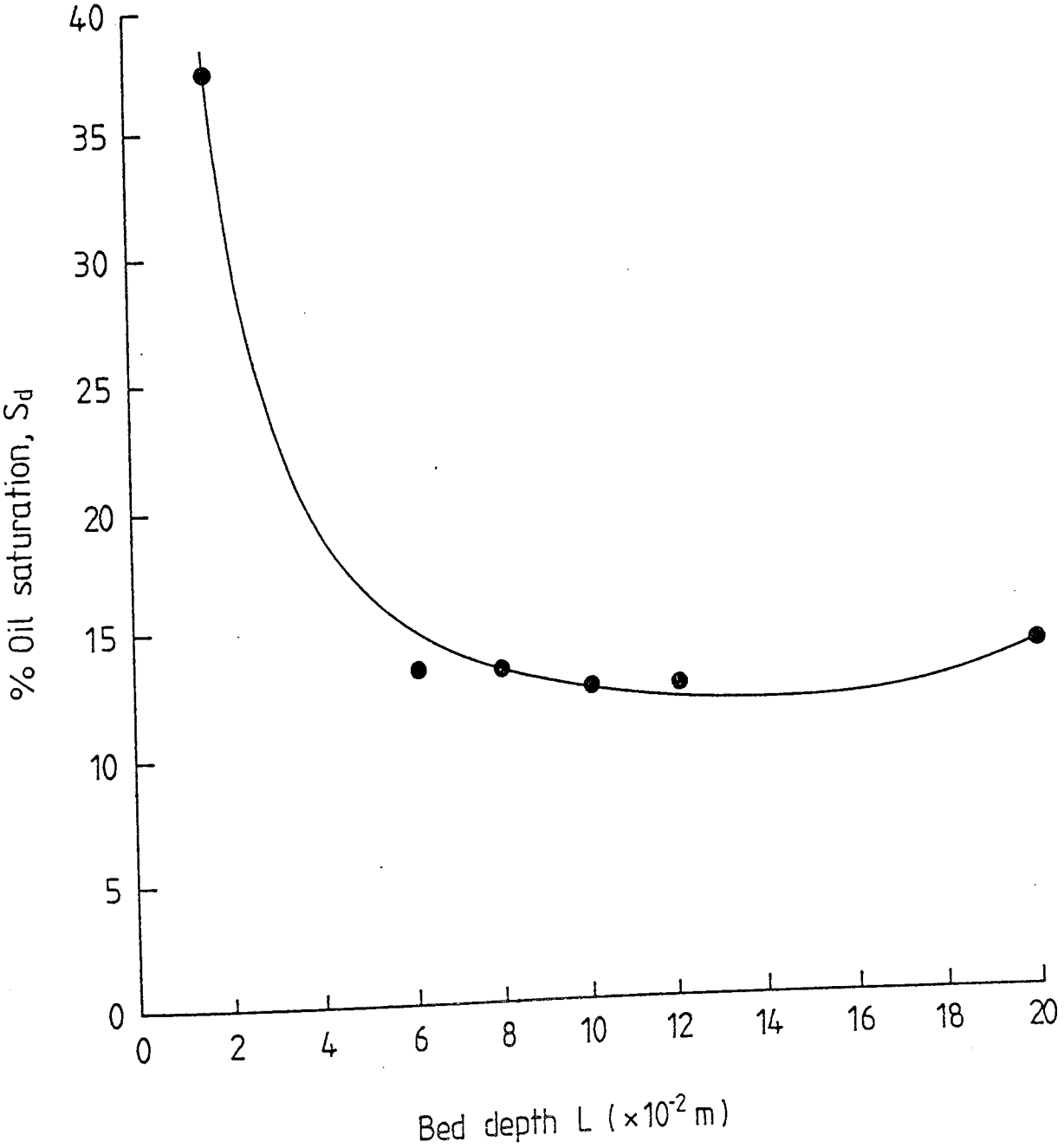

Figure 9·5 Saturation vs Bed depth
Ballotini 93 μm, 20×10^{-2} m Bed depth, 3×10^{-2} m/s velocity and 0·4% Dispersed phase concentration.

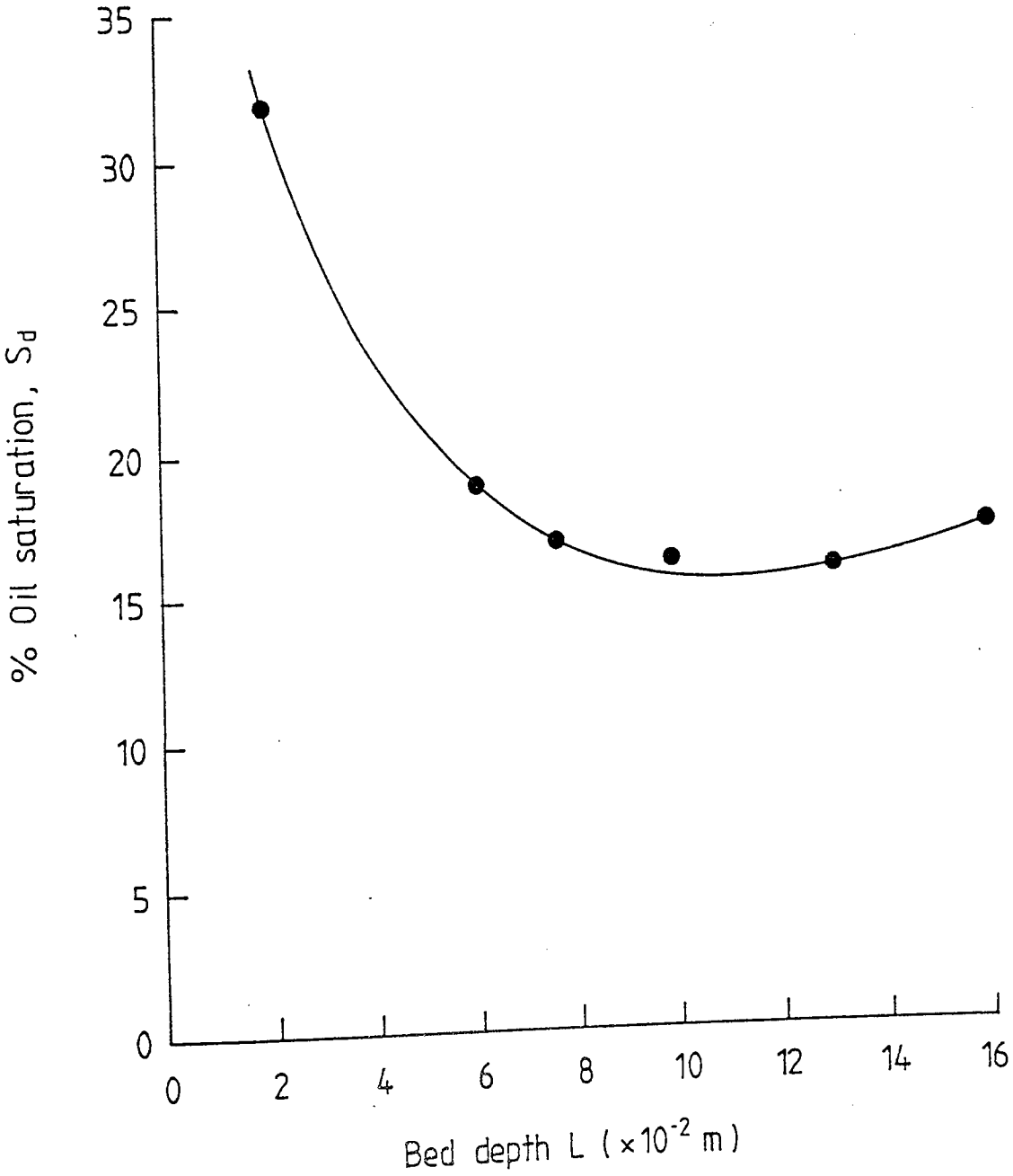

Figure 9·6 Saturation vs. Bed depth
Ballotini size, 93 μm. 20×10^{-2} m Bed depth
3×10^{-2} m/s Velocity, and 0·6 V/V Dispersed phase concentration(%).

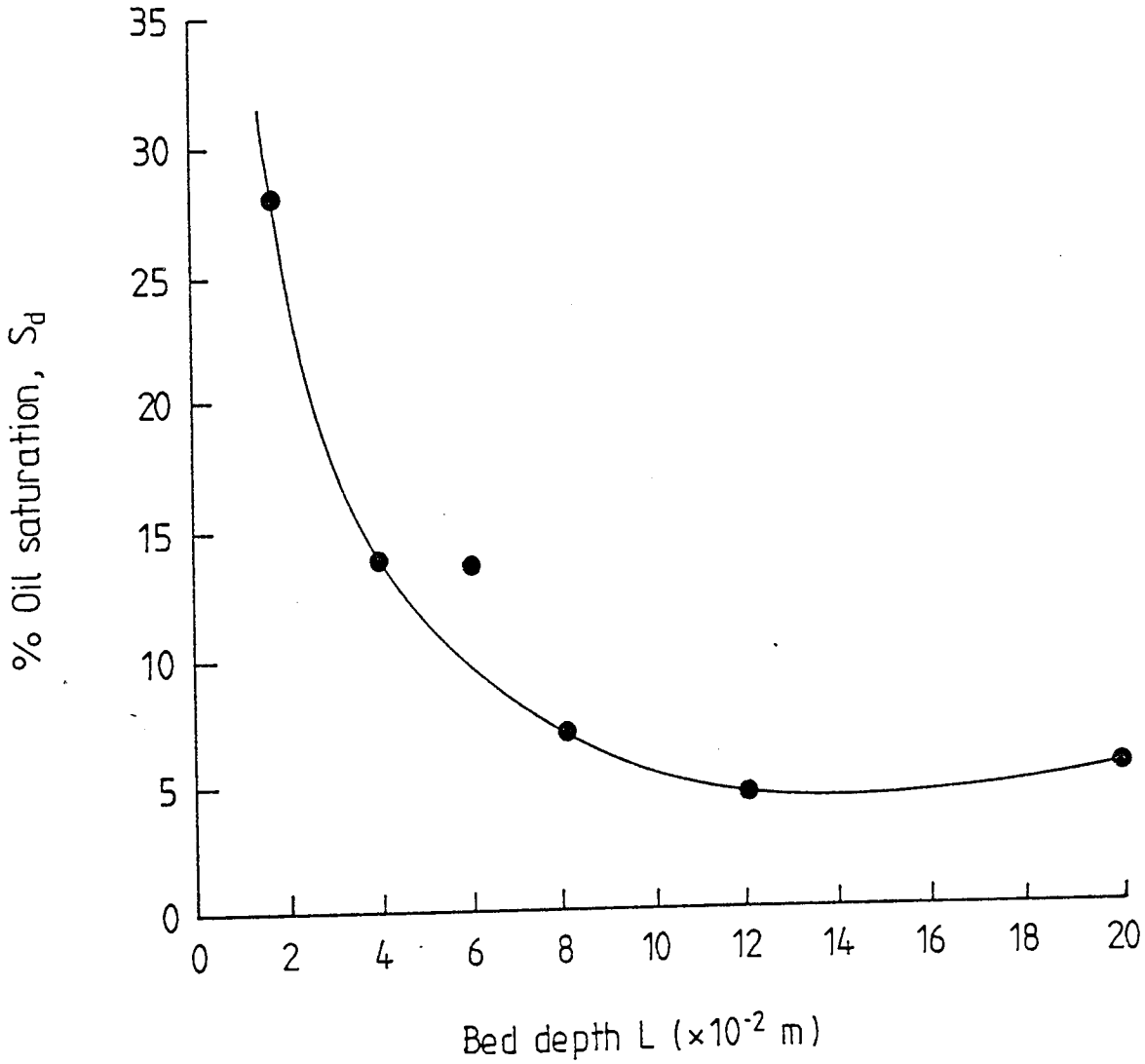

Figure 9·7 Saturation vs. Bed depth
Ballotini 367 μm, 20×10^{-2} m Bed depth
5×10^{-2} m/s velocity and 1% V/V Dispersed phase concentration.

Figures 9.5 to 9.7 are typical profiles from 83 experiments covering superficial velocity in the range 3-5 x 10^2 m/s and bed depth in the range of 0.05-0.2m. The complete data have been deposited in the Department of Chemical Engineering.

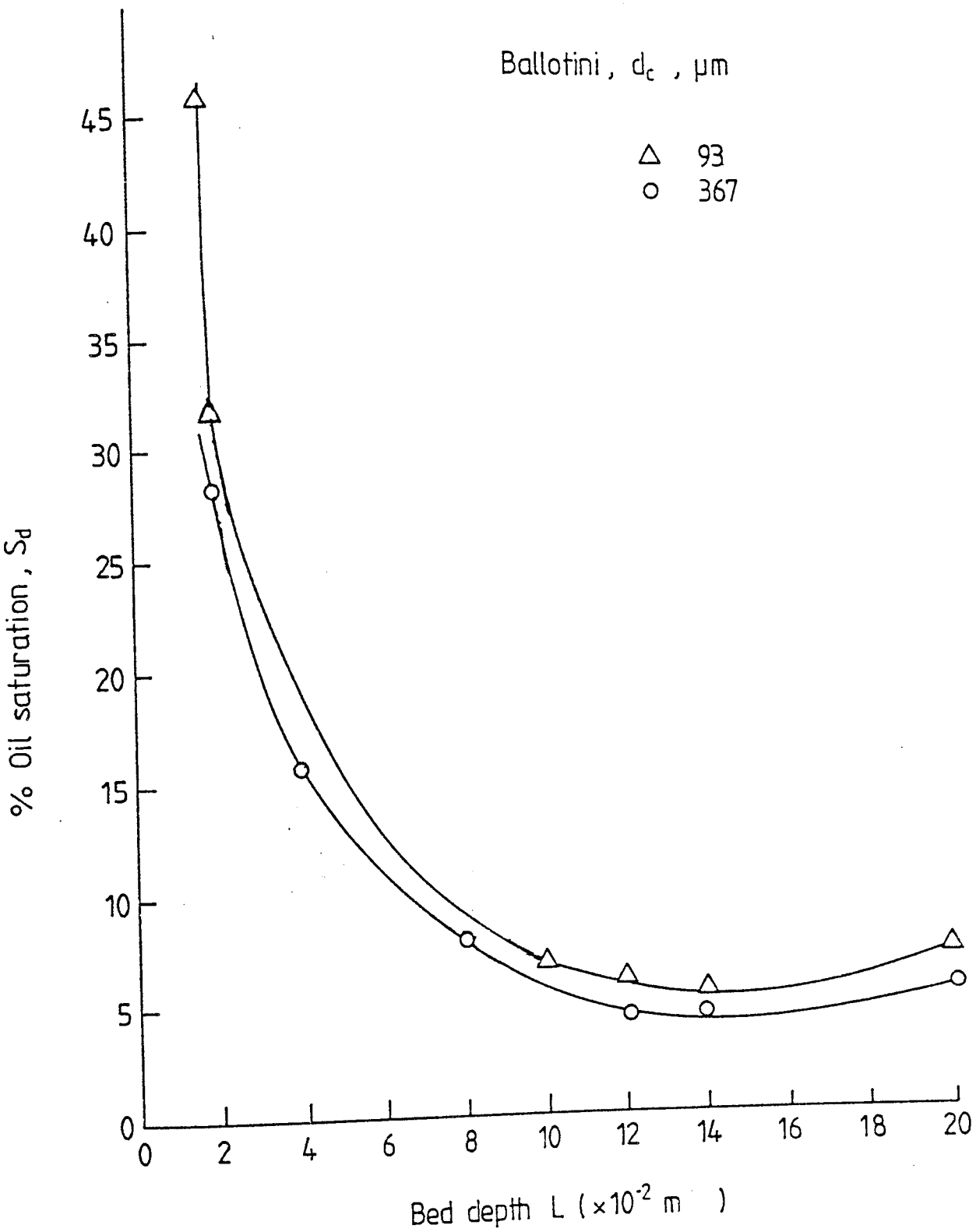

Figure 9·8 Effect of Ballotini on Saturation vs Bed depth. 20×10^{-2} m Bed depth, 5×10^{-2} m/s velocity and 1% V/V dispersed phase concentration.

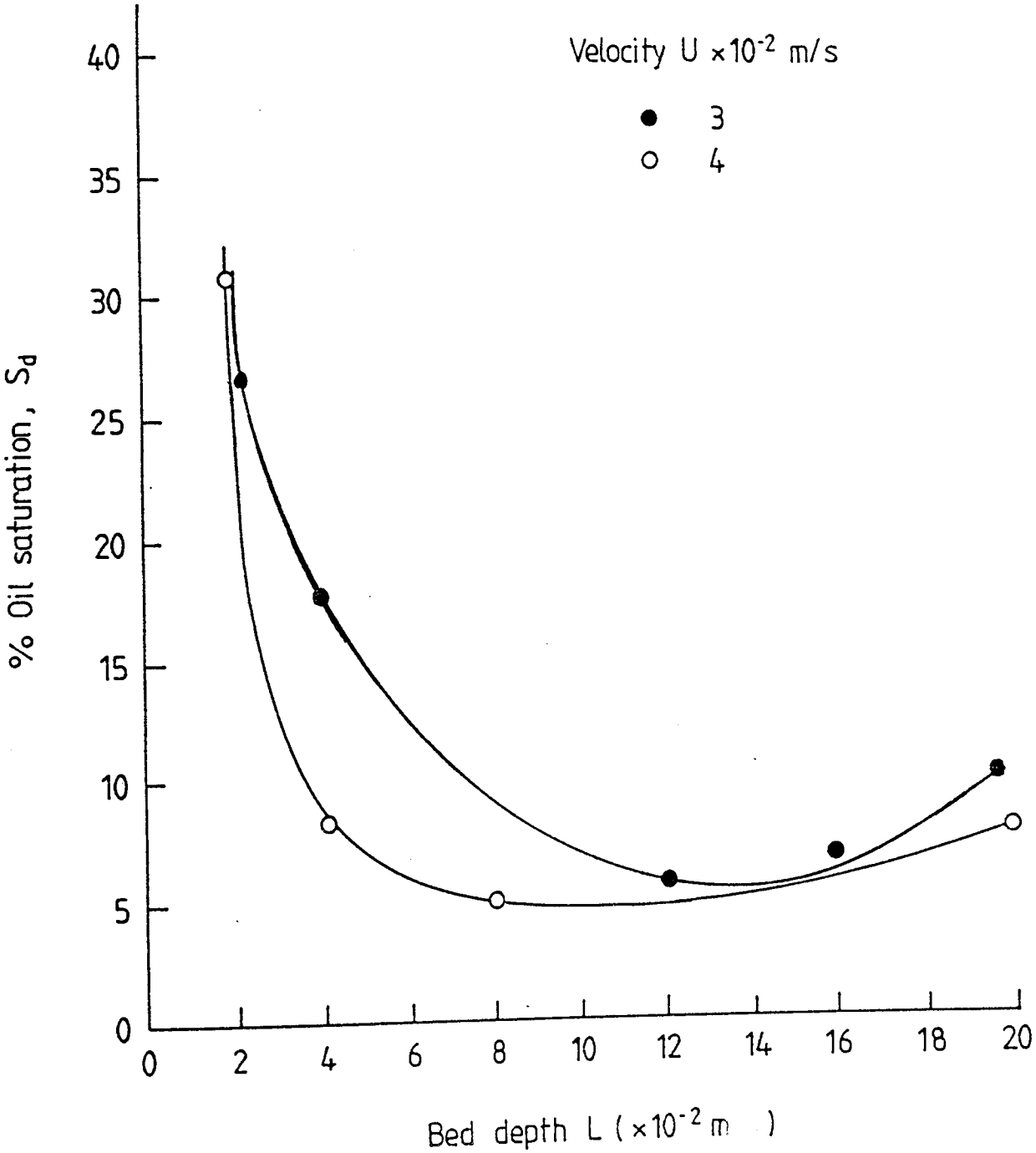

Figure 9·9 Effect of velocity on Saturation vs Bed depth Ballotini size 267 μm and 20×10^{-2} m Bed depth.

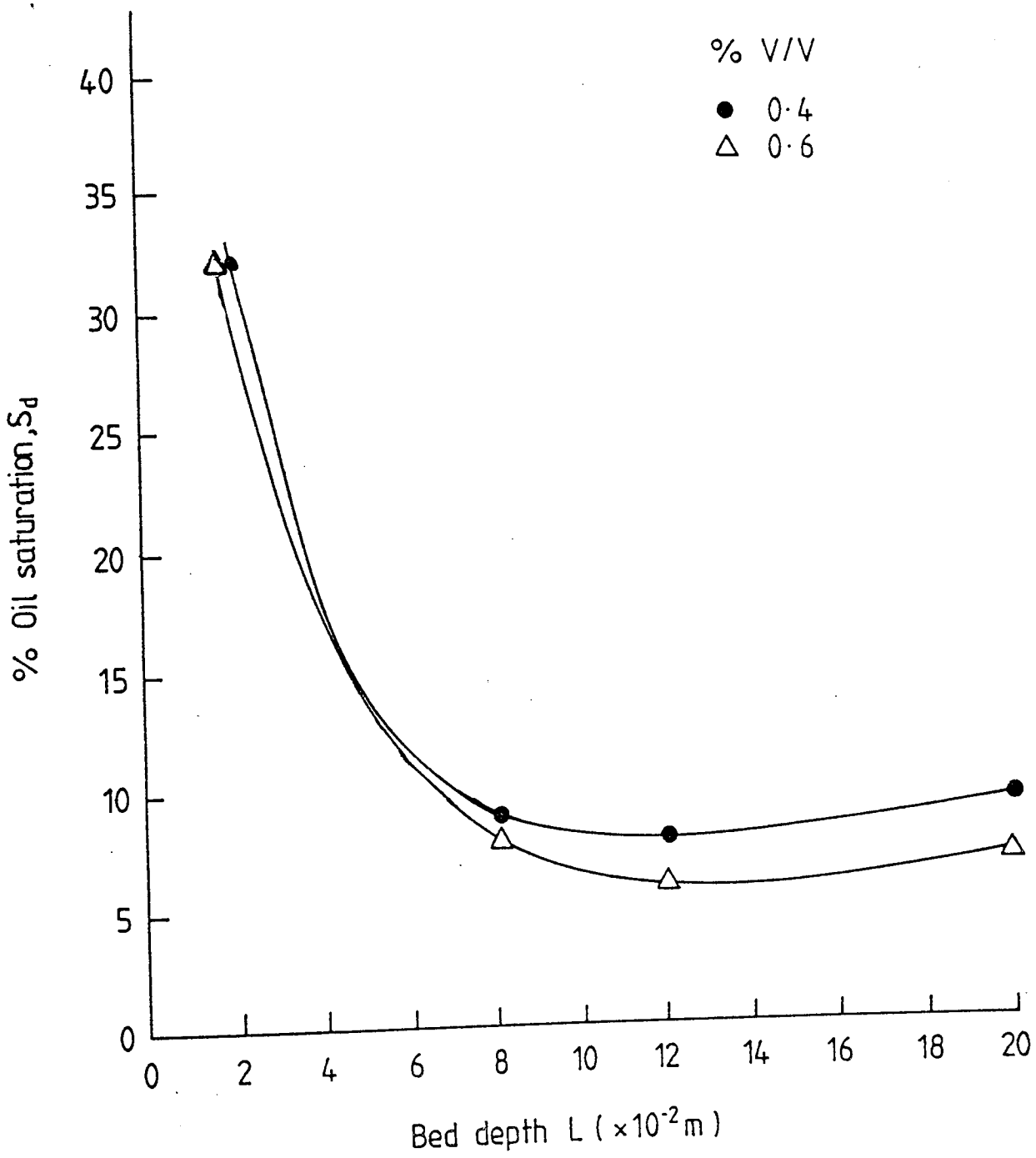

Figure 9·10 Effect of concentration of dispersed phase on Saturation vs Bed depth.
Ballotini 93 μm, 20×10^{-2} m Bed depth. Velocity 5×10^{-2} m/s

Bed Height (m)	Superficial Velocity m/s ($x10^{-2}$)	$\frac{\mu_c UL}{\Delta p_1}$	$\frac{e_1^3 dc^2}{180(1 - e_1)^2}$
0.08	3.04	8.75	7.2
0.08	3.978	9.5	7.2
0.08	5.038	11.15	7.2
0.12	3.04	10.94	7.84
0.12	3.978	13.2	7.84
0.12	5.038	14.5	7.84
0.16	3.04	11.29	6.66
0.16	3.978	13.88	6.66
0.16	5.038	16.57	6.66
0.2	3.04	12.87	6.45
0.2	3.978	16.36	6.45
0.2	5.038	19.60	6.45

Table 9.5. Comparing Ko Using Two Different Equations for Ballotini Size 267μm.

Bed Height (m)	Superficial Velocity m/s ($x10^{-2}$)	$\frac{\mu_c UL}{\Delta p_1}$	$\frac{e_1^3 d_c^2}{180 (1 - e_1)^2}$
0.08	3.04	9.72	10.92
0.08	3.978	10.9	10.92
0.08	5.038	12.08	10.92
0.12	3.04	11.93	12.59
0.12	3.978	14.31	12.59
0.12	5.038	16.75	12.59
0.16	3.04	12.5	13.59
0.16	3.978	15.27	13.59
0.16	5.038	17.58	13.59
0.2	3.04	13.67	14.81
0.2	3.978	17.35	14.81
0.2	5.038	20.1	14.81

Table 9.6. Comparing K_o Using Two Different Equations for Ballotini Size 367μm

CHAPTER TEN

DISCUSSION OF RESULTS

CHAPTER TEN

DISCUSSION OF RESULTS

10.1. Prediction of filter coefficient

The filter coefficient provides a measure of the overall drop coalescence efficiency of a bed and is defined as

$$\lambda = \frac{-\log_e \left\{ \frac{\text{outlet drop number density}}{\text{inlet drop number density}} \right\}}{L} \qquad 10.1.$$

In this chapter an equation is proposed to predict the filter coefficient for a ballotini bed coalescer(68).

10.2. Theoretical comparison of capture mechanisms

Many mechanisms have been suggested for drop capture in Chapter 4. Although each mechanism contributes to overall drop capture; it is important to determine their relative contribution in drop capture in order to produce an equation for estimation of the drop capture in a coalescer.

The variables investigated in this experimental study involved drop diameter, packing size, and superficial velocity. Direct interception was not included in the analysis since the efficiencies cannot be compared directly and this mechanism only becomes significant when the drop size exceeds the effective aperture diameter. Inertial impaction was also excluded since drop density is less than continuous phase density.

The comparison was made with Happel's cell expression (59) for an assemblage of spheres, A_s, characterising the flow parameter for viscous flow.

The overall efficiency is:

$$\eta_T = \eta_I + \eta_D + \eta_G + \eta_L \qquad 10.2.$$

where $\eta_I = \frac{3}{2} \left(\frac{d_p}{d_c}\right)^2$

$$\eta_D = 4.04 \ (A_s)^{\frac{1}{3}} \left(\frac{d_c U}{D}\right)^{-\frac{2}{3}}$$

$$\eta_G = \frac{d^2 p \ (\rho_d - \rho_c) g}{18 \ \mu_c U}$$

$$\eta_L = 2A_s \left(\frac{d_p}{d_c}\right)^2 \left(\frac{9}{5} \frac{4Q}{9\pi R^2 \ \mu_c U \ d_p^2}\right)^{\frac{1}{3}}$$

where

I is Interception mechanism

D is Diffusion mechanism

G is Sedimentation mechanism

L is London forces mechanism

All four mechanisms investigated were found to be relevant to coalescence of secondary dispersion, and the calculated values of η_T are presented in table 10.1. The domain associated with each mechanism is also expressed qualitatively in table 10.2., where its significance is recorded if its contribution is greater than 5% of the total efficiency.

Figure 10.2. indicates that at high velocity, interception is the most important mechansim. Figure 10.3.

DROP DIAMETER dp (μm)	SUPERFICIAL VELOCITY, U($x10^{-2}$ m/s)						
	2.0	2.5	3.0	3.5	4.0	4.5	5.0
5	0.0194	0.0177	0.01724	0.0168	0.01657	0.01632	0.01611
10	0.0518	0.05124	0.0507	0.0503	0.0499	0.0497	0.0494
25	0.2887	0.2873	0.2861	0.2852	0.2846	0.784	0.2833

Table 10.1. Total Capture Efficiency for the Range of Velocities and Drop Diameters Encountered in Secondary Dispersion Coalescence for Ballotini Size 367μm

DROP DIAMETER dp (μm)	SUPERFICIAL VELOCITY, U($\times 10^{-2}$ m/s)						
	2.0	2.5	3.0	3.5	4.0	4.5	5.0
5	IL	IL	IL	IL	IL	IL	IL
10	IL	IL	IL	IL	IL	IL	IL
25	IL	IL	IL	IL	IL	I	I
30	I	I	I	I	I	I	I

Table 10.2. Significant of Different Capture Mechanisms at 5% Contribution Level for Range of Velocities and Drop Diameters Encountered in Secondary Dispersion Coalescence for Ballotini Size 367μm.

DROP DIAMETER dp (μm)	SUPERFICIAL VELOCITY, U($x10^{-2}$ m/s)						
	2.0	2.5	3.0	3.5	4.0	4.5	5.0
5	IL	IL	IL	IL	IL	IL	IL
10	I	I	I	I	I	I	I

Table 10.3. Significance of Different Capture Mechanisms at 5% Contribution Level for Range of Velocities and Drop Diameters Encountered in Secondary Dispersion Coalescence for Ballotini Size 147.5μm.

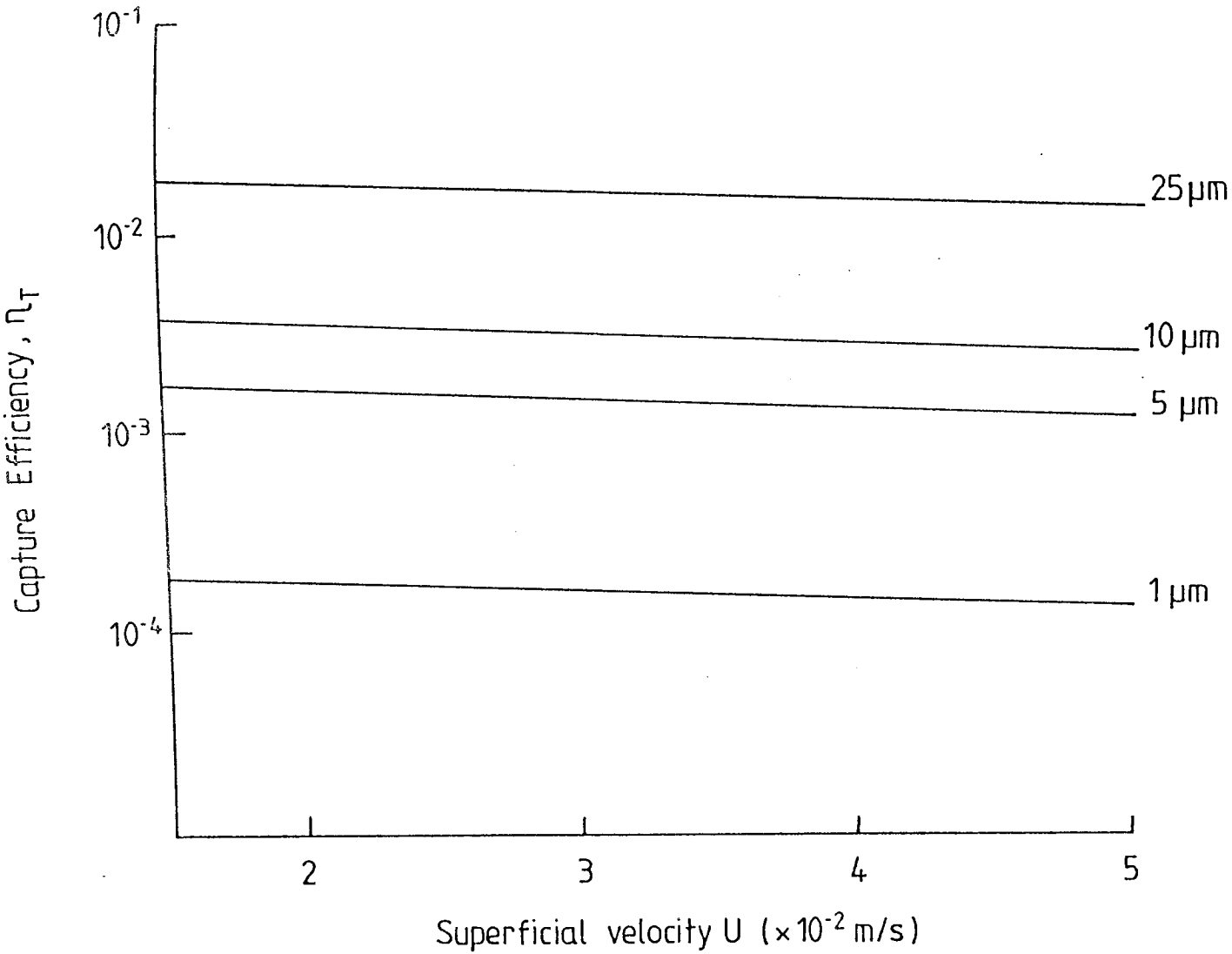

Figure 10·1 Variation of total capture efficiency with velocity for different drop sizes.

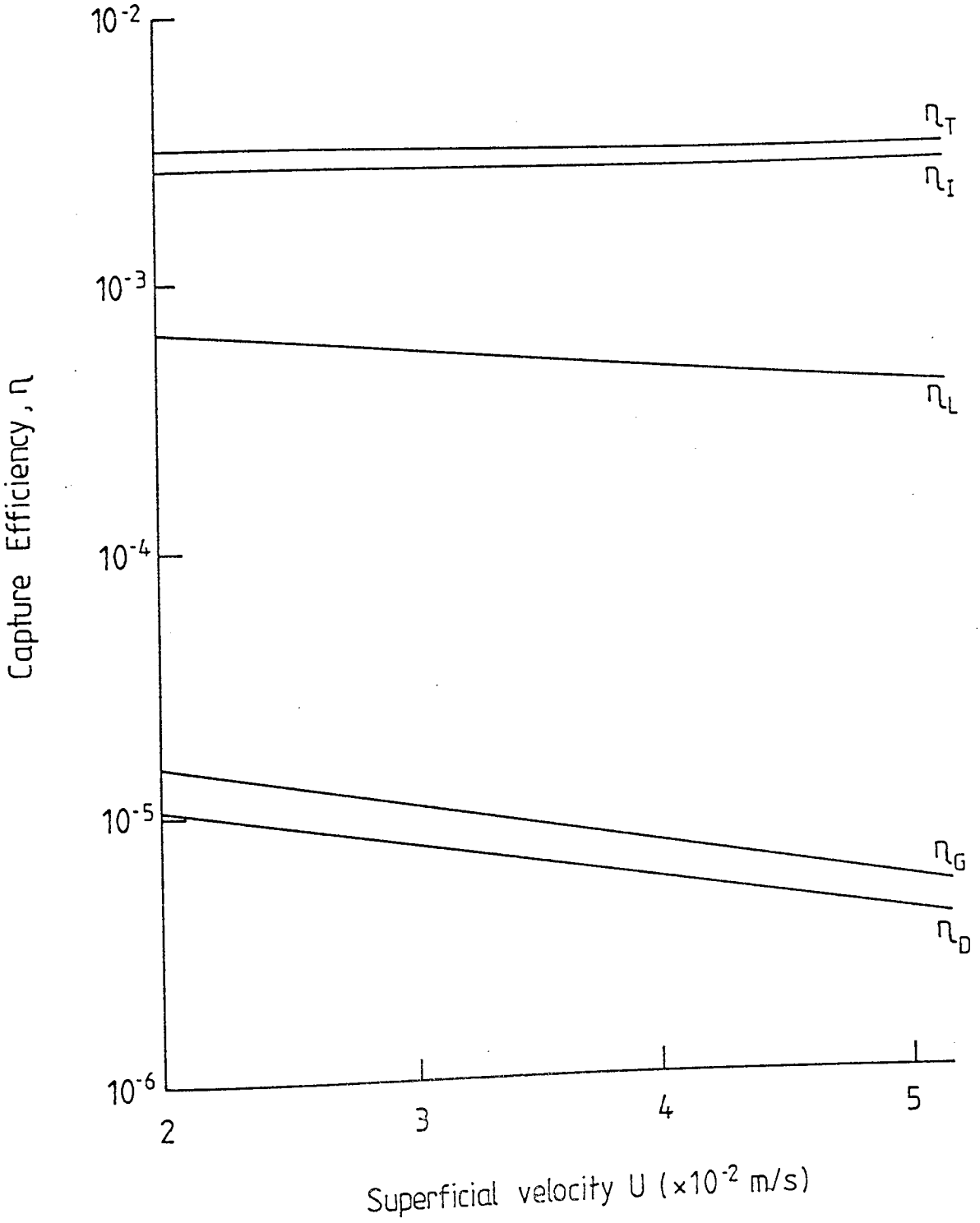

Figure 10·2 Variation of capture efficiency with velocity at 10 μm.

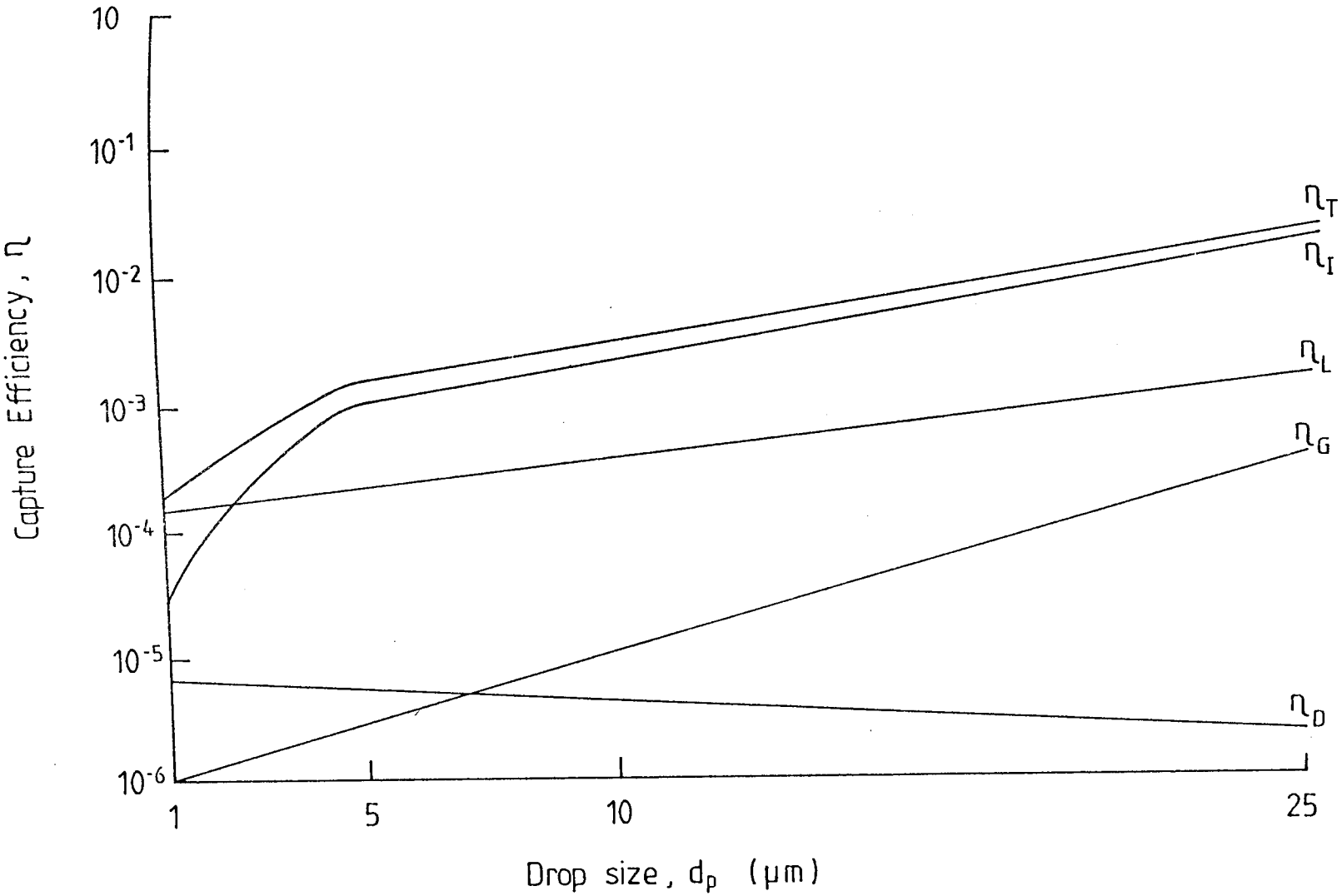

Figure 10·3 Variation of capture efficiency with drop size at 4×10^{-2} m/s.

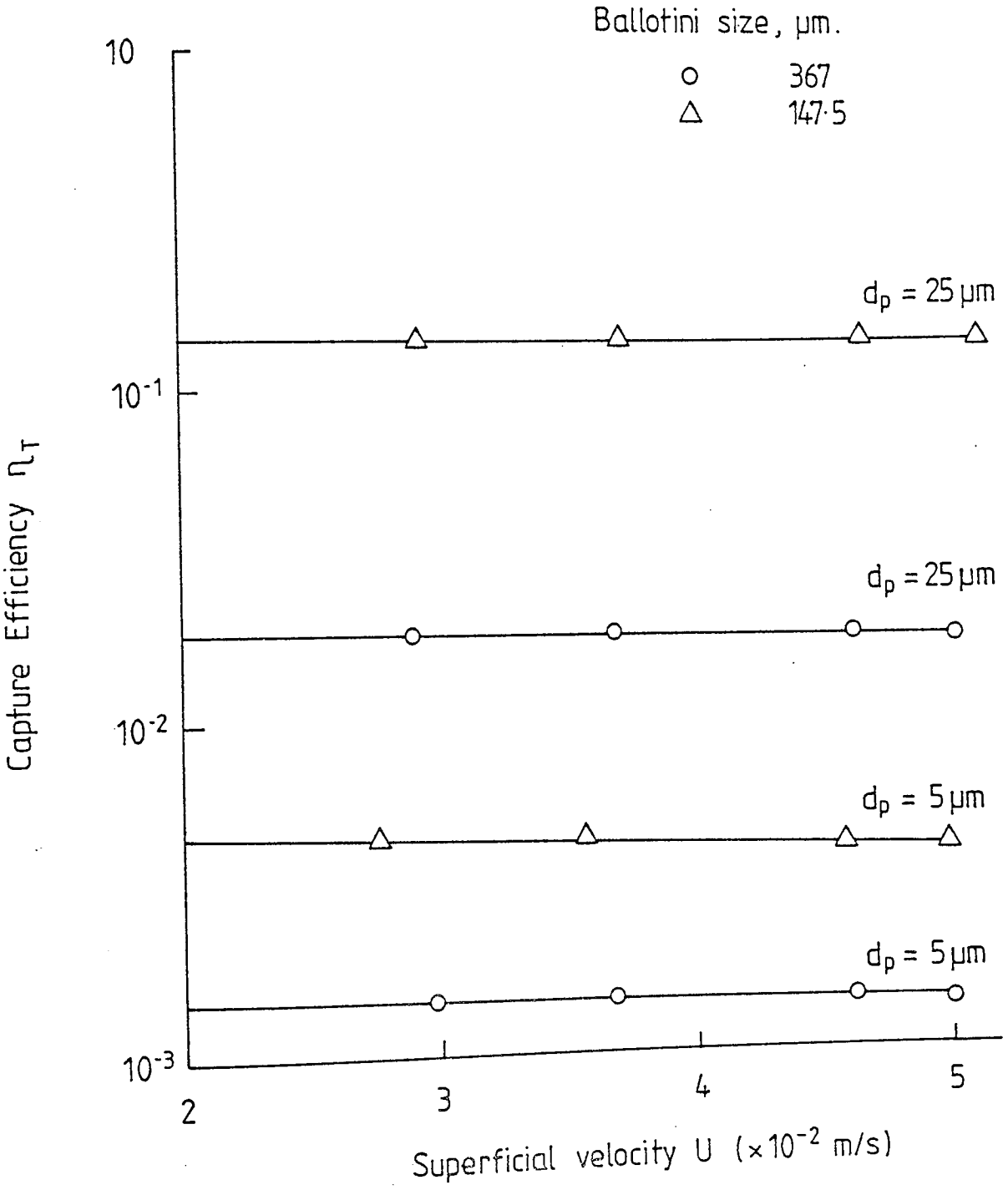

Figure 10·4 Variation of total capture efficiency with velocity for different Ballotini sizes.

shows that for drops less than 5μm diffusion becomes the most significant mechanism, whereas for drops larger than 5μm, interception and sedimentation are the significant mechanisms. Also the significance of London van der Waal's mechanism increases as the inlet drop size decreases, and its contribution to drop capture increases as the packing size is increased, Figure 10.2. and 10.3.

From the above discussion, for drops larger than 5μm the contribution of diffusion is negligible and this mechanism may be eliminated from the overall capture efficiency.

From Figure 10.4. it can be seen that as ballotini size in the bed increased the total capture efficiency decreased, this supports what has been reported in section 8.4.

10.2.1. Screening of mechanisms

Different formulae have been proposed when more than one capture mechanism is important. Spielman and Goren (16) have shown that the collection efficiency by simultaneous interception and diffusion is of the form:

$$\eta_{ID}\ RN_{pe} = f(N_{Ad},\ A_s U\ a_p^3/Da_c^2) \qquad 10.3.$$

if retardation is neglected. After substitution of

$$D = K'T/6\pi\mu_c a_p$$

$$\frac{A_s U a_p^3}{Da_c^2} = \frac{6\pi\mu_c U A_s a_p^4}{K' T a_c^2} = \frac{2}{3}\frac{Q}{K'T}\frac{1}{N_{Ad}} \qquad 10.4.$$

and as $A_s R^3 N p_e = A_s \frac{a_p^3}{a_c^3}\left(\frac{2a_c U}{D}\right) = \frac{4}{3}\frac{Q}{K'T}\frac{1}{N_{Ad}}$ 10.5.

from equations 10.4. and 10.5.

$$\eta_{ID} R N_{pe} = R\ (N_{Ad},\ K'T/Q) \qquad 10.6.$$

From equation 10.6. the group (K'T/Q) is very nearly constant in most experimental studies so ($\eta_{ID} R N_{pe}$) depends on N_{Ad} alone.

The dimensionless collection efficiency is then

$$\frac{N_{ID}}{\eta_I} = \frac{N_{ID}}{1.5\ R^2 A_s} = \frac{N_{ID} R N_{pe}}{1.5\ A_s R^3 N_{pe}} = \frac{F(N_{Ad}, K'T/Q)}{2(Q/K'T)N_{Ad}} = G(N_{Ad}, K'T/Q) \qquad 10.7.$$

If the collection efficiency by London attraction and diffusion can be approximated by the sum of their respective efficiencies then,

$$\frac{\eta_{LD}}{1.5R^2 As} = \frac{\eta_L}{1.5R^2 A_s} + \frac{\eta_{LD}}{1.5R^2 A_s}$$

or

$$\frac{\eta_{LD}}{\eta_I} = f(N_{Ad}) + 2.22\ N_{Ad}^{2/3}\left(\frac{K'T}{Q}\right)^{\frac{2}{3}} \qquad 10.8.$$

where $\eta_D = 4.04 A_s^{\frac{1}{3}} N_{pe}^{-\frac{2}{3}}$

SUPERFICIAL VELOCITY $x10^{-2}$	$\frac{\eta_{ILD}}{\eta_I}$	$\frac{\eta_T}{\eta_I}$	DIFFERENCE %
2.0	1.1747	1.2	2.1
2.5	1.1741	1.1926	1.55
3.0	1.1736	1.18	0.54
3.5	1.1732	1.1707	0.21
4.0	1.17299	1.16259	0.88
4.5	1.17277	1.1575	1.3
5.0	1.17258	1.1518	1.76

Table 10.4. Total Capture Efficiency for Ballotini Size 376 x 10^{-6}m Inlet Drop Size 10 x 10^{-6}m.

There were two assumptions to be made, firstly, the coalescence rate exhibited first order kinetics when expressed as a function of the intermediate phase saturation S'', and secondly that the fraction of newly captured drops is negligible ie. $S''' \rightarrow 0$.

Despite differences between absolute values of local saturation, attributable to different operating parameters of the system and packing media, the shapes of the saturation profiles exhibit several common factors. There is a maximum value of the saturation at the inlet face which appears to have a constant value, independent of superficial velocity, as the bed depth, $l \rightarrow 0$. Secondly the local saturation decays with bed depth at a rate which depends on velocity to a minimum value, which remains constant as far as the exit face. The profiles found by Shalhoub (48) and Bitten (13) indicate a slight increase in local saturation just upstream of the exit face for which no explanation was given. In this experimental study, it was not possible to measure the saturation profile without interfering with the coalescence process, but as presented in the previous section, by using pressure drop measurements across the bed and relative permeability correlations, the saturation profiles for the system were obtained. These profiles are in excellent agreement with those of previous workers. Typical data from a number of studies are presented in Figures 10.6. and 10.7.

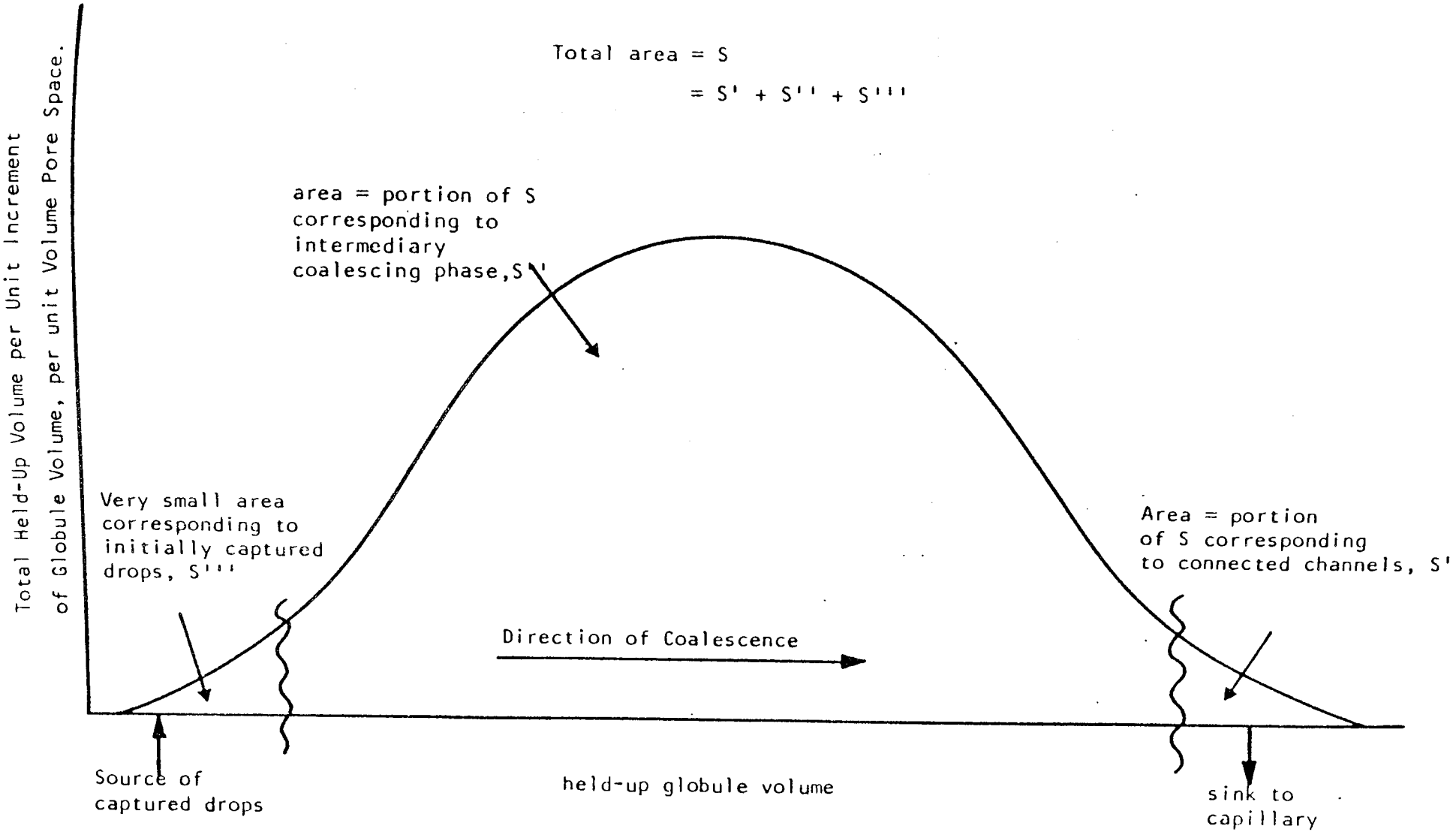

Figure 10.5. Qualitative distribution of the total volume of held-up oil over individual held-up globule volumes. Drops are captured at the left hand of the spectrum. Dispersed phase is transferred to successively larger drops by coalescence eventually leaving the capillary conduction at the right.

10.3.2. Mathematical description of saturation profiles

Based on the general trends shown by experimental data Austin (66) proposed an idealised saturation profile, illustrated in Figure 10.8. Since the saturation at the inlet face cannot be infinite, a small length L_I where the saturation has a constant value, S_I, was proposed. S_I was assumed to be independent of velocity. Thereafter, the saturation decays exponentially at a rate characterised by the value of K which is a function of velocity. The decrease continues until a final value of saturation, S_E, is attained which is also dependent on velocity.

ie. $S = S_I \qquad 0 < \ell \leq L_I$

$$S = (S_I - S_E)e^{-K(\ell - L_I)} + S_E \qquad L_I \leq \ell \leq L \qquad 10.10.$$

This expression was fitted to the saturation profile to find the value of K by regressional analysis according to Appendix D. The value of S_E was taken as the lowest value of the saturation before the slight increase in local saturation at the bed exit.

In Figures 10.9/10/11 some of the experimental and predicted saturation profiles are presented. These demonstrate that the model can be used to mathematically represent the system, the only drawback being that the inlet saturation, S_I, predicted is always higher than the experimental values obtained.

Since the drop capture near the inlet face is high and the inlet drop size distribution is a polydispersion,

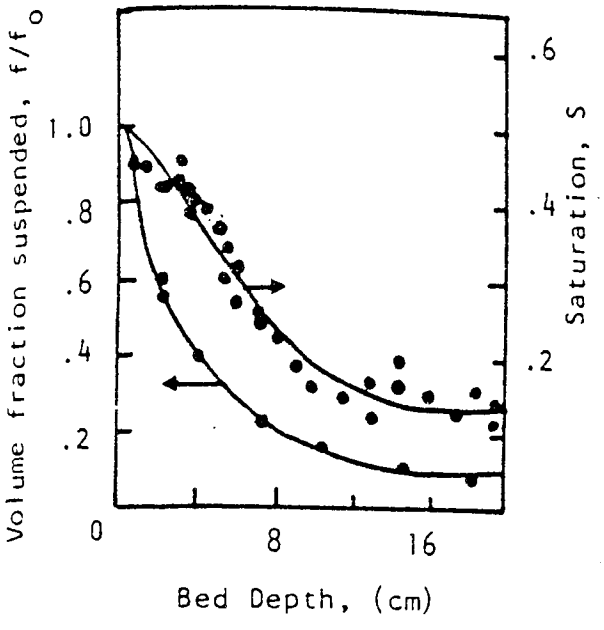

d_c = 0.5mm, μ_d = 50 cP

u = 0.3 cm/s, $f_o = 2 \times 10^{-4}$

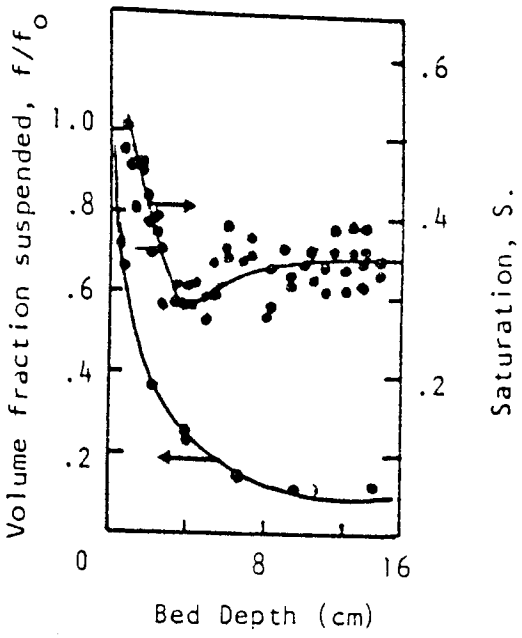

d_c = 0.36 mm, μ_d = 500 cP

u = 0.3 cm/s, $f_o = 8 \times 10^{-4}$

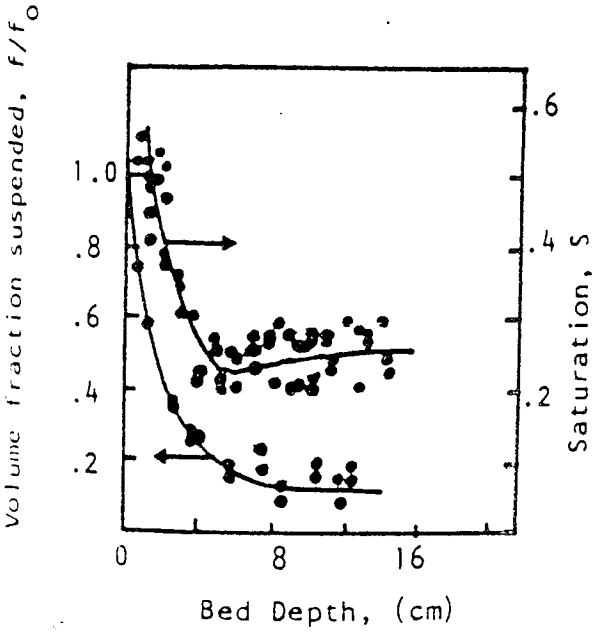

d_c = 0.36, μ_d = 500 cP

u = 0.3 cm/s, $f_o = 2. \times 10^{-4}$

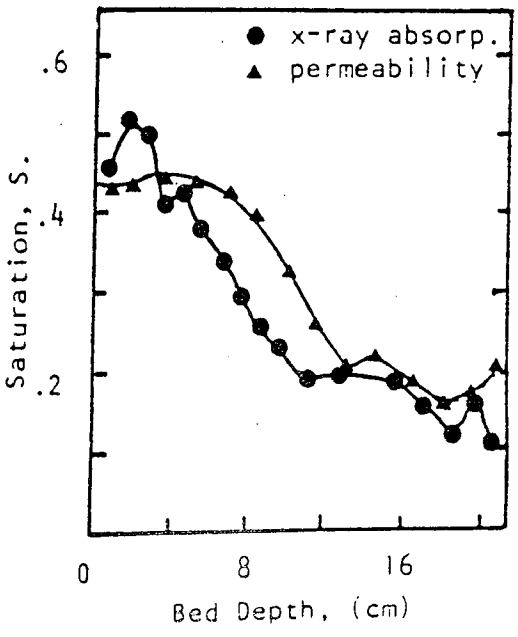

d_c = 0.36 mm, μ_d = 50 cP

u = o.6 cm/s, $f_o = 2 \times 10^{-4}$

Figure 10.6. Variation of Volume Fraction of Suspended Drops and Dispersed Phase Saturation with Bed Depth. (Data of Spielman and Su)

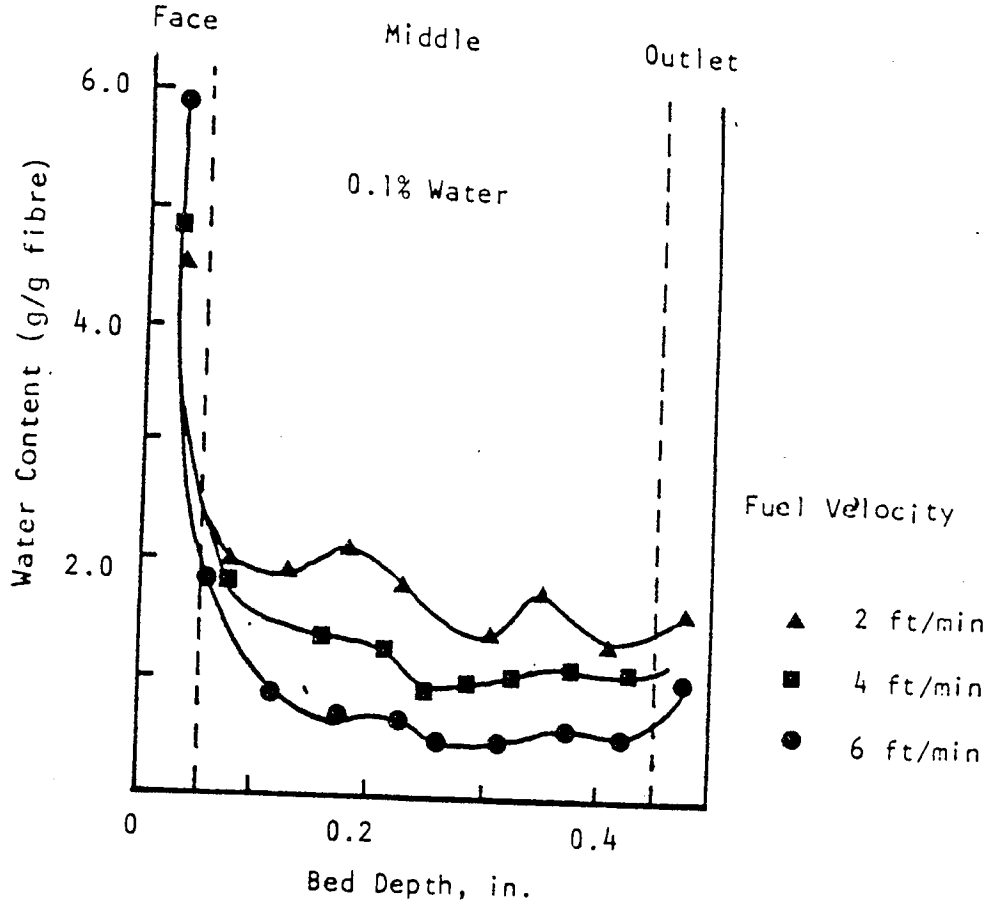

(a) ½ inch thick fibreglass coalscer (6 lb/ft^3).

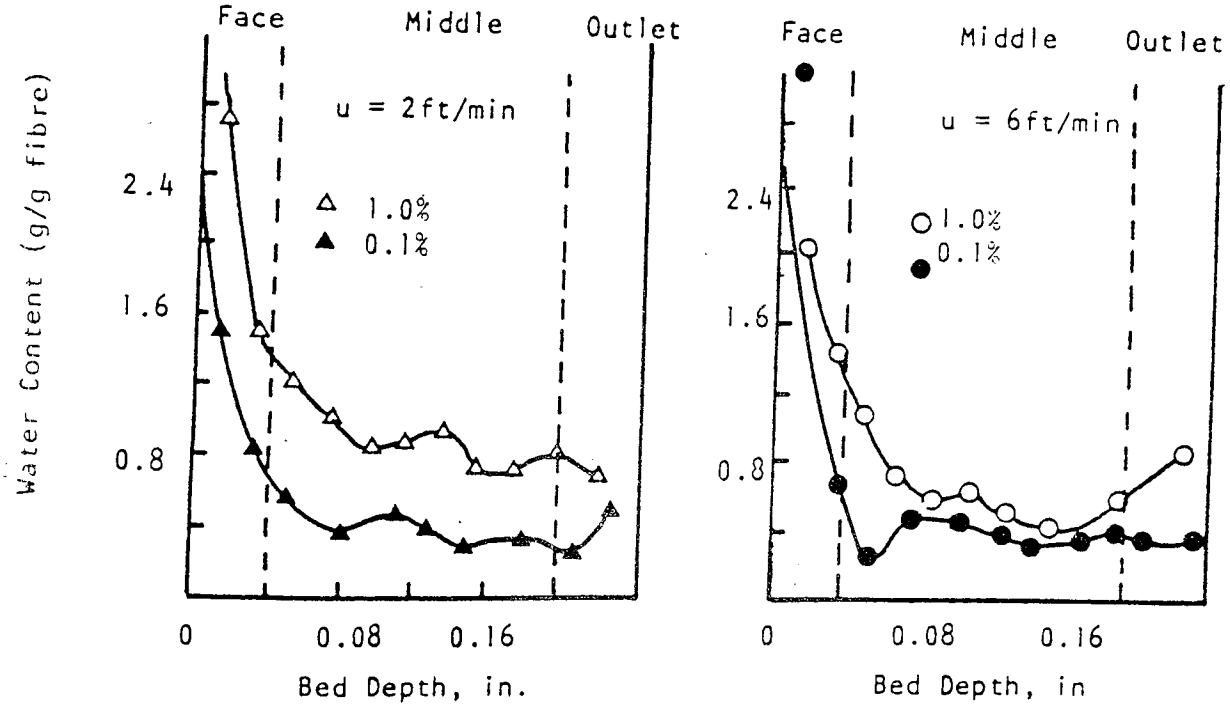

(b) ½ inch thick fibreglass coalscer (14 lb/ft^3)

Figure 10.7. Variation of Hold-Up with Bed Depth.
(Data of Bitten and Fochtman).

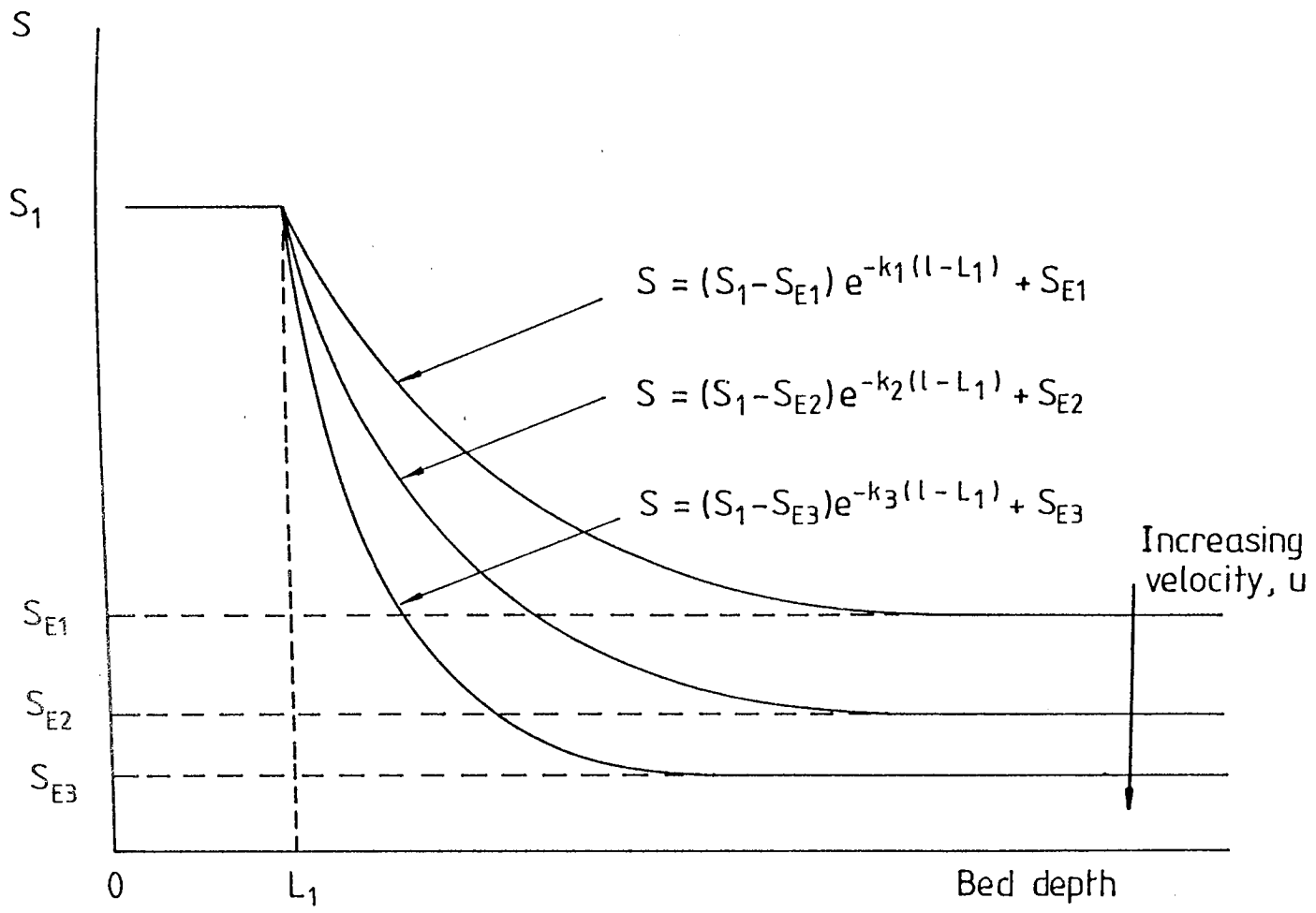

Figure 10·8 Idealised saturation profiles.

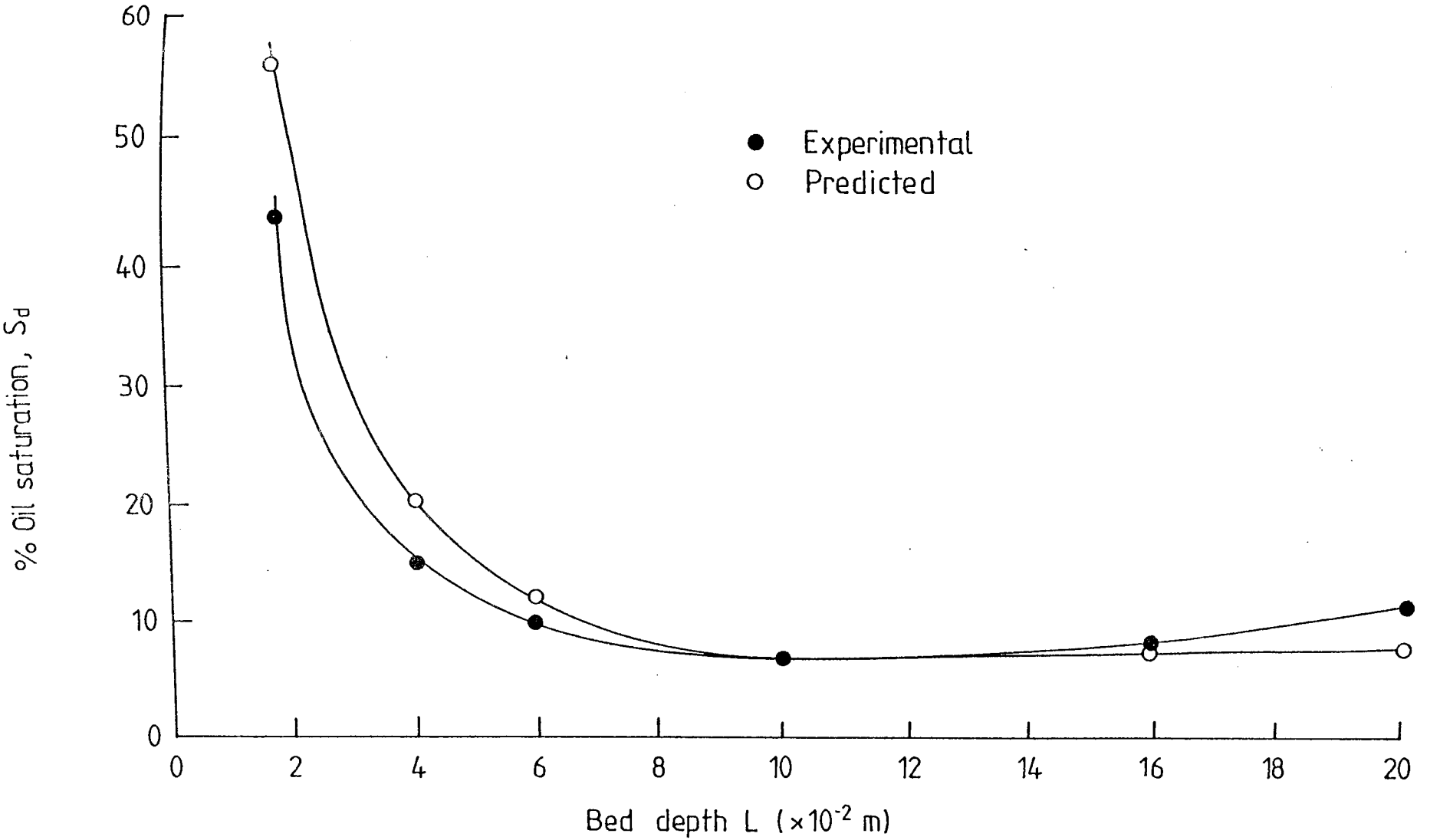

Figure 10·9: Experimental and predicted dispersed phase saturation vs. Bed depth for 93 μm Ballotini, 20×10^{-2} m Bed depth, 5×10^{-2} m/s velocity and 1% V/V Dispersed phase concentration.

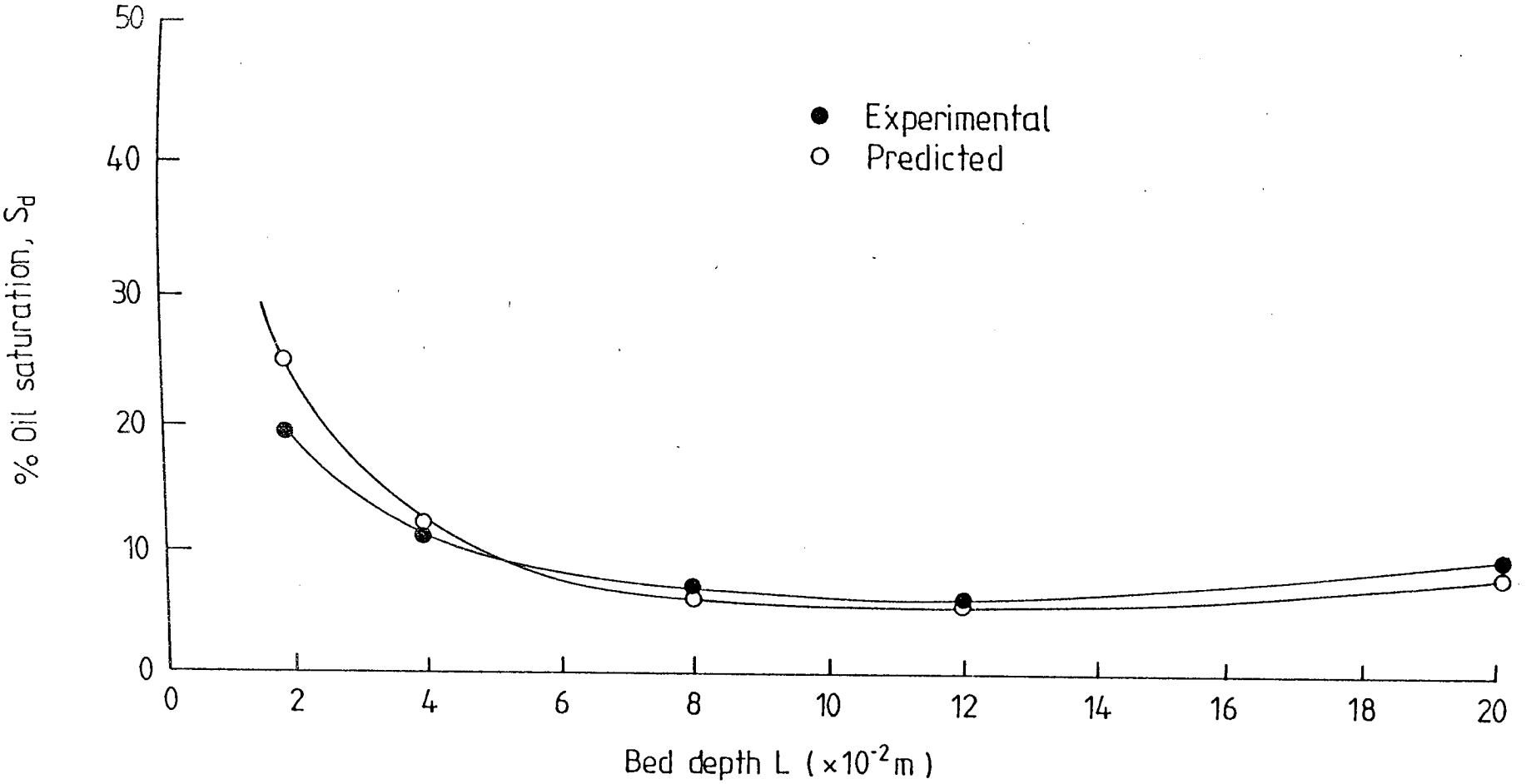

Figure 10·10 Experimental and predicted dispersed phase saturation vs. Bed depth for 367 μm Ballotini size, 20×10^{-2} m Bed depth, 4×10^{-2} m/s velocity and 1% V/V Dispersed phase concentration.

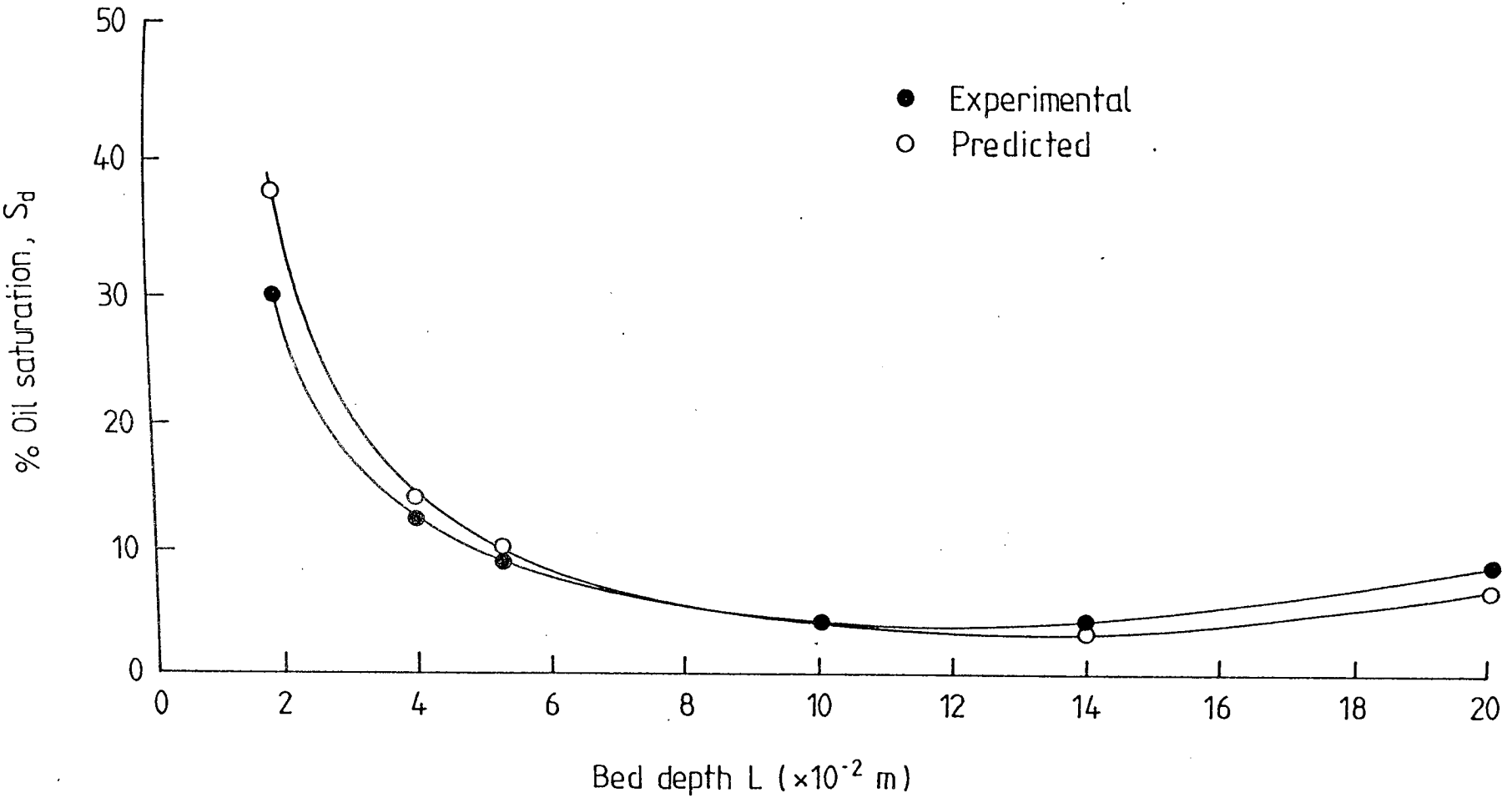

Figure 10·11 Experimental and predicted dispersed phase saturation vs. Bed depth for 367 μm Ballotini size, 3×10^{-2} m/s velocity, and 1% V/V Dispersed phase concentration

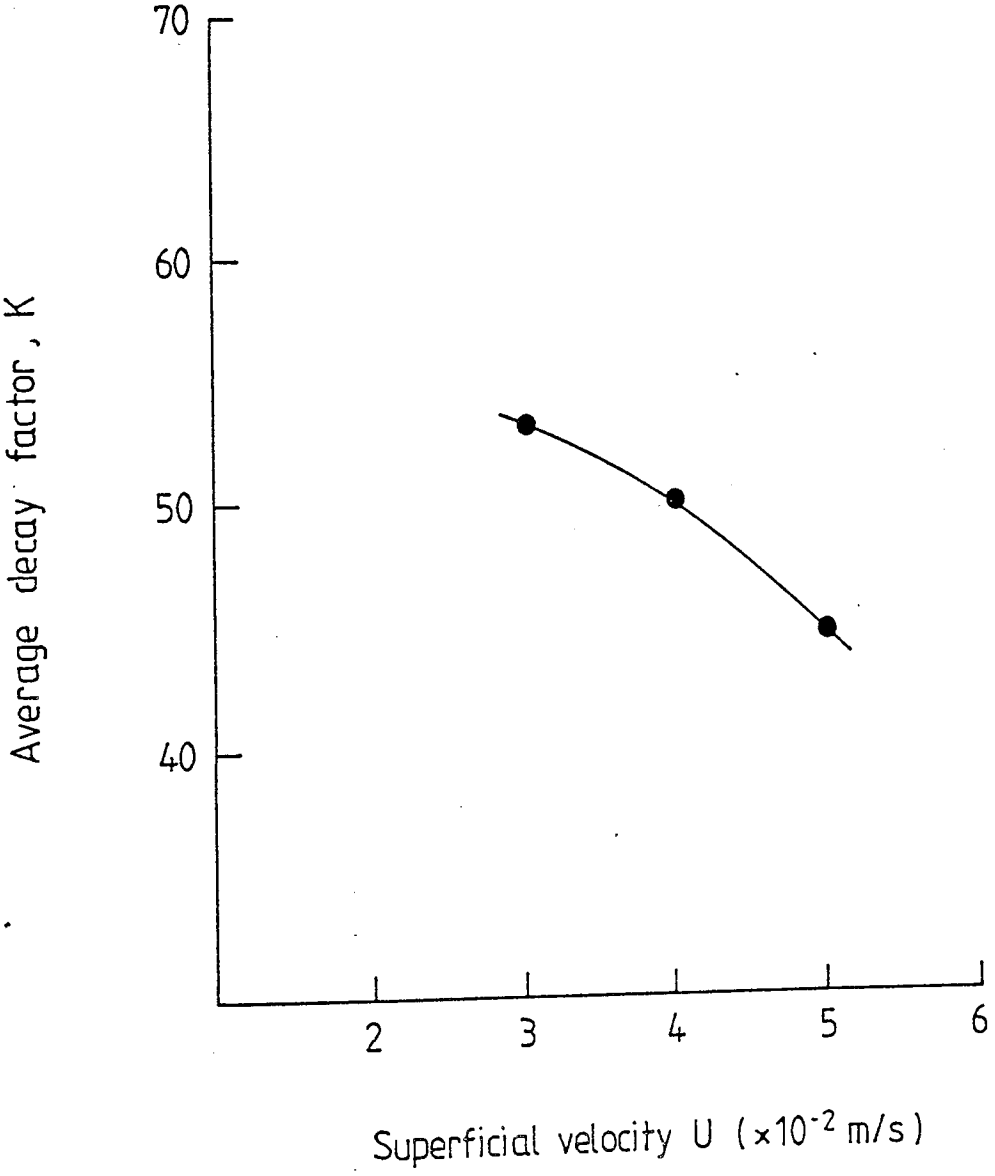

Figure 10·12 Average decay factor vs. velocity.
Ballotini 367 μm, 16×10^{-2} m Bed depth
1% V/V Dispersed phase concentration.

a saturation equivalent to the void fraction of the bed of mixed spheres would be expected. Brown (32) gave a correlation between void fraction and the diameter ratio $\frac{d_p}{d_a}$ which for a mean drop size 25μm and aperture diameter of 99.6μm, $\frac{d_p}{d_a} = 0.251$ gives $e_p = 0.437$ corresponding to a saturation of 0.56. This value is in close agreement with the data of Spielman and Su (34) and with the value obtained from relative permeability calculations in this study. This value will be used as a reference when predicting values of S_I. The experimentally determined profiles all indicate that decay of saturation with bed depth occurs very close to the inlet face implying that L_I is very small. However, since the saturation must be zero at the inlet face, in the absence of flooding, a small finite value of L_I was fixed at 1cm from the bed inlet. After a value for the rate of decay, K, has been found, L_I can be taken to be as small as the length of single ballotini layer. Then assuming the saturation profiles are unchanged, a new value of K can be calculated. Although the saturation will increase from 0 to S_I within a small distance from the inlet face, ie. $<<L_I$, omission of the thin section of the saturation profile from the integration of equation 10.10. will not incur any significant error.

In Figure 10.12. the average value of K obtained has been plotted against superficial velocity. The value of K decreases with an increase in superficial velocity suggesting that for the experiments $S_I \rightarrow S_E$ nearer to the inlet of the bed. This may be due to the fact that, despite the greater

influx of captured drops at higher velocities, the existence of larger hydrodynamic forces causes the drops to progress through the bed more quickly.

10.4. Two phase pressure drop prediction

10.4.1. Derivation of proposed equation

As the Carman-Kozeny equation proved to be successful for correlation of single phase pressure drops, it was used as the basis for this model. However the Carman-Kozeny equation must be modified since during two phase flow, the bed consists effectively of a mixture of spheres of different diameters which possess different values of specific surface, a.

Two equations have been proposed to describe two phase pressure drop, one for large ballotini sizes of 267μm and 367μm, the other for small ballotini sizes of 93μm and 147.5μm.

10.4.2. Derivation of proposed equation for ballotini sizes

For single phase flow through an element of bed δ_L

$$\frac{\delta P_1}{\delta L} = \frac{K \mu_c U(1 - e_1)^2 a_1^2}{e_1^3} \qquad 10.11.$$

For two phase flow,

$$\frac{\delta P_2}{\delta L} = \frac{K \mu_c U(1 - e_2)^2 a_2^2}{e_2^3} \qquad 10.12.$$

where $e_2 = e_1(1 - s)$

and

$$a_2 = \frac{\frac{6e_1 s}{d_p} + 6\frac{(1 - e_1)}{d_c}}{1 - e_1 \quad (1 - s)} \qquad 10.13.$$

for a mixture of spheres, Appendix C.

Substituting for e_2 and a_2 into equation 10.12. and taking the limit as $\delta L \to 0$.

$$\frac{dP_2}{dL} = 36K\mu_c U \frac{\left(\frac{e_1 s}{d_p} + \frac{(1 - e_1)}{d_c}\right)^2}{e_1^3 \ (1 - S)^3} \qquad 10.14.$$

By integration of equation 10.14., two phase pressure drop may be determined between the limits of 0 and L.

$$\Delta p_2 = \frac{36K\mu_c U}{e_1^3} \int_0^L \frac{\left(\frac{e_1 s}{d_p} + \frac{(1 - e_1)}{d_c}\right)^2}{(1 - S)^3} \, d\ell \qquad 10.15.$$

Similarly from equation 10.11. and substituting for a_1

$$\Delta p_1 = \frac{2.25 \ \mu_c \ U(1 - e_1)^2 L}{e_1^3 \ dc^2} \qquad 10.16.$$

$$\Delta p_2 = \frac{36K\mu_c U}{e_1^3} \int_0^L f(s) \, d\ell \qquad 10.17.$$

by letting $b = \frac{1}{d_p}$ and $c = \frac{1}{d_c}$

Where

$$f(s) = \frac{\left(\frac{e_1 s}{dp} + \frac{1 - e_1}{d_c}\right)^2}{(1 - s^3)} \qquad 10.18.$$

the right hand side of equation 10.18. becomes

$$f(S) = \frac{b^2 e_1^2 S^2 + 2bce_1 S(1 - e_1) + (1 - e_1)^2 C^2}{(1 - S)^3} \qquad 10.19.$$

to simplify the coefficients

$$d = b^2 e_1^2,\ f = 2bce_1 (1 - e_1),\ i = (1 - e_1)^2 c^2$$

equation 10.19. will be

$$f(S) = \frac{dS^2 + fS + i}{(1 - S)^3}$$

considering equation 10.17., the integration of f (S) cannot be performed in one stage since discontinuity appears in the mathematical description of the saturation profile. When $0<\ell<L_T$ $S = S_I$ and is independent of ℓ therefore

$$\int_0^{L_I} f(S)\, d\ell = \frac{(dS_I^2 + fS_I + i)\, L_I}{(1 - S_I)^3}$$

when $L_I<\ell<I_/S_I = (S_I - S_E)e^{-K(\ell - L_I)} + S_E$

let $g = (S_I - S_E)$; $h = S_E$

and substituting

$$v = g^{e^{-K(\ell - L_I)}} + h$$

$$\frac{dv}{dl} = -Kg^{e^{-K(\ell - L_I)}} = K(v - h)$$

$$dl = \frac{dv}{K(v - h)}$$

when $\ell = L_I$, $v = g + h$

$\ell = L$, $v = g\, e^{-K(L - L_I)} + h$

$$\therefore \int_{L_I}^{L} f(S)\, d1 = \int_{g+h}^{ge^{-K(L-L_I)}} f(V) - \frac{dv}{K(V-h)}$$

$$= \frac{1}{K} \int_{ge^{-K(L-L_I)}-h}^{g+h} \frac{f(V)}{(V-h)}\, dv$$

$$= \frac{1}{K} \int_{ge^{-K(L-L_I)}+h}^{g+h} \frac{dv^2 + fU + i}{(V-h)(1-V)^3}\, dv \qquad 10.20.$$

Evaluation of the integral given by equation 10.20. is completed in Appendix E.

The total pressure drop across the bed

$$\Delta p_2 = \frac{36K\mu_c U}{e_1^3} \int_0^{L_I} f(S)\, d\ell + \int_{L_I}^{L} f(S)\, d\ell \qquad 10.21.$$

for small ballotini size <147.5μm, and from the experimental results, table 10.6.

$K = 2.26$

$$\Delta p_2 = \frac{81.36\mu_c U}{e_1^3} \int_0^{L_I} f(S)\, dl + \int_{L_I}^{L} f(S)\, d\ell \qquad 10.22.$$

for large ballotini size >267μm, and from the experimental results, table 10.5.

$K = 7$

$$\Delta p_2 = \frac{252\mu_c U}{e_1^3} \int_{L}^{L_I} f(S)\, dl + \int_{L_I}^{L} f(S)\, d\ell \qquad 10.23.$$

The two phase pressure drop may be predicted from single phase pressure drop (71). For single phase pressure drop

$$\frac{\delta P1}{\delta L} = \frac{K\mu_c (1 - e_1)^2 a_1^2 U}{e_1^3} \qquad 10.24.$$

where $a_1 = \frac{6}{a_c}$ for spheres

$$\Delta p_1 = \frac{36K\mu_c(1 - e_1)^2 LU}{e_1^3 d_c^2} \qquad 10.25.$$

dividing equation 10.15. by 10.24.

$$\frac{\Delta p_2}{\Delta p_1} = \frac{d_c^2}{(1 - e_1)^2 L} \int_0^L f(S)\, d\ell \qquad 10.26.$$

$$\int_0^L f(S)\, d\ell = \int_0^{L_I} f(S)\, d\ell + \int_{L_I}^{L} f(S)\, d$$

$$\frac{\Delta p_2}{\Delta p_1} = \frac{d_c^2}{(1 - e_1)^2 L} \int_0^{L_I} f(S)\, d\ell + \int_{L_I}^{L} f(S)\, d\ell \qquad 10.27.$$

In this case the predicted two phase pressure drop is the same for all ballotini sizes, due to cancellation of Kozeny constant by dividing with single phase pressure drop.

Bed Height (m)	e_1	$K = \frac{e_1^3 \, d_c^2}{180 \, (1 - e_1)^2}$
0.08	0.402	7.2
0.08	0.402	7.2
0.08	0.402	7.2
0.12	0.41	7.84
0.12	0.41	7.84
0.12	0.41	7.84
0.16	0.395	6.66
0.16	0.395	6.66
0.16	0.395	6.66
0.2	0.392	6.45
0.2	0.392	6.45
0.2	0.392	6.45

Table 10.5. Experimental Evaluation of Kozeny Constant for 267μm.

Bed Height (m)	e_1	$K = \frac{e_1^3 \, d_c^2}{180 \, (1 - e_1)^2}$
0.08	0.42	2.66
0.08	0.42	2.66
0.08	0.42	2.66
0.12	0.395	2.03
0.12	0.395	2.03
0.12	0.395	2.03
0.16	0.392	1.97
0.16	0.392	1.97
0.16	0.392	1.97
0.2	0.41	2.4
0.2	0.41	2.4
0.2	0.41	2.4

Table 10.6. Experimental Evaluavtion of Kozeny Constant for 147.5μm.

10.5. Queueing drop model

10.5.1. Derivation of queue length equation

The function of this model is to predict the filter coefficient using average saturation data. It is based on the hypothesis that drops are captured in the entry section of the bed where they accumulate until coalescence into a dispersed phase continuum occurs. The dispersed phase is then conveyed in discrete channels to the release sites located on the exit face of the coalescer. The model recognises an analogy between drops waiting to coalesce into a dispersed phase continuum and 'customers' queueing at a service facility.

Austin (68) made the following assumptions

(i) Poisson arrival distribution of mean arrival rate, λ.

(ii) Exponential service distribution of mean service rate, μ.

(iii) Queue discipline is on a first come, first served basis.

(v) No simultaneous arrivals or service, which eliminates terms of second order int.

(vi) Under steady state conditions, the number in the system exceeds the number of service channels, ie. $n \geq \mu$ and there are no constraints governing the queue length. The resulting equation was,

$$Lq = \sum_{n=1}^{\infty} \frac{n \rho^n \gamma^{n(n-1)}}{\sum_{n=1}^{\infty} \rho^n \gamma^{n(n-1)}} \qquad 10.28.$$

Derivation of this equation is in Appendix F.

10.5.2. Filter coefficient

The filter coefficient may be related to the fraction of customers, f_n which undergo 'balking' from

$$f_n = \gamma^{2n}; \quad f_{n-1} = \gamma^{2n-2} \qquad 10.29.$$

for steady state conditions when $n = L_q$

$$f_{Lq} = \gamma^{2Lq} \qquad 10.30.$$

the filter coefficient λ_c is given by

$$\lambda_c = \frac{-\log_e(1 - f_{Lq})}{L} \qquad 10.31.$$

substituting for f_{Lq} from equation 10.29. and the bed depth

$$\lambda_c = \frac{-\log_e(1 - \gamma^{2L_q})}{2\ dc\ N_L} \qquad 10.32.$$

The experimental filter coefficient λ_e was determined by using Vinson and Churchill's equation

$$\lambda_e = \frac{-\log_e \{0.128(U\ d_c\ \mu_c)^{-0.4} - 0.089\}}{L} \qquad 10.33.$$

Table 10.7. lists the values of λ_e and λ_c, and it can be noticed that the average difference between the filter coefficient is 20% so either equation can be used to measure the filter coefficient, for practical purposes. The length of the 'queue' may be estimated from experimental data if the quantity of the dispersed phase held in the packing interstices is transformed into a number of drops of characteristic diameter, dp. If 'balking' is solely responsible for a separation efficiency of less than 100% then dp may be taken, so the mean linear diameter of the inlet dispersion

$$L_q = \frac{3e_1 \, dc \, D^2 S N_L}{dp^3} \qquad 10.34.$$

Also comparing the results of equations 10.32. and 10.33. the maximum difference between both sets of results does not exceed 16%, this is also shown in Figures 10.13,14, 15.

Superficial Velocity $\times 10^{-2}$ m/s	Ballotini Size $\times 10^{-6}$ m	Bed Height m	λ_e	λ_c
3	147.5	0.12	54.66	56.63
3	267	0.16	39.8	39.5
5	93	0.12	54.5	33.2
3	267	0.12	52.6	35.26
5	367	0.2	29.9	21.3
3	93	0.16	42.15	43.57
4	267	0.2	13.47	10.97
3	147.5	0.16	41	43

Table 10.7. Comparison Between Calculated and Experimental Filter Coefficient.

Ballotini Size µm	Phase Ratio	Bed Depth (m)	Superficial Velocity m/s	No of Channels As Observed From Exit	No. of Exit Drops in Seconds
93	1.0	0.12	5	2	$\frac{15}{31}$, $\frac{5}{30}$
93	1.0	0.08	5	2	$\frac{35}{37}$, $\frac{10}{48}$
93	0.4	0.12	3	1	$\frac{23}{39}$
93	0.6	0.12	4	2	$\frac{12}{50}$, $\frac{10}{56}$
93	0.6	0.12	5	2	$\frac{16}{32}$, $\frac{7}{58}$
93	1.0	0.16	3	2	$\frac{8}{12}$, $\frac{20}{16}$
267	1.0	0.2	3	2	$\frac{10}{12}$, $\frac{10}{24}$
267	1.0	0.12	5	2	$\frac{10}{18}$, $\frac{10}{17}$
367	1.0	0.2	3	1	$\frac{10}{28}$
367	1.0	0.2	5	2	$\frac{12}{16}$, $\frac{10}{18}$
147.5	1.0	0.08	3	2	$\frac{25}{18}$, $\frac{10}{8}$
147.5	1.0	0.12	3	2	$\frac{25}{12}$, $\frac{10}{30}$
100	0.4	0.05	5	1	10
100	0.4	0.05	3	1	2/60

Table 10.8. The Effect of Ballotini Size, Phase Ratio, Bed Depth, Superficial Velocity on the Number of Exit Drops Per Second.

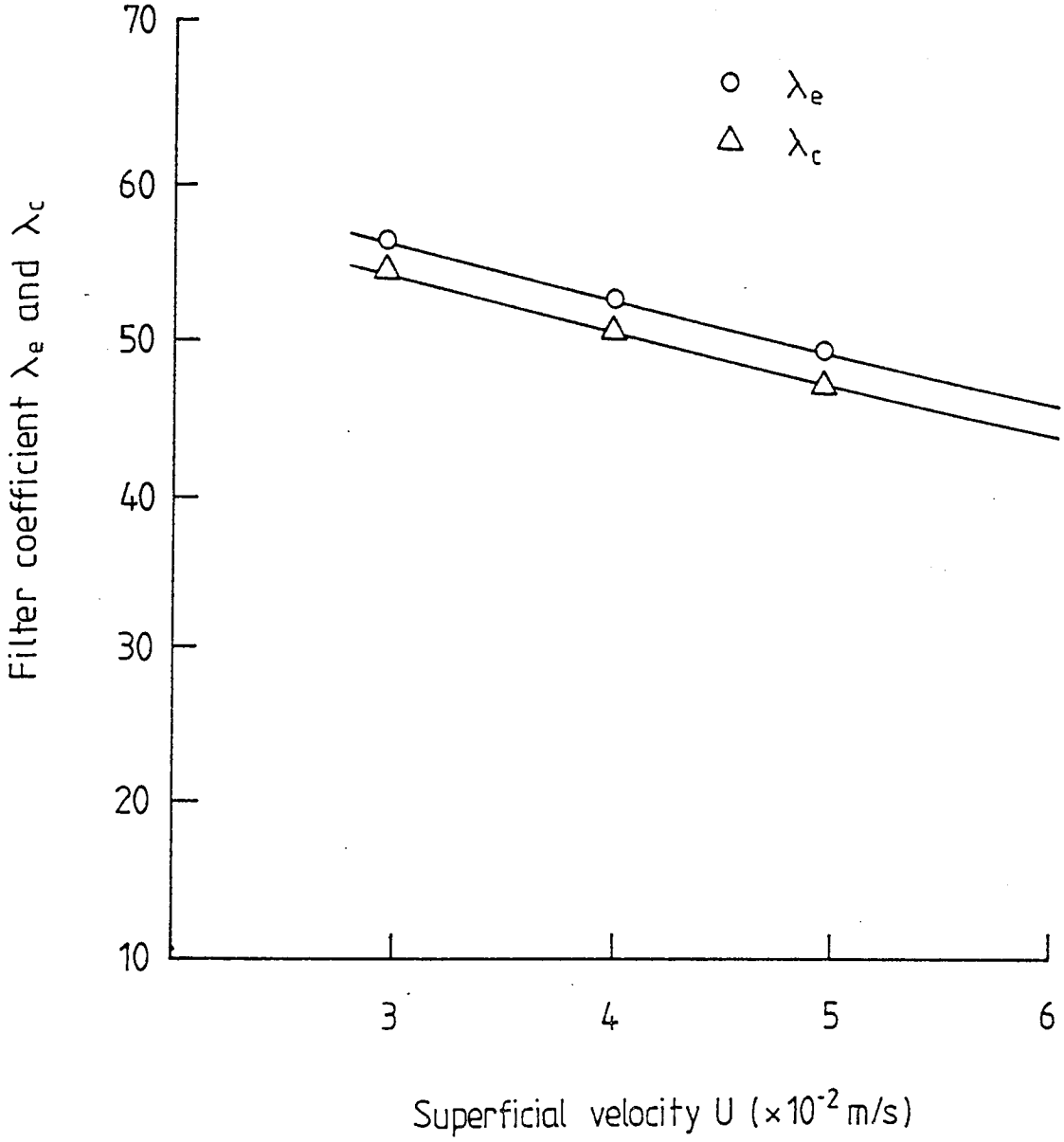

Figure 10·13 The filter coefficient vs. superficial velocity for Ballotini size, 147·5 μm, Bed depth 12×10^{-2} m, 1% V/V Dispersed phase concentration.

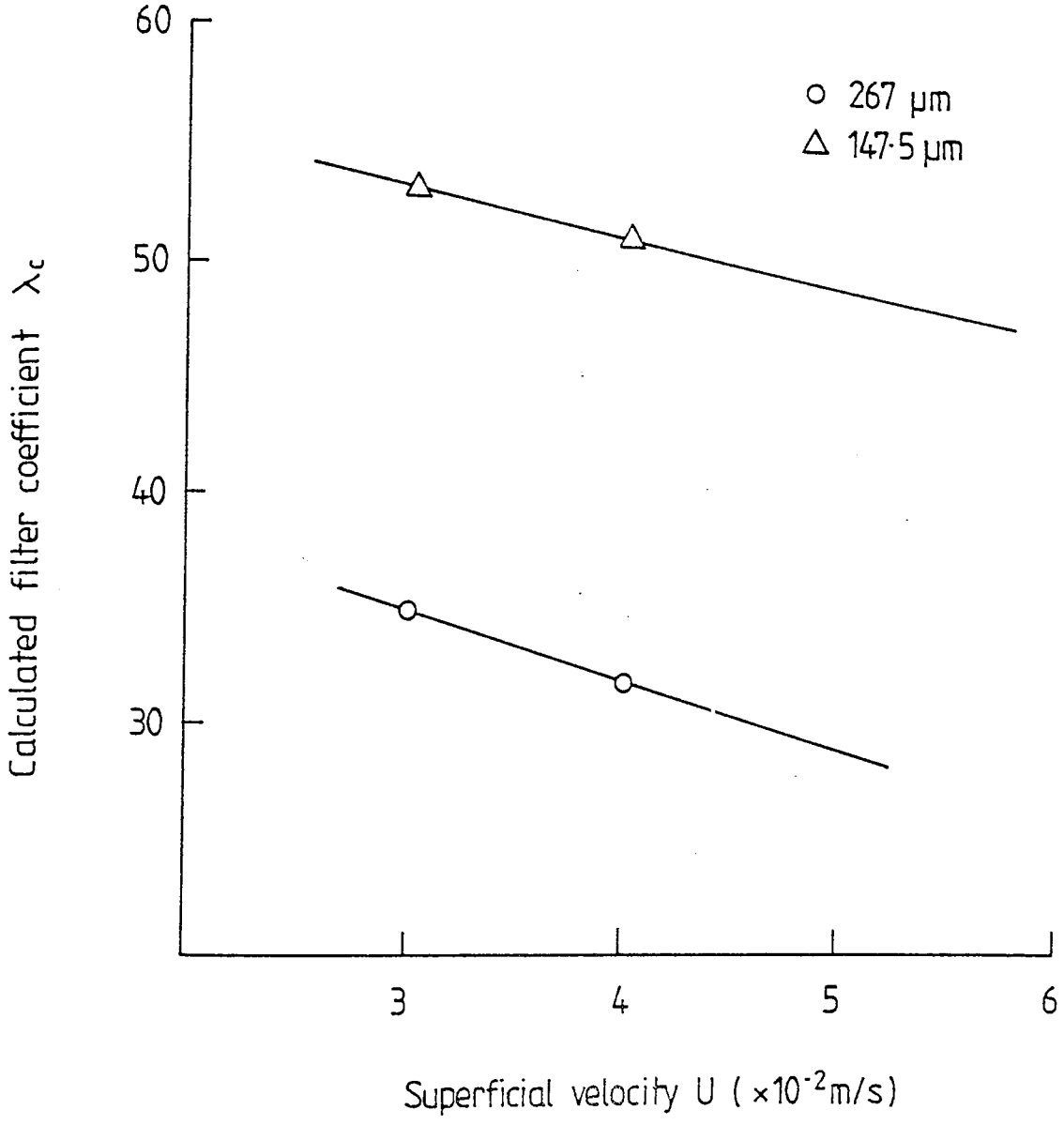

Figure 10·14 Calculated filter coefficient vs. superficial velocity Ballotini sizes 147·5 μm, 267 μm. Bed depth 12×10^{-2}m/s 1% V/V Dispersed phase concentration.

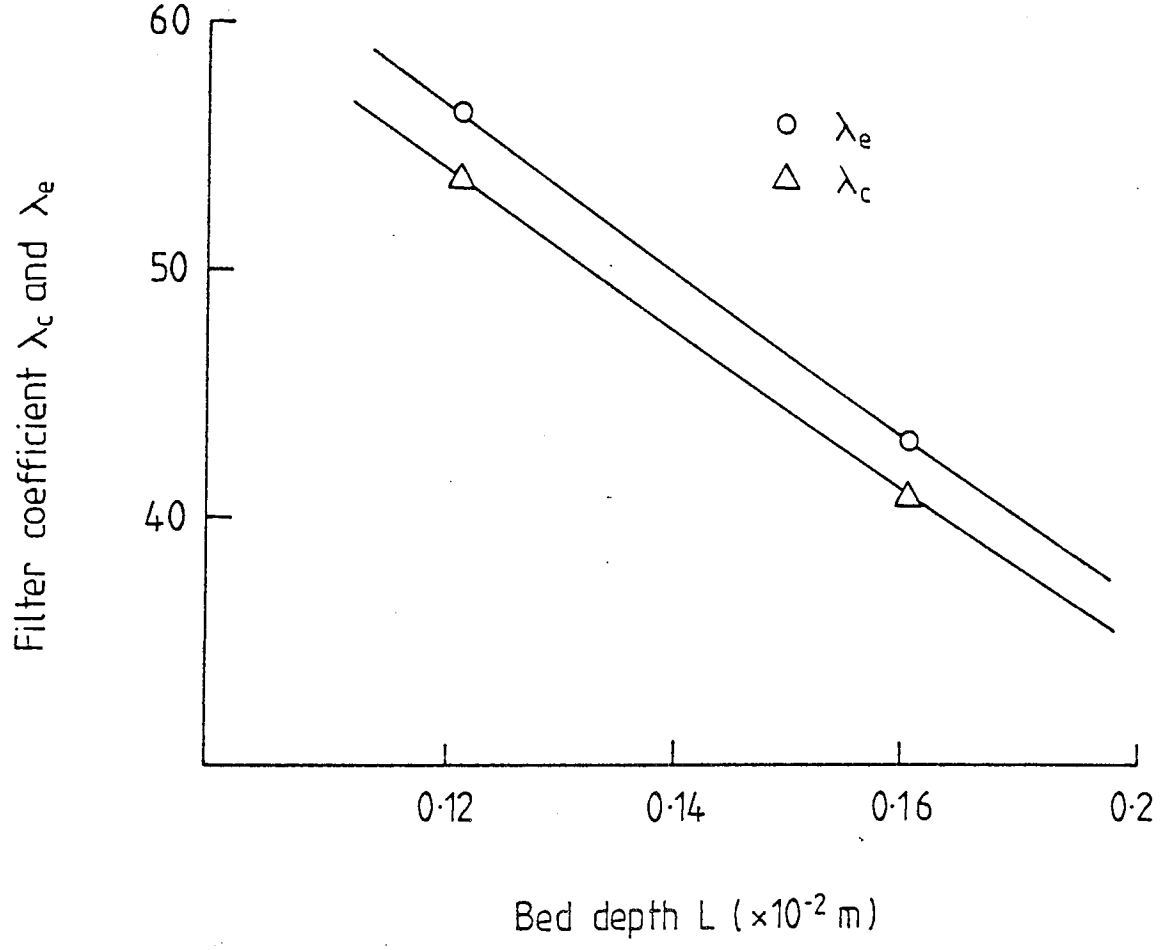

Figure 10·15 The filter coefficient vs. Bed depth.
Ballotini size 147·5 μm, Velocity 3×10^{-2} m/s
1% V/V Dispersed phase concentration.

CONCLUSIONS

CONCLUSIONS

1. There is a maximum velocity above which breakthrough of the dispersion occurred. There is a maximum bed depth above which drop redispersion occurred. The maximum velocity and the maximum bed depth depended on the size of ballotini. For ballotini size 93μm the maximum bed depth was 0.16m and the maximum velocity of 3.978×10^{-2}m/s; at these conditions the separation efficiency was 90%. For 367μm the maximum bed depth before redispersion occurred was 0.2m, and a maximum velocity of 5×10^{-2}m/s; at these conditions the separation efficiency was 55%.

2. The Carman-Kozeny equation was modified to correlate the two phase pressure drop. This modification was found to depend on the size of ballotini, ie. two equations were proposed, one to express the two phase pressure drop for ballotini sizes 93μm and 147.5μm, equation 10.21., the other equation 10.22. is for 267μm and 367μm.

3. The filter coefficient derived from the queueing drop model section 10.5.2. gave a satisfactory result compared with the Vinson and Churchill equation, 10.28.

4. The Macdonald equation was satisfactory to correlate the results of the single phase pressure drop for low Reynolds numbers.

$$\frac{\Delta p_1}{L} = \frac{18\mu_c \, U(1 - e_1)^2}{d_c^2 \, e_1^3}$$

5. The size of ballotini in the third forepart of the bed affects the coalescence efficiency and the exit drop size; the other two thirds do not have any effect on the coalescence efficiency.

6. The overall capture efficiency can be expressed by

$$\frac{\eta_T}{\eta_I} \text{ or } \frac{\eta_{ILD}}{\eta_I}$$

The capture efficiency mechanism depended on the superficial velocity and on ballotini size for drop diameters less than 25μm and the major capture mechanism was interception.

7. The saturation profiles obtained using relative permeability correlations and the experimental pressure drop data, shows the variation of saturation across the bed depth. The maximum saturation at the forepart of the bed decreases with the bed height until it reaches a constant value. The outlet saturation increases slightly.

8. A mechanism of coalescence of secondary dispersion is proposed based upon theoretical and experimental study. Almost 90% of secondary drops are captured by indirect interception; the next main capture mechanism is London van der Waal's forces. The drops reside in the fore-part of the bed either attached to the packing or intercepted by pores, where coalescence occurs until they attain such a size when hydrodynamic forces exceed the restraining interfacial tension and adhesion forces.

The primary drops are then squeezed through the packing interstices in a zigzag or straight ahead fashion within fixed channels of flow. The primary drops flow through these channels in a form of groups with constant interval times. The number of these channels, the number of the primary drops and the interval times depend on the concentration of the dispersed phase.

9. The two phase pressure drop can be predicted by using equation 10.23. for ballotini sizes less than 147.5μm, and using equation 10.24. for ballotini sizes larger than 267μm.

   The two phase pressure drop can also be predicted from single phase pressure drop using equation 10.27. which is applicable for all sizes of ballotini.

10. From primary experiments, it was concluded that as the ballotini size in the bed decreased the separation efficiency increased, until it reached a certain size (93μm) after which the separation efficiency started to decrease due to fluidisation in the bed.

The above conclusions are based on experiments (Chapter 5) covering bed depth - 0.05-0.20m, ballotini size 93μm-367μm and superficial velocity 3×10^{-2} m/s-5×10^{-2} m/s but because of it's bulk only selected data are plotted. The complete lists of data have been deposited in the Department of Chemical Engineering.

RECOMMENDATION FOR FURTHER WORK

RECOMMENDATION FOR FURTHER WORK

The following areas are worth further investigation.

1. Further investigation is needed, into separation using a glass mesh holder instead of the stainless steel mesh. This would eliminate any effects due to different surface energy between the ballotini packing and the steel mesh holder. However there is no evidence that so-called 'junction effects' described for primary drop dispersions exists with smaller spherical drops.

2. A study of performance of a packing consisting of two beds of different ballotini sizes. The smaller size ballotini (93μm) should be used at the inlet of the bed, since coalescence takes place within the lower third of the bed, and the saturation has it's highest value in the same plane of the bed. The use of larger size ballotini (367μm) to form the outlet may reduce the pressure drop, and does not affect the separation efficiency and exit drop size.

   Study would also be worthwhile with the two different sizes of ballotini, separated by free liquid to observe the release mechanisms of primary drops from each part of the bed, and the effect on pressure drop and saturation profiles. (However the unrestricted release from the first part would obviously differ from that in the real case.)

3. As an extension of this study, investigation could be made into ageing of ballotini, to see whether it has an effect on the coalescence mechanism. In the present study it was observed that the longer the ballotini was used, the exit drops had a tendency to accumulate on the top of the packing. This phenomena did not occur with new ballotini. The effect was not attributable to dirt deposition because of the rigorous cleaning procedures used. Surface 'etching' may have been a factor due to the cleaning process.

4. More study is needed on drop release mechanisms, since these determine the exit drop size distribution. In this study release by chaining has been noticed for the first time in oil-in-water systems. Attarzadeh also noticed this release mechanism but for water-in-oil system.

5. As an extension to this study, further investigation could be made of bed performance for ballotini size in the range of 147.5μm-267μm. It was shown that total pressure drop can be expressed by two equations, one for ballotini size larger than 267μm. The point of overlap therefore remains to be determined.

6. Improvements to the queueing model would be advantageous to cover the assumptions from which deviations occur in practice, eg. (a) the variation in useful channels with phase ratio and flow rate, and, (b) the distribution of entering drop sizes. So far as (a) is concerned an

empirical correlation factor could be introduced, eg. on the basis of the preliminary observations shown in table 10.8. Allowance for (b) would clearly be more complex mathematically, involving initially characterisation of the drop size distribution.

APPENDICES

APPENDIX A

Physical properties of liquid system

The physical properties of the liquid system were determined as a function of temperature. The temperature coefficient of density for both continuous and dispersed phases is low in the range between 14°C and 26°C.

Density of water $\rho_c = 998 + 2$ kg/m^2 (R)

Density of Toluene $\rho_d = 867 + 3$ kg/m^3 (R)

The remaining relevant properties are presented as a function of temperature in Figures A.1., A.2., and A.3.

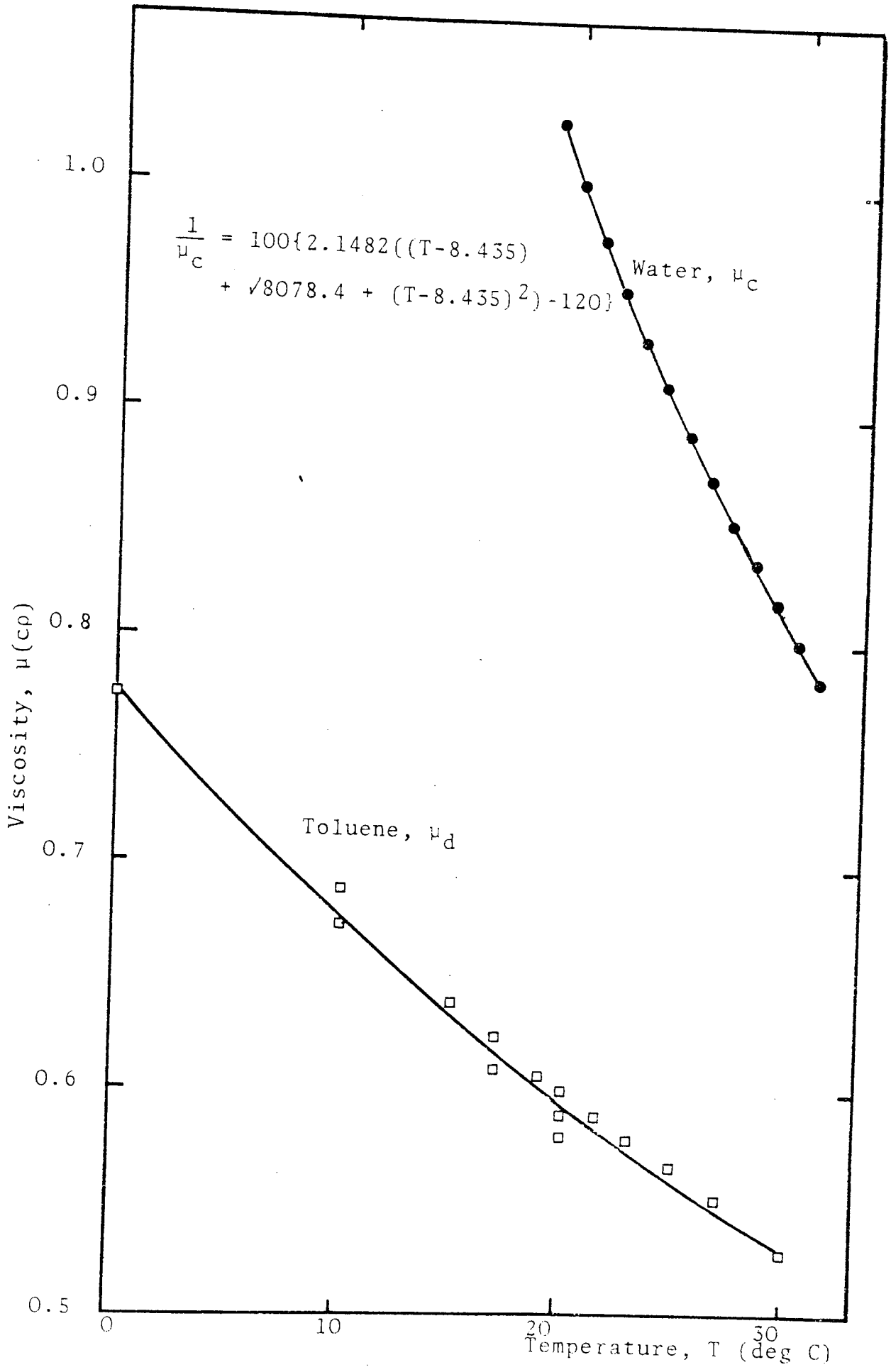

FIG. A.1 Phase Viscosities as a Function of Temperature

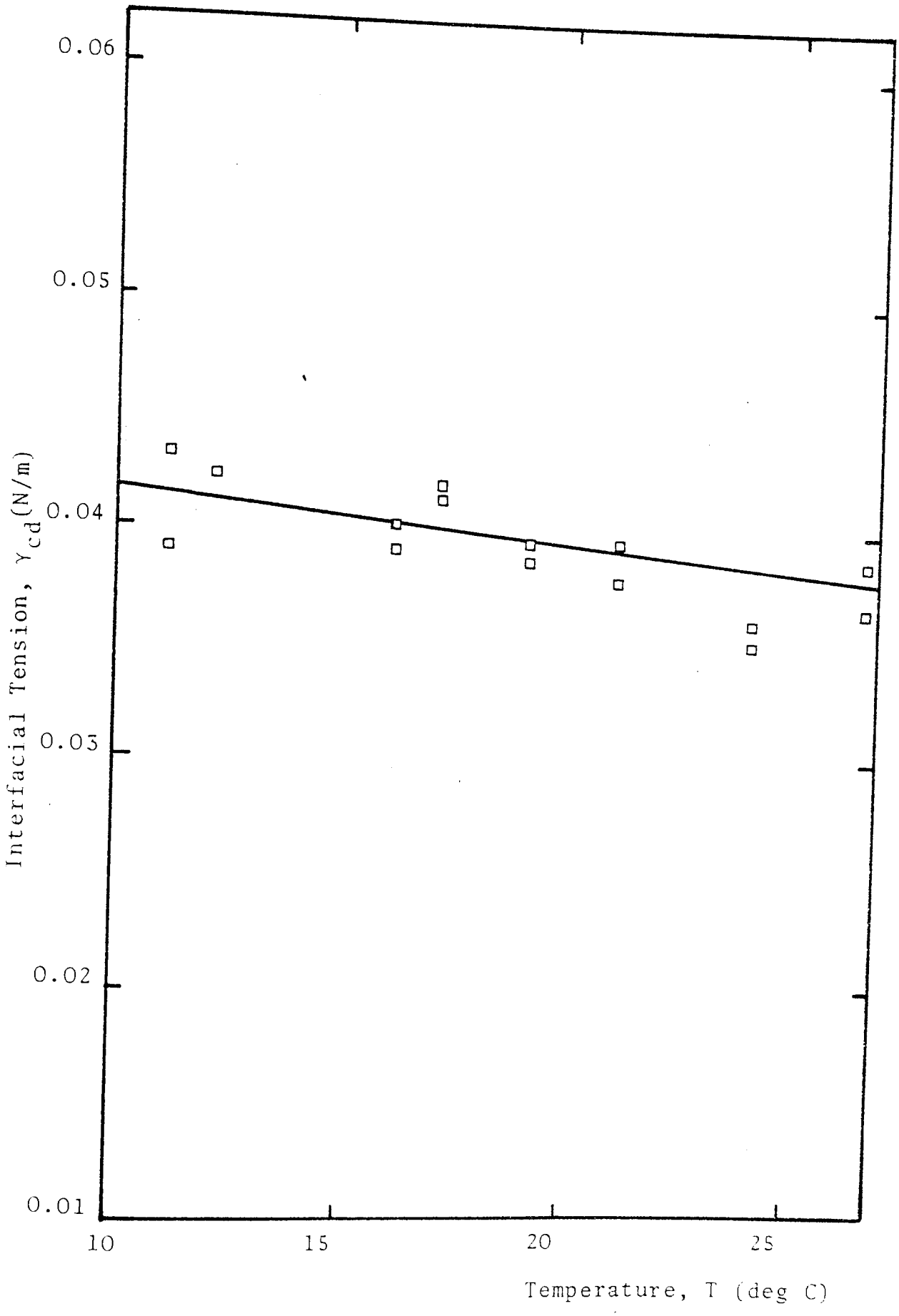

Fig. A.2 Interfacial Tension for Toluene/Water System as a Function of Temperature

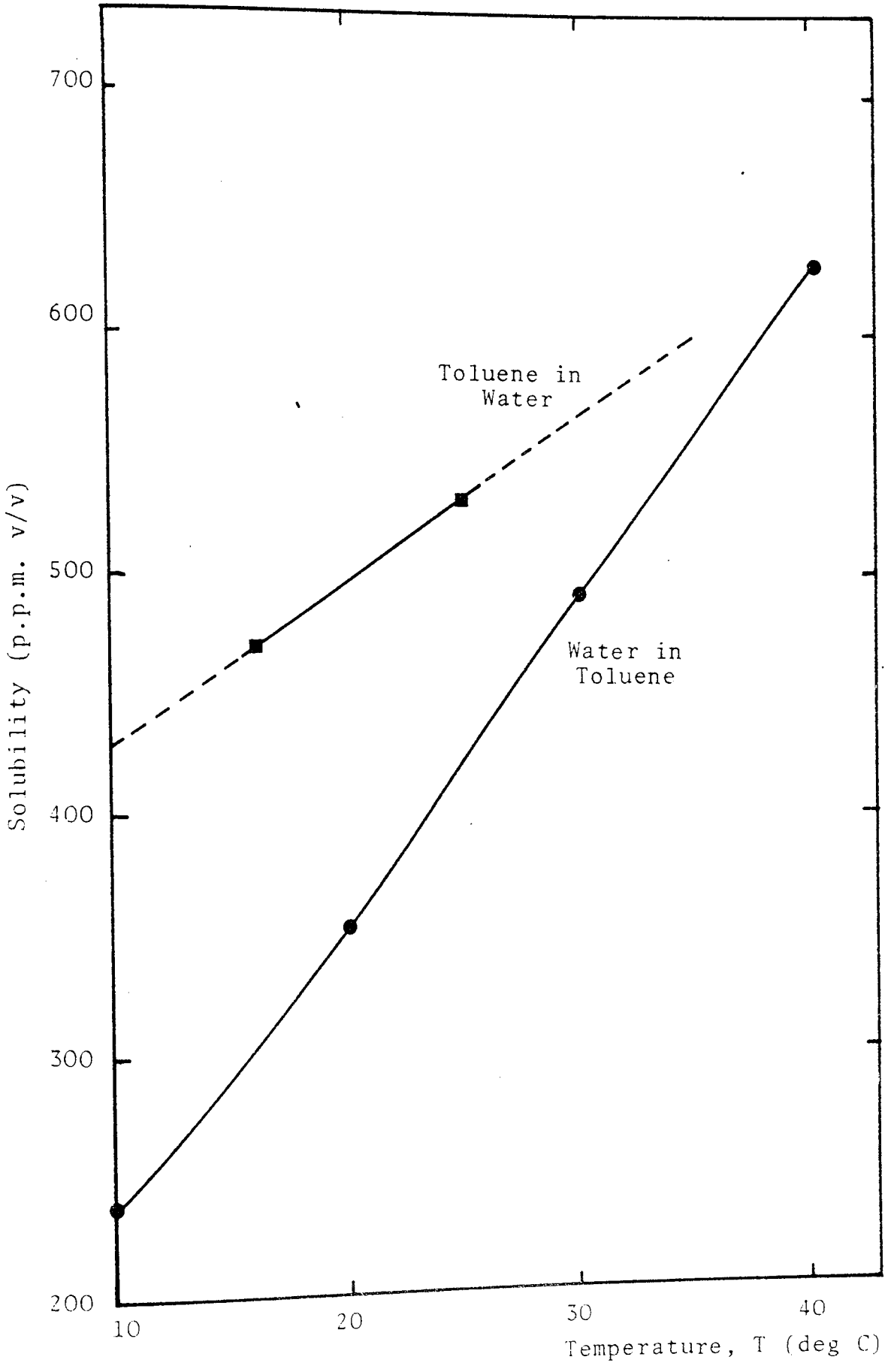

Fig. A.3 Mutual Solubility of Toluene/Water System as Function of Temperature

APPENDIX B

Bed voidage determination

Packing thickness = 5×10^{-2} m

Initial reading = 20.3×10^{-2} m

Volume Collected $\times 10^{-6} m^3$	New Reading $\times 10^{-2}$ m	Distance Drop $\times 10^{-2}$ m
50	15.9	4.4
50	11.6	4.3
50	7.3	4.3
50	1.2	6.1

Distance drop per $50 \times 10^{-6} m^3$ above the packing =

$$\left(\frac{4.4 + 4.3 + 4.3}{3}\right) \times 10^{-2} = 4.333 \times 10^{-2} \text{m}$$

From the last reading

$$6.1 \times 10^{-2} - 5.0 \times 10^{-2} = 1.1 \times 10^{-2} \text{m}$$

This contains $12.7 \times 10^{-6} m^3$ water, but water collected is $50 \times 10^{-6} m^3$

$\therefore$ Hold up of water = $50 \times 10^{-6} - 12.7 \times 10^{-6} = 37.29 \times 10^{-6} m^3$

Volume of packing = $57 \times 10^{-6} m^3$

$\therefore$ Packing voidage = $e_1 = \frac{57 - 37.29}{57} = 0.345$

This procedure was repeated three times to obtain the average value of e_1.

APPENDIX C

Evaluation of specific surface for coalescer containing drops of dispersed phase

$$\text{Specific surface, } a = \frac{\text{(Surface area of drops+surface area of spheres)}}{\text{(Volume of drops+volume of spheres)}}$$

Np = Number of drops per unit volume of bed

surface area = $Np\pi dp^2$

volume = $Np\pi \frac{dp^3}{6}$

N_c = Number of grains per unit volume of bed

surface area = $N_c\pi d_c^2$

volume = $N_c\pi\frac{d_c^3}{6}$

e_1 = void fraction of sphere

$$N_c = \frac{6(1 - e_1)}{\pi d_c^3}$$

e_p = void fraction of drops

$$Np = \frac{6(1 - e_p)}{\pi d_p^3}$$

e_2 = two phase effective voidage

$$e_2 = (e_p + e_1) - 1$$

$$e_p = (e_2 - e_1) + 1$$

$$\text{Saturation } S = 1 - \frac{e_2}{e_1}$$

$$\therefore \quad a = \frac{\left\{\frac{6}{d_p}(e_1 - e_2) + \frac{6}{d_c}(1 - e_1)\right\}}{(1 - e_2)}$$

$$a = \frac{\left\{\frac{6}{d_p} e_1 S + \frac{6}{d_c}(1 - e_1)\right\}}{\{1 - e_1(1 - S)\}}$$

APPENDIX D

Regressional analysis used in the evaluation of the Decay Factor k. From equation 10.24. the saturation profile is

$$S = (S_I - S_E)_3^{-k(1 - L_I)} + S_E \qquad D.1.$$

Rearranging and linearising

$$\log_e(S - S_E) = \log_e(S_I - S_E) - k(1 - L_I) \qquad D.2.$$

Equal $\log_e y = \log_e a + bx$ D.3.

1. Coefficients a, b

$$b = \frac{\sum x_i \log_c y_i - \frac{1}{n} (\sum x_i) (\sum \log_e y_i)}{\sum x_i^2 - \frac{1}{n} (\sum x_i)^2} \qquad D.4.$$

$$a = \exp \left(\frac{\sum \log_e y_i}{n} - \frac{\sum x_i}{n}\right) \qquad D.5.$$

2. Coefficient of determination

$$r^2 = \frac{\{\sum x_i \log_e y_i - \frac{1}{n} \sum x_i \sum \log_e y_i\}^2}{\{\sum x_i^2 - \frac{(\sum x_i)^2}{n}\} \{\sum (\log_e y_i)^2 - \frac{(\sum \log_e y_i)^2}{n}\}}$$

From the saturation vs bed depth graph obtained from relative permeability calculations the experimental values of S_I, S_E and changing S with L are obtained and used in the programme to obtain the coefficients of equation D.3.

APPENDIX E

Integration of two phase pressure drop equation

The solution of the equation describing the pressure drop ratio was reduced to the integration of the following polynomial expression.

$$\int_{L_1}^{L} f(s)\, dl = \frac{1}{k} \int_{g}^{g+h} \frac{(dV^2 + fV + i)}{-k(L - L_I) + h\,(V - h)(1 - V)^3}\, dV \qquad \text{E.1.}$$

Integration is performed by partial fractions

$$\frac{dV^2 + fV + i}{(V - h)(1 - V)^2} = \frac{A}{(1 - V)} + \frac{B}{(1 - V)^2} + \frac{C}{(1 - V)^3} + \frac{D}{(V - h)}$$

$$dV^2+fV+i = A(1-V)^2(V-h) + B(1-V)(V-h) + C(V-h) + D(1-V)^3$$

$$= A\{V^3 - V^2\,(2 + h) + V(1 + 2h) - h\}$$

$$= B\{-V^2 + V\,(h + 1) - h\} + C\{V - h\}$$

$$= D\{-V^3 + 3V^2 - 3V + 1\}$$

equating coefficients

V^3 : $0 = A-D$

V^2 : $d = -(2+h)A - B+3D$

V : $f = (1+2h)A + (h+1)B + C-3D$

V° : $1 = -hA - hB - hC +D$

This equation gives:

$$A = D = \frac{dh^2+fh+i}{(h^2-2h+1)(1-h)}$$

$$B = \frac{(f+2d)h - d+i}{(h^2-2h+1)}$$

$$C = \frac{(d+f+i)(1-h)}{(h^2-2h+1)} -$$

these expressions are independent of v, it is possible to integrate equation A.5.1.

$$\int_{g}^{g+h} e^{-k(L-L_I)+h} \quad \frac{(dV^2 + fV + i)}{(V - h)(1 - V)^3} dv$$

$$= \{-A \log_e (1-V) + \frac{B}{(1-V)} + \frac{C}{2(1-V)^2} + D \log_e (V-h) \int_{g}^{g+h} e^{-k(L-L_I)}$$

APPENDIX F

Derivation of queue length equation

Assuming λ = poisson arrival distribution of mean arrival rate

μ = exponential service distribution of mean service rate

M = number of channels having an identical service rate

n = number of units (drops) in the system

The number in the system exceeds the number of service channels i.e. $n \geq M$.

The fractions of drops which join the queue $tn = e^{\frac{-\alpha n}{\mu}}$ F.1.

Now : mean service rate = $M\mu$

mean arrival rate = $f_n \lambda$

If there are n units in the queueing system, the probability that there are n units in the system at time t + dt is $\rho_n(t + dt)$. If the processes which cause a transition from this state are independent of time which is true for steady state operation,

$$\rho_n = (t + dt) = \sum_m T_{mn} (dt)\ \rho m\ (t) \qquad \text{F.2.}$$

considering the transition probabilities

$$Tn,n(dt) = 1 - (M\mu + f_n\lambda)dt \qquad \text{F.3.}$$

$$T_{n+1,n}(dt) = M\mu\, dt \qquad \text{F.4.}$$

$$T_{n-1,n}(dt) = f_{n-1}\,\lambda\, dt \qquad \text{F.5.}$$

Let $\gamma = e^{-\frac{\alpha}{2\mu}}$

Then $f_n = \gamma^{2n}$; $f_{n-1} = \gamma^{2n-2}$ F.6.

substituting equations F.3., F.4. and F.5. in equation F.2. noting that $\rho_n(t+dt) = \rho_n(t)\, dt + d\rho_n$

gives the following

$$\rho_n(t)\, dt + d\rho_n = [M\mu\rho_{n+1}(t) + 1 - (M\mu + {}^{2n}\lambda)\, \rho_n(t) + \gamma^{2n-2}\, \rho_{n-1}(t)]dt \qquad \text{F.6.}$$

dividing by dt and setting $\frac{d\rho n}{dt} = 0$ for steady state conditions,

$$M\mu\, \rho_{n+1} + \gamma^{2n-2}\lambda\rho_{n-1} - (M\mu + {}^{2n}\lambda)\rho_n = 0 \qquad \text{F.8.}$$

equation F.8. takes a special form for n = 0 since ρ_{-1} does not exist and there is zero probability of moving from the state, n = 0 by completion of a service operation.

i.e. $\rho_{-1} = 0$; $n\mu\rho_n = 0$; $\gamma^{2n} = 1$

$$\therefore \quad \mu\rho_1 - \lambda\rho o = 0 \qquad \text{F.9.}$$

dividing equation F.8. by μM, and defining the utilisation factor $\rho = \frac{\lambda}{\mu M}$,

$$\rho_{n+1} + \rho\gamma^{2n-2}\, \rho_{n-1} - (1 + \rho^{2n})\rho_n = 0 \qquad \text{F.10.}$$

for $n \geq M$

If $n \geq m$ equation F.10. becomes

$$(n+1)\rho_{n+1} + \rho^{2n-2}\rho_{n-1} - (n+\rho^{2n})\rho_n = 0 \qquad \text{F.11.}$$

$$\rho_1 = \rho P \quad \text{where } \rho = \frac{\lambda}{\mu}$$

The general solution of these equations is obtained by successively increasing the value of n,

$$P_n = \frac{\rho^n \gamma^{n(n-1)}}{n1} Po \qquad 1 \leq n \leq M \qquad \text{F.12.}$$

$$P_n = \frac{\rho^n \gamma^{n(n-1)} M^M}{M1} Po \qquad M \leq n \qquad \text{F.13.}$$

The sum of the probabilities for all possible states of the system must be unity

$$\therefore \quad \sum_{n=1}^{\infty} P_n = 1$$

from equation A.6.13.

$$\sum_{n=1}^{\infty} \frac{\rho^n \gamma^{n(n-1)} M^M Po}{M1} = 1 \qquad \text{F.14.}$$

hence

$$Po = \frac{M1}{M^M \sum_{n=1}^{\infty} \rho^n \gamma^{n(n-1)}} \qquad \text{F.15.}$$

The length of the queue, L_q is given by

$$L_q = \sum_{n=1}^{\infty} n P_n$$

$$\therefore \quad L_q = \sum_{n=1}^{\infty} \frac{n\,\rho^n\,\gamma^{n(n-1)}}{\sum_{n=1}^{\infty} \rho^n\,\gamma^{n(n-1)}} \qquad \text{F.16.}$$

APPENDIX G

Determination of the Hamaker constant

An Equation to determine the Hamaker constant was given by Sherony and Kintner (23) for a system of two immiscible liquids and a solid

$$Q = 6\pi r^2 \left(\sqrt{\sigma_c^d} - \sqrt{\sigma_c^d}\right) \left(\sqrt{\sigma_s^d} - \sqrt{\sigma_c^d}\right)$$

where r is the intermolecular distance σ_c^d, σ_d^d, σ_s^d are the London-van der Waal's component to the surface tensions of the continuous, dispersed, and solid phases respectively.

Fowkes (98) determined $6\pi r^2$ equal to $1.44 \times 10^{-18} m^2$ for water and hydrocarbon systems.

$\sigma_c^d = 0.0218$ N/m for water

$\sigma_c^d = 0.0285$ N/m for toluene

$\sigma_c^d = 0.078$ N/m for glass

$$Q = 1.44 \times 10^{-18} \left(\sqrt{0}.0285 - \sqrt{0}.218\right) \left(\sqrt{0}.078 - \sqrt{0}.0218\right)$$

$$Q = 0.401 \times 10^{-20} \text{ J}$$

APPENDIX H

Parameters used in comparison of capture mechanisms and filter coefficients

Parameter	Symbol	Value
Collector diameter	d_c	267μm
Dispersed phase density	d	866.9 kg/m^3
Continuous phase density	c	1000 kg/m^3
Dispersed phase viscosity	μ_d	0.58×10^{-3} Ns/m^2
Continuous phase viscosity	μ_c	1.00×10^{-3} Ns/m^2
Boltzman's constant	K'	1.38048×10^{-23} J/K
Absolute temperature	T	293°K
Hamaker constant	Q	0.401×10^{-20} J
Hydrodynamic function	A_s	37.98

NOMENCLATURE

NOMENCLATURE

The symbols have the following meanings except where specifically indicated in the text:

a	specific surface area (m^2/m^3)
a_c	collector radius (m)
a_p	drop radius (m)
A	flow parameter (-)
A_c	surface area of container per unit volume of bed (m^2/m^3)
A_{cap}	area of capillary available for flow (m^2)
A_F	Happel's cell flow parameter for assemblage of cylinders (-)
A_S	Happel's cell flow parameter for assemblage of spheres (-)
b	width of capillary (m)
B	radius of smallest droplet (μm)
C	fractional concentration of dispersion (-)
d	channel diameter (m)
d_a	aperture diameter (m)
d_c	collector diameter (m)
$\bar{d}_c$	average collector diameter (m)
d_{ce}	effective collector diameter (m)
d_H	hydraulic radius (m)
d_p	drop diameter (m)
d_{pc}	critical drop diameter for release (m)
d_{pe}	exit drop size (m)
	molecular diffusion coefficient (m^2/s)
D	diameter of coalescing bed (m)

D	diameter factor (μm)
E	packing voidage
e	voidage factor (-)
f_p	friction factor (-)
f_w	correction factor for wall effect (-)
F_{Ad}	adhesion force (N)
F_{DL}	double layer force (N)
F*	dimensionless drag force (-)
g	acceleration due to gravity = 9.81 (m/s^2)
h	drop/collector separation (m)
	film thickness for capillary flow (m)
H	dimensionless separation between drop and collector = h/a_p (-)
H*	dimensionless separation at rear stagnation point
I	mass capture rate (m^2/s)
j	rate of particle capture per unit sphere length ($\eta o/ms$)
k	relative permeability (-)
	saturation profile parameter characterising rate of decay (-)
k'	Boltzman constant K'
K	Kozeny constant (-)
K_o	shape factor (-)
ℓ	distance into coalescing bed from inlet face (m)
L	bed depth (m)
L	radius of droplet (μm)
L_e	effective path length (m)
L_E	length of bed near exit face having constant saturation value (m)

L_I length of drop near inlet face having constant saturation value (m)

n number of drops (-)

L_q length of queue

n_o number of drops entering interval ℓ from inlet face (-)

n_1 number of drops leaving ℓ from inlet face (1)

N_{Ad} adhesion number = $\frac{4Q}{9\pi R^2 A} \cdot \frac{1}{\mu_c U d_p^2}$ (-)

N_{DL} double layer group = $\frac{\kappa d_p}{2}$ (-)

N_{EZ} electrokinetic group = $\frac{2 \zeta_p \zeta_c}{(\zeta_p^2 + \zeta_c^2)}$ (-)

N_G gravity number = $\frac{d_p^2 (\rho_d - \rho_c) g}{18 \mu_c U A}$ (-)

N_{pe} Peclet number = $\frac{d_c u}{D}$ (-)

N_R interception number = $\frac{d_p}{d_c}$

N_{Re} Reynolds number = $\frac{d_c u \rho_c}{\mu_c}$ (-)

N_{Re} Reynolds number = $\frac{d_c u \rho_c}{\mu_c}$ (-)

N_{sh} Sherwood number = $\frac{I}{\pi d_c D C}$ (-)

N_{stk} Stoke's number = $\frac{d_p^2 \rho_c u}{9 \mu_c d_c}$ (-)

ΔP pressure drop (N/m^2)

i flowrate of pahse i (m^3/s)

Q Hamaker constant (J)

Q total volumetric flowrate (m^3/s)

r distance from centre of cylinder or sphere (m)

r_{22} intermolecular distance (m)

R interception number = $\frac{dp}{dc}$ (-)

R_d direct interception number = $\frac{dp}{da}$ (-)

S local saturation of dispersed phase (-)

$\bar{S}$ average saturation of dispersed phase (-)

S_c local saturation of continuous phase (-)

S_d local saturation of dispersed phase when used in conjunction with S_c (-)

S_E saturation near exit face of bed (-)

S_I saturation near inlet face of bed (-)

t time (s)

T temperature (°K)

T tortuosity factor (-)

u superficial velocity (m/s)

u_1 aqueous superficial velocity for single phase (m/s)

u_2 aqueous superficial velocity for two phase flow (m/s)

u_{cap} interstitical velocity (m/s)

X cross sectional area (m^2)

Greek letters

α volume of solids in the bed = $1 - e_1$ (-)

β fraction of collisions between drops that resulted in coalescence

γ interfacial tension (N/m)

ε dielectric constant of continuous phase

σ	surface tension (N/m)
η	drop capture efficiency (-)
η_c	coalescence efficiency (-)
μ	viscosity (Ns/m^2)
ρ	density (kg/m^3)
λ	theoretical filter coefficient (m^{-1})
ν	kinematic viscosity (m^2/s)
ψ	streamline function for drop/collector system (-)
Θ	polar coordinate for drop/collector system (rad.)
ϕ_i	ith particle shape parameter (-)
κ	reciprocal Debye length

Subscripts

1	single phase flow
2	two phase flow
c	continuous phase
C	calculated phase
d	dispersed phase
e	experimental
f	bed of firbres
s	bed of spheres
D	diffusion
D	direct interception
G	gravity (sedimentation)
I	interception
II	inertial impaction
L	London van der Wall
T	total

REFERENCES

REFERENCES

1. Richardson, J.G., Colloid Sci., 15, 404 (1950).

2. Taylor, G.I., Proc, Roc. Soc., London, A138, 41 (1931).

3. Rumscheidt, F.D., Mason, S.G., J. Colloid Sci., 16, 238 (1961).

4. Sherman, P., "Emulsion Science", Academic Press, London (1968).

5. Bonnet, C.F., U.S. Pat. 2, 260, 798, 609, (1940).

6. Hanson, G.B., U.S. Pat. 2, 325, 850, Aug (1943).

7. Sadek, S.E., Hendricks, C.D., Ind. Eng. Chem. Fund. 13, (2), 139-42 (1974).

8. Outlook, "Waste Water Treatment with Air Flotation", Process Engineering, 1, (11), 996 (1973).

9. Sallabanks, L.G.A., "Treating Ballast Water Oily Waste", I.Ch.E. Meeting, University of Surrey, Guildford, May (1975).

10. Farley, R., Valentin, F.H.H., A.I.Ch.E. - I. Chem. E. Symposium Series 1, (1965).

11. Tuerk, H., Dechema-Monogr., 74, 205-19, (1974).

12. Robertson, D., J. Appl. Phsy., 44, (9), 3924-7, (1973).

13. Bitten, J.F., Fochtman, E.G., J1. Coll, and Interfac. Sci., 31 (92), 312 (1971).

14. Hazlett, R.N., Ind. Eng. Che. Fundam., 8 (4), 625 (1969).

15. Vinson, C.G., Churchill, S.W., The Ch. Eng. J., 1, 110 (1970).

16. Spielman, L.A., Goren, S.L., Enviro. Sci. & Tech., 4 (2), 135 (1970).

17. Rosenfeld, J.I., Wasan, D.T., Can. J. Chem. Eng., 52, 3 (1974).

18. Davies, G.A., Jeffreys, G.V., Filt. and Sep., July/ August, 349 (1965).

19. Rajagopalan, R., Tien, C., Can. J. Ch. E., 55, 246 (1977).

20. Attarzadeh, G.R., Ph.D., Thesis, Univeristy of Aston (1979).

21. Langmuir, I., Office of Technical Service, Washington D.C., OSRD Resport No. 865 (1942).

22. Hazlett, R.N., Ind. Eng. Chem. Fundam., 2 (3), 520 (1970).

23. Sherony, D.G., Kintner, R.C., Can. J. Chem. Eng., 49, 314, (1971).

24. Spielman, L.A., Fitzpatrick, J.A., J. Coll. & Inter. Sci., 42 (3), 607 (1973).

25. Hamaker, H.C., Physica, 4, 1058 (1937).

26. Rosenfield, J.I., Wasan, D.T., Proc. I.S.E.C. 74, Lyons, 319 (1974).

27. Wilkinson, D., Mumford, C.J., Jeffreys, G.V., A.I.Ch. E.J., 21 (5), 910 (1975).

28. Redmon, O.C., Chem. Eng. Progr., 59, 87 (1963).

29. Bitten, J.F., J1, Coll. and Interfac. Sci., 33 (2), 265 (1970).

30. Smith, T.N., Chem. Eng. Sci., 29, 583 (1974).

31. Spielman, L.A., Goren, S.L., Ind. Eng. Chem., 62, 10 (1970).

32. Brown, G.G., "Unit Operations", John Wiley, N.Y. (1950).

33. Spielman, L.A., Goren, S.L., Ind. Eng. Chem. Fund., 11 (1), 66 (1972).

34. Spielman, L.A., Su, Y.P., Ind. Eng. Chem. Fund., 16 (2), 272 (1977).

35. Hazlett, R.N., Ind. Eng. Chem. Fundam., 8 (4), 633 (1969).

36. Sherony, D.F., et al, Can. J. Chem. Eng. 49, 321, (1971).

37. Langden, W.M., I.E.C.Fund., 5 (4), 625 (1969).

38. Lindenhofen, H.E., Filt. and Sep. Sept/Oct., 567 (1969).

39. Davies, G.A., Jeffreys, G.V., Filt. and Sep., July/ August (1969).

40. Garrison, M., Van Loenen, W.F., U.S. Patent, 1, 947, 709, (1934).

41. Burtis, T.A., Kirkbride, C.G., Trans. A.I.Ch.E. 42 (3), 413 (1946).

42. Spielman, L.A., Ph.D. Thesis, University of California, Berkely, (1969).

43. Rosenfeld, J.I., Ph.D. Thesis, I.I.T., Chicago, (1973).

44. Redman, O., Chem. Eng. Prog., 59, 87, (1963).

45. Sherony, D.F., M.Sc.Thesis, I.I.T. Inst. of Tech., Chicago, (1965).

46. Bitten, J.F., J. Coll and Interfac. Sci., 33 (2), 265 (1970).

47. Wilkinson, D., Ph.D. Thesis, University of Aston, (1974).

48. Shalhoub, N.G., Ph.D. Thesis, University of Aston, (1975).

49. Langdon, W.M., et al, Envirom. Sci. and Tech., 6 (10), 905 (1972).

50. Singhal, A.K., Dranchuk, P.M., Can. J. Ch. Eng., 53, 3 (1975).

51. Shah, B.S., M.Sc. Thesis, Illinois Institute of Technology, Chicago (1975).

52. Mason, G.J., Coll. Interfac. Sci., 35 , 286 (1971).

53. Hogg, R., et al, Trans. Fara. Soc., 62, 1638 (1966).

54. Ridgeway, R., Jarbuck, K.J., Brit. Chem. Eng., 12, 384 (1967).

55. Verman, L.C., Barnerjee, S., Nature, 151, 584 (1946).

56. Thomas, R.J., Mumford, C.J., Int. Solvent Extraction Conf., Hague, Vol. 1, 400 (1971).

57. Spielman, L.A., Goren, S.L., Ind, Eng. Chem. Fund., 11, 73 (1972).

58. Happel, J., A.I.Ch.E.J., 5, 174 (1959).

59. Happel, J., Brenner, H., "Low Reynolds Number Hydrodynamics", Prentice-Hall, pp. 533, Englewood Cliffs, New Jersey (1965).

60. Perry, R.H., Chilton, C.H., "Chemical Engineers Handbook", 5th Edition, McGraw Hill, Tokyo, (1973).

61. Payatukes, A.C., et al, A.I.Ch.E.J., 19, 581, 67 (1973).

62. Calibration Data, "Metric Series Rotameters", G.E.C., Elliott Automation Group (1975).

63. Fattah, A.F.M., Ph.D. Thesis, University of Aston, (1975).

64. Malvern Electronics - Malvern Particle Sizer 2200, Instruction Manual, Malvern, England (1981).

65. Irani, R.R., Callis, C.F., "Particle Size:Measurement, Interpretation and Application", John Wiley (1963).

66. Coulter Electronics, L.T.D. Coulter Counter Model ZB Instruction Manual, Dunstable, England, (1980).

67. Polichronakis, C.I., M.Sc. Thesis, University of Aston, (1972).

68. Austin, D.G., Ph.D. Thesis, University of Aston, (1979).

69. Ibrahim, S.Y., M.Sc. Thesis, University of Aston, (1981).

70. Tonna, J.A., B.Sc. Project Report, University of Aston, (1983).

71. Baez, S., Ph.D. Thesis, University of Aston, (1983).

72. Sareen, S.S., et al, A.I.Ch.E.J., 12 (6), 1045 (1966).

73. Ergun, S., Chem. Eng. Proj., 48m 98 (1952).

74. Macdonald, I.F., et al, Ind. Eng. Chem. Fund., 18, 199 (1979).

75. Jones, P.J., Word Oil, 129, (2), 170 (1949).

76. Ali, A.M., "Cost and Optimization Eng.", McGraw Hill Book Co. N.Y. (1970).

77. Boyadzhieu, L., et al, Filt. and Sep, pp. 42-43, Jan-Feb (1981).

78. Grilc, V., et al, Chem. Eng. Res. Des., 62 (1984).

79. Lindenhofen, H.E.m Filt, and Sep., July/August, 317 (1968).

80. Lloyd, N.E., J. Coll. Sci., 14, 441 (1959).

81. Lissant, K.J., J. Coll. Inter. Sci., 22, (1966).

82. Lungdgnen, T.S., J. Fluid. Mech., 51, 273 (1972).

83. Becher, P., J1, Coll. Interfac. Sci., 24, pp. 91-96 (1967).

84. Mumford, C.J., Hemeri, A.L., A.A.A., I.S.E.C., Hague, Vol. 2, 1591 (1974).

85. Dullien, F.A.L., A.I.Ch.E.J., 21, 299 (1975).

86. Elgar, C., B.Sc. Project Report, University of Aston, Jan (1974).

87. Bikerman, J.J., Ind. Eng, Chem., 57 (1), pp. 59-62, (1965).

88. Carpenter, C.W., Jr-Bail, P.T., Bobek, J.E., Soc. Petrol Eng. Jnl., March (1962).

89. Carroll, B.J., Lucassen, R., "Theory and Practice of Emulsion Technology" Symp., Soc. Chem. Ind., Brunel University, pp. 29-41 (1974).

90. Chembers, D.B., "Oil Water Separation using Fibrous Materials", I.Ch.E. Symposium: Separation of Liquid Dispersions, Manchester, November (1977).

91. Heller, J.P., Procc. Symp. "Fundamentals Transport Phenomenon Porous Media", 2nd, IAHR - ISSS Vol. 1, University of Guelph, Ontario, Canada (1972).

92. Hermanie, P.H.J., Van deer Waarden, M., J. Coll. Inter. Sci., 21, pp. 513-521 (1933).

93. Douglas, E., Elliott, I.G., Trans, Inst. Marine. Eng., 74, (5), 164 (1962).

94. Dudgeon, C.R., Honille Blanche, I., 785 (1966).

95. Brinkman, H.C., Appl. Sci. Res., A1, 27, 81, A2, 190 (1949).

96. Boyadzheiv, L., et al, Filt. and Sep., Jan/Feb (1981).

97. Bear, J., "Dynamics of Fluids in Porous Media", American Elsevier, New York, (1972).

98. Fowkes, F.M., et al, Eng. Sci. Tech., 4, 510 (1970).

99. Fowkes, F.M., Ind. Eng. Chem. 56, (12), 40 (1964).

100. Collins, R.E., "Flow of Fluids Through Porous Materials", Reinhold, New York (1961).

101. Cornell, D., Katx, D.L., Ind. Eng. Chem., 45, 2145 (1952).

102. Franklin, J.S., Eff 1., Water Treat. Jl., Oct (1973).

103. Friedlander, S.K., A.I.Ch.E.J., 3, 43 (1957).

104. Friedlander, S.K., J. Colloid. Inter. Sci. 23, 157 (1967).

105. Fuchs, N.A., "The Mechanics of Aerosols", Pergamon, Oxford, pp. 408 (1964).

106. Gabriel, J.C., Parry, G., Filt. and Sep., 253, May/June (1977).

107. Gammon, H., Filt. and Sep., 409, July/August (1973).

108. Carman, P.G., Trans. Inst. Chem. Eng., 15, 150 (1937).

109. Ghosh, M.M., Brown, W.P., J. Water Pollution Control Fed., 47 (8), 2101 (1975).

110. Haring, R.E., Greenkom, R.A., A.I.Ch.E.Jl., 16, 477 (1970).

111. Harkins, W.D., "The Physical Chemistry of Surface Films", Reinhold, New York (1952).

112. Hazlett, R.N., Carhart, H.W., Filt. and Sep., July/ August, (1972).

113. Hitit, H.A., Ph.D. Thesis, University of Aston, (1972).

114. Allak, A.M.A., Ph.D. Thesis, University of Aston, (1973).

115. Treybal, R.E., "Liquid Extraction", McGraw Hill, N.Y., (1963).

116. Ullman, J.H., B.Sc. Project Report, University of Aston, (1974).

117. Filter Coalescer Elements, British Patent, BP155823.

118. Lawrence, P.A., Eric, M.D., Brit. Pat. Appl. 2050557 (1981).

119. Hartland, S., Vohra, D.K., J. Colloid Interfac. Sci., 77 (2) (1980).

120. Rushton, P., Davies, G.A., Filt. and Sep., 17 (2), (1980).

121. Hisakaza, S., et al, Chem. Pharm. Bull., 27 (12), (1979).

122. Root, T.A., Pat. Appl. 9059 (1980).

123. Scheele, G.F., Pendergrass, J.H., Chem. Eng. Commun.5, (1980).

124. Scheele, G.F., Clork, D.B., Chem. Eng. Commun. 5, (1980).

125. Chambers, D., Walker, B., U.S. Pat. 4199447 (1975).

126. Hartland, S., Gakis, N., Proc. Royal. Soc. London Series A, 369 (1979).

127. Sagart, N.H., Quinn, M.J., Can. J. Chem. Eng., 57, (1979).

128. Rushton, E., Davies, G.A., Inter. J. Mult. Flow, 4 (4) (1978).

129. Sagart, N.H., Quinn, M.J., Can. J. Chem. Eng., 56, (1978).

130. Acharya, A., Ulbrecht, J.J., A.I.Ch.E. Journal, 24 (1978).

131. Golob, J., Modio, R., Trans. Instn. Chem. Eng., 55, (1977).

132. Hendricks, C.D., I.E.E.E. Trans. on Ind. Applicat. Sept/Oct, (1977).

133. Jones, A.F., Wilson, S.D.R., J. Fluid Mech., 87 (2), (1978).

134. Spielman, L.A., Ind. Eng. Chem. Fund., May (1977).

135. Rose, H.E., Rizk, A.M.A., Rroc. Inst. Mech. Engrs., 160, 493 (1949).